台灣山岳冰河

Freie Universität Berlin

Dissertation at the Department of Earth Sciences

Photo: Glacial sediments in Nanhuta Shan, Taiwan, October 2000

Geomorphological studies on the late Pleistocene and early Holocene glaciation in selected high mountain ranges in Taiwan

Robert Hebenstreit

Freie Universität Berlin

Geomorphological studies on the late Pleistocene and early Holocene glaciation in selected high mountain ranges in Taiwan

Geomorphologische Untersuchungen zur spätpleistozänen und frühholozänen Vergletscherung ausgewählter Hochgebirge in Taiwan

Dissertation

zur Erlangung des akademischen Grades
Doktor der Naturwissenschaften (Dr. rer. nat.)

am Fachbereich Geowissenschaften
der Freien Universität Berlin

vorgelegt von
Robert Hebenstreit

Berlin, 2012

Erstgutachterin:	Prof. Dr. Margot Böse
Zweitgutachter:	Prof. Dr. Karl Tilman Rost
Tag der Disputation:	21. Oktober 2011

Preface and acknowledgements

The following thesis is submitted in partial fulfilment of the requirements for the degree *Doktor der Naturwissenschaften* at the Department of Geosciences at the Freie Universität Berlin, Germany. This dissertation comprises major parts of the research project *Jungpleistozäne und holozäne Relief- und Klimageschichte im Hochgebirge von Taiwan* supervised by Prof. Dr. Margot Böse and supported by the German Research Foundation (Deutsche Forschungsgemeinschaft, no. Bo 659/16-1), the National Science Council of Taiwan and the German Academic Exchange Service. It was organized in cooperation with the National Taiwan University, the Nordic Laboratory for Luminescence Dating of the Aarhus University in Roskilde (Denmark), the Laboratory of Ion Beam Physics at the ETH Zurich (Switzerland) and three National Parks in Taiwan. For two and half years I was supported by a scholarship from the Berlin Senate (*NaFöG*), which I appreciated very much.

Four field campaigns were undertaken in Taiwan during the period between spring 2000 and spring 2002. A first version manuscript of this dissertation was compiled and parts of the results were submitted for publication in summer 2004. They were published as two scientific articles in 2006. Data, which make up a major part of this project, were processed with a delay of several years due to problems concerning external laboratory analyses, which were not accounted by the author. Therefore, the work on this dissertation was nearly completely interrupted for about five years. After the data were available, final results were submitted for publication in April 2010 and were published online in December 2010. The manuscript of this dissertation was subsequently completely revised and updated with new information from the latest literature. The final version was compiled in spring and summer 2011.

The text is organized into eight chapters. The introducing **chapter 1** gives the main motivation, the background of this work and a short overview on previous research on the paleoclimate in East Asia and Taiwan. **Chapter 2** introduces the study area with its regional physio-geographic setting. The description of the applied methods makes up **chapter 3**. The following three **chapters 4 to 6** comprise the results, which were previously published in the three articles in scientific journals. They are ordered chronologically according to their

publication date and referred to in the text as **publication 1** (Hebenstreit et al., 2006), **publication 2** (Hebenstreit, 2006) and **publication 3** (Hebenstreit et al., 2011) or as the respective chapters 4, 5 and 6. Due to the reasons noted above, important analytical results could be published only with delay in the third paper - that means after the synthesis in the second paper. However, they confirm in general the previous results and refine them. Additional results, which are not part of the publications, are presented in the supplementary **chapter 7**. A comprehensive review on Pleistocene glaciations in the Asian-Pacific region and some concluding remarks are given in **chapter 8**.

As the whole project resembled a work in progress and knowledge increased over time, doubling and reinterpretation of content in the publications and the dissertation text were not totally avoidable since they concern – strictly speaking – the same subject from different points of view. Furthermore, to make the text readable as a whole, some introducing descriptions and methodological considerations from the papers are additionally put into the introducing chapters. However, it was tried to avoid repetitions as far as possible.

This work would not have been possible without the help of numerous contributors. My very first thank is due to **Margot Böse**, who invited me to take part in this project, which widened not only my scientific view and interests, but brought me also many unforgettable personal experiences. Thanks a lot also for her patience and permanent insisting to bring this dissertation to a successful end.

Christina Klose was my partner in this project from the periglacial and present morphodynamic side. Although our discussions were often controversial, they were also interesting and inspiring. **Susan Ivy-Ochs** did the sample preparation for the exposure dating and **Peter Kubik** made the AMS measurements and the first version age calculation. Thank you both very much for useful comments and corrections on the manuscript of the third paper. Thanks to **Andrew Murray** for analysing the OSL samples at the Risø Lab, for corrections in the first paper and for a long discussion together with **Christian Schlüchter** and **David Patley,** who all convinced me in the end that the whole thing makes sense.

Many thanks are also due to **Jiun-Chuan Lin, Ping-Mei Liew**, their students and assistants, especially **Chia-Hung Jen**, from the NTU for their patient help in Taipei with all the logistics and technical problems of this project and their talent to make impossible things happen.

A very special thank goes to **Mr. and Mrs. Tai** for some financial support, but even much more for introducing the culinary and cultural highlights of Taiwan.

Mountain guide **Wen-Chih Lin** is the secret hero behind the scenes. His field experience and outdoor cooking art helped us to find our way through the bamboo jungle and to survive on remote rock summits in the Taiwanese mountains. **Helge Martens** and **Yen-Chao Kuo** were my field partners during the first expedition to Nanhuta Shan. Thank you for joining and your help. **Hao-Tsu Chu** and **Chien-Fu "O.B." Yang** provided useful information about the field areas.

Many thanks go to **Marion Müller**, **Jens Lock**, **Manuela Burmeister** for their help in the sediment lab and to **Peter Röper** for many useful comments on the grain size data.

Thanks to **Anne Beck, Jörg Riekert** and **Nathalie von Möllendorff** for giving some English text corrections and also to **Chia-Han Tseng** and **Ying-Wei Lin** for their help with Chinese translations and characters. Many thanks are due to the reviewers of the papers **Christian Schlüchter, Steven Porter, Andrew Hein and Georg Delisle** for comments, which improved the papers considerably.

After my come back to the office in Berlin-Lankwitz I had a very inspiring communication and discussion with my colleagues of the Arbeitsgruppe Böse. The atmosphere in the group was an invaluable source of motivation to finish this dissertation. Special thanks go to **Dirk Wenske, Christopher Lüthgens and Tony Reimann** for helping me patiently with the computer stuff, especially with the GIS applications and for discussions about the OSL data.

Some more personal thanks go to my friends **Hung-Ling** and **Yi-Hsiang** who showed me much of the life in Taipei and helped me to understand the Taiwanese lifestyle from another point of view, and to **Ricardo**, who kept the house with a broken leg in a foreign country, which nearly challenged my first field trip. ¡Gracias, Chico para tu paciencia! Thank you, **Tino** for reading the last version manuscript about the strange stones with eagle eyes and for giving me company and warmth in many years.

Thank you all, *謝謝* !

Robert Hebenstreit

Berlin, summer 2011

Contents

Preface and acknowledgements **1**

Summary **6**

Zusammenfassung **7**

CHAPTER 1 Introduction **8**

1.1 Motivation, background and aims of this work 8

1.2 Paleoclimatic environment in the western Pacific and East Asian region 9

1.3 Previous research on former glaciations in Taiwan 12

CHAPTER 2 The study area **17**

2.1 Geographical units, topography and altitudinal zonation of Taiwan and the location of the study areas 17

2.2 Short outline of the present climate in Taiwan and the regional atmospheric circulation 21

2.2.1 Circulation and air masses *21*

2.2.2 Precipitation *23*

2.2.3 Temperature *27*

2.2.4 Characteristics of annual and diurnal variations of air temperature in Nanhuta Shan *28*

2.3 Geologic-tectonical setting and morphodynamics in the Taiwanese orogen 30

2.3.1 Plate tectonics and geological provinces *30*

2.3.2 Geologic setting in the Nanhuta Shan massif *32*

2.3.3 Seismicity *34*

2.3.4 Mountain uplift *34*

2.3.5 Present morphodynamics and erosion in the Taiwanese mountain belt *35*

CHAPTER 3 Methods **38**

3.1 Methodical framework and strategic approach of this work 38

3.2 Some principles and theoretical aspects of glacio-geomorphological analyses 39

3.3 Key landforms of glacial erosion 40

3.3.1 Glacial valleys and associated key features *40*

3.3.2 Cirques and associated landforms *42*

3.3.3 Roches moutonnées *42*

3.3.4 Small scale erosional features *43*

3.4 Glacigenic depositions 43

3.4.1 Definitions *43*

3.4.2 Characteristics of glacial deposits and problems associated with their identification in high mountain environments *44*

3.4.3 Erratics *46*

3.5 Applied techniques and field work 47
3.5.1 Remote sensing, aerial photo and topographic map interpretation, positioning 47
3.5.2 Setup of a meteorological station in Nanhuta Shan and the ascertainment of a four-year dataset of temperature and precipitation 48
3.5.3 Elementary geological mapping 48
3.5.4 Sedimentological analyses 49
3.6 Sediment dating by means of optically stimulated luminescence (OSL) 50
3.6.1 Introduction 50
3.6.2 Principles of luminescence dating 50
3.6.3 Sampling and applied measurement protocol 51
3.6.4 Application for glacial sediments and associated problems 52
3.7 Rock surface exposure dating using in situ produced terrestrial cosmogenic nuclides (TCN) 53
3.8 Calculations of equilibrium line altitudes 54
3.8.1 Principles and Definitions 54
3.8.2 Geometrical reconstruction of present and former ELAs and the ΔELAs 56
3.8.3 Calculation of the modern theoretical ELA in Taiwan and some theoretical climatological considerations 57
3.8.4 Adjustment for postglacial uplift and sea level rise 59

CHAPTER 4 Sedimentological results and OSL dating 61

CHAPTER 5 Present and former equilibrium line altitudes in the Taiwanese high mountain range 75

CHAPTER 6 Application and results of the ^{10}Be surface exposure dating in Nanhuta Shan 83

CHAPTER 7 Supplement to chapters 4 to 6 98

7.1 Geomorphological evidence from Hsueh Shan 99
7.2 Geomorphological evidence from Nanhuta Shan and updated ELA calculations 102

CHAPTER 8 Concluding remarks 110

8.1 Excurse with a wider view: Pleistocene and Holocene glaciations and ELAs in the western Pacific and East Asian region 110
8.2 Some concluding paleoclimatic implications of the results or: Where did the snow come from? 117
8.3 Critical remarks on paleoclimate estimations in mountain areas inferred from ELA reconstructions and comments on future research 118

Overall bibliography 121

Appendix 136

List of publications 145
Curriculum Vitae 146

Summary

Taiwan is a subtropical mountainous island situated at the tropic of cancer in the monsoonal western Pacific region. Its high mountain ranges are not glaciated at present, but since they reach nearly 4000 m they provided favourable conditions for late Pleistocene and early Holocene glacier advances. Their isolated position may provide useful high altitude paleoclimatic information for comparison with marine and continental climate archives and other glaciated areas in the region. At the beginning of this project, only little was known about former glaciations on the island based on the work of early researchers, but detailed sedimentological or chronological information was missing.

This study focuses on a detailed geomorphologic field mapping and the description and analysis of glacial landforms and deposits concerning their geometry, composition and morphostratigraphical correlation. For a chronological constrain, optically stimulated luminescence and rock surface exposure dating with in situ produced cosmogenic ^{10}Be were applied on glacigenic sediments and glacial boulders, respectively, which allows an independent temporal correlation of different geomorphologic evidences. The central Nanhuta Shan massif in NE-Taiwan had the best preserved glacial landforms and thus studies were focused there. Comparative observations were made in Hsueh Shan and in Yushan.

The main finding of this study is, that glaciers advanced repeatedly in the Taiwanese mountains during the last glacial cycle. Large scale glacio-erosional landforms indicate a last glacial equilibrium line altitude below 3000 m with a depression of about 1000 m. Although, age control is still poor for this maximum stage a correlation with the marine isotope stage (MIS) 4 is assumed. Independently derived OSL and ^{10}Be exposure ages from different small scale glacial sediments in Nanhuta Shan yielded a reliable timeframe for a Lateglacial to early Holocene stage with two possible sub-stages at 12 - 15 ka and 9.5 ka and ELA depressions of 610 m and 510 m, respectively.

These results correspond basically with the paleoclimatic proxies and other glacial records from the region and suggest a larger mountain glacier extent in East Asia during the MIS 4 than during MIS 2 and a re-advance during the Lateglacial and Holocene. Full glacial advances are interpreted in terms of an increased influence of the westerly circulation, whereas Holocene glaciations seem to be related to monsoon intensification.

Zusammenfassung

Die subtropische Gebirgsinsel Taiwan liegt am nördlichen Wendekreis im monsunal beeinflussten westlichen Pazifik. Ihre Hochgebirge sind gegenwärtig unvergletschert, doch bei Gipfelhöhen von fast 4000 m boten sie günstige Bedingungen für spätpleistozäne und frühholozäne Gletschervorstöße. Die isolierte Höhenlage verspricht sowohl wertvolle paläoklimatische Informationen im Vergleich mit marinen und kontinentalen Klimaarchiven, als auch mit anderen Vergletscherungsgebieten der Region. Zu Beginn dieses Projektes war die Vergletscherungsgeschichte der Insel kaum bekannt und wenige frühe Forschungen beinhalten keine detaillierten sedimentologischen und chronometrischen Untersuchungen.

Ziele dieser Arbeit waren eine detaillierte geomorphologische Beschreibung, Analyse und Kartierung von glazialen Geländeformen und Sedimenten hinsichtlich ihrer Geometrie, Zusammensetzung und morphostratigraphischer Lagebeziehung. Für eine zeitliche Eingrenzung ihrer Ablagerung wurden glaziale Sedimente und Blöcke mit optisch stimulierter Lumineszenz und in situ produziertem kosmogenem ^{10}Be datiert, was einen unabhängigen Vergleich der verschiedenen glazialen Befunde ermöglicht. Feldarbeiten konzentrierten sich auf das Massiv des Nanhuta Shan in NO-Taiwan mit den besterhaltenen Glazialformen. Ergänzende Untersuchungen erfolgten im Hsueh Shan und Yushan.

Hauptergebnis dieser Untersuchung ist der Nachweis einer mehrphasigen Vergletscherung der Taiwanesischen Gebirge während des letzten Glazialzyklus'. Glazial-erosive Großformen belegen eine Schneegrenze von unter 3000 m, was einer Absenkung von 1000 m entspricht. Bisher wenig gesicherte Datierungen deuten für die Maximalausdehnung ein Alter im marinen Isotopenstadium (MIS) 4 an. Die Datierung kleinräumiger glazialer Sedimente und Einzelblöcke im Nanhuta Shan ergab belastbare OSL- und ^{10}Be Expositions-Alter eines spätglazialen und frühholozänen Stadiums mit möglichen Vorstößen um 12 - 15 ka und um 9.5 ka und entsprechenden Schneegrenzabsenkungen von 610 m und 510 m. Die Ergebnisse korrespondieren im Wesentlichen mit Paläoklima-Proxies und glazialen Befunden aus der Region und legen für Ostasien eine größere Gebirgsgletscherausdehnung im MIS 4 als im MIS 2 und einen spätglazialen/ holozänen Wiedervorstoß nahe. Hochglaziale Gletschervorstöße werden einem stärkeren Einfluss der Westwinddrift zugeschrieben, während holozäne Vergletscherungen mit einer Verstärkung des Monsunsystems erklärt werden.

CHAPTER 1

Introduction

1.1 Motivation, background and aims of this work

The presently observed global climate change is reason for ongoing scientific, political and social debates worldwide about cause and forcing mechanisms of climate fluctuations. Their effect on global ecosystems and cultured land is discussed as well as the predicted increase of related natural hazards, which resemble an enormous risk for life, settlement areas and the economic basis of the people in the affected territories (IPCC, 2007). To implement suitable preventive activity and to establish reliable predictions for future climate change it is essential to increase the understanding of the forcing factors of the climate system including knowledge about natural climate variability.

The paleoclimatology and the ice age[1] research try to reconstruct the nature and magnitude of climate fluctuations as well as the related modification of ecosystems during the Earth's history on geological timescales. Because these fluctuations are not directly measurable, geological, paleontological or geomorphological indicators, so called proxy data, are used for the reconstruction of the past climate (Bradley, 2000).

The extent of mountain glaciers and the altitude of their equilibrium line[2] are usually taken as a valuable climate proxy, because the ice mass balance of a glacier reacts sensitively to climate change, especially to changes in temperature, precipitation and radiation, which result in short-time variations of the glacier's length and volume (e.g. Ohmura et al., 1992; Oerlemans, 2005; Kerschner and Ivy-Ochs, 2008). The analysis of landforms and sediments left by former glacial activity allows therefore conclusions about former climate fluctuations

[1] The more or less popular term "ice age" is used here in a sense of planetary conditions with partially ice cover, which started in the Eocene (*c.* 35 Ma) and remains until today (Ehlers and Gibbard, 2007). For differentiation between colder and warmer periods the terms "glacial"/ "glaciation" and "interglacial" are used respectively (Gibbard and West, 2000).

[2] = snowline, cf. section 3.8 for definition

and their timing. Due to a lack of other climate records, former mountain glaciations are often the principle source of high altitude paleoclimate data in a particular region.

The paleoclimate of the Taiwanese high mountain range and its former glaciations in particular are still poorly known in detail. However, the mountain ranges of Taiwan have excellent potential for former glaciations, because they reach altitudes of far above 3000 m ([3]). Moreover, the unique location of the island in East Asia is of particular paleoclimatic interest, because it represents the intersection of two regional climatic transects. As an isolated high mountain area at the junction of the Eurasian continent and the western Pacific Ocean the island promises useful terrestrial paleoclimatic information in an oceanic environment. Proxy data from Taiwan may potentially mediate between marine climate archives and continental records (cf. section 1.2). The reconstruction of the equilibrium line altitude at the tropic of cancer represents furthermore a regional connection between the Pleistocene mountains glaciations on the inner tropical Malay Archipelago and those in the mid-latitude regions of Northeast Asia on a meridional coastal transect (cf. section 1.4).

The main objective of this work is therefore the reconstruction of the extent and the chronology of presumed former glaciations by a description and mapping of glacial landforms and deposits including detailed sedimentological and geochronological analyses of the deposits in three selected, presently not glacierized mountain ranges in Taiwan, the Nanhuta Shan[4], the Hsueh Shan and the Yushan (cf. section 3.1 for a methodological outline). In addition, the respective depressions of the glacier equilibrium line altitude (ELA) will be estimated to allow comparison with former mountain glaciations elsewhere and with other paleoclimatic indicators on a regional and global scale. This project aims therefore to close a lack of knowledge in paleoclimatic research in the western Pacific and East Asian region.

1.2 Paleoclimatic environment in the western Pacific and East Asian region

During the Quaternary, the Earth was subject to dramatic climate variations resulting in glacial periods with repeated advances of glaciers and large ice sheets, which covered and shaped wide areas of the continental surface interrupted by periods with warmer conditions and less ice extent during the interglacials (Benn and Evans, 1998; Gibbard and West, 2000;

[3] Except as noted otherwise, all altitudes refer to the sea level (a.s.l.), cf. section 3.5.1.

[4] Shan = Chinese for mountain or mountains, cf. chapter 2 for study area location and appendix table A1 for remarks on Chinese transcriptions

Ehlers and Gibbard, 2007). These fluctuations are attributed to cyclical changes in the Earth's orbital parameters (Milankovic, 1941; Hays et al., 1976; Berger, 1988).

The glacial cycles are recorded in oxygen isotope variations ($\delta^{18}O$) of the conserved shells of oceanic microfossils found in cores from sea floor deposits. The $\delta^{18}O$ reflect both, the ocean water temperature and the isotopic composition of the sea water, of which the latter is a measure for the ice volume bound on land. These variations are referred to as the marine isotope stages (MIS) (Emiliani, 1955; Shackleton and Opdyke, 1973). Oxygen isotope variations are also found in the glacier ice itself, for example in ice cores from the Greenland ice sheet[5], where they are considered to be a proxy for air temperature (Grootes et al., 1993) and reflect clearly the transition from the last glacial maximum (LGM) [6] via the Lateglacial with unstable climatic conditions to the onset of the Holocene at about 11.5 ka before present (B.P., Johnsen et al., 1992; Alley et al., 1993).

The continental glacier advances resulted in a global sea level lowering (Fairbanks, 1989; Bard et al., 1990), which led to profound changes of the paleo-geographical environment in the Asian-Pacific region during the last glacial cycle[7]. Large parts of the East Asian/ Australian continental shelves were exposed, including the entire East China Sea (apart from the Okinawa Trough), the Yellow Sea, the northern part of the South China Sea and large areas of the Sunda and the Sahul Shelves with a total area of some 390 million km^2 (Sun et al., 2000). The published values for sea level drop in the western Pacific area range from 120 m (Hanebuth et al., 2000; Liu et al., 2004) to 160 m (Yao et al., 2009) at the last glacial maximum (LGM), which makes, however, a negligible difference in the exposed area (fig. 1.1).

Like at present, the western Pacific warm pool (WPWP) existed during the last glacial period. Sea surface temperatures (SST) were reduced there by only 2 - 3 °C (Thunell et al., 1994; Lea et al., 2000; Stott et al., 2002; Gagan et al., 2004). Nevertheless, the sea level low stand has prevented the warm Kuroshio sea current from entering the Sea of Japan (Ryu et al., 2005).

[5] Examples are the Greenland Ice-core Project (GRIP) and the Greenland Ice Sheet Project 2 (GISP2), cf. publications 1 and 3 for comparative diagrams.

[6] The LGM is defined as the period with maximum global ice volume at about 21 ka B.P., which does not necessarily correspond with the lowest local temperatures (Bard, 1999) or the maximum regional glacier extent (Ehlers and Gibbard, 2007).

[7] The last glacial period is here referred to as the "last glaciation" or the "last glacial"; the last glacial/ interglacial period as the "last glacial cycle", which is more or less synonymous with the stratigraphic subepoch Late Pleistocene (Gibbard et al., 2010).

It reduced also the water exchange through the Luzon Strait into the South China Sea (Wang, 1999), which both resulted in an enhanced thermal seasonality of the surface water in higher latitudes and in the remained marginal seas with winter SST reduction of 5 °C (Ijiri et al., 2005) or even up to 9 °C (Huang et al., 1997). The existence of a possible land bridge connecting the Ryukyu Island Arc to Taiwan is still under debate (Ujiie and Ujiie, 1999). The post-glacial sea level rise and the transgression into the marginal seas occurred rapidly during the Holocene with major pulses at about 14, 12 and 9.5 ka and an up to 5 m higher sea level than at present during the Mid-Holocene (Liu et al., 2004; Yao et al., 2009).

Climatic variations in the western Pacific area are closely related to changes in the East Asian monsoon system[8]. Paleoclimatic information about these changes is derived from multi-proxy records in various terrestrial archives like e.g. loess (e.g. Zhou et al., 1996; An, 2000; Porter, 2001a), glacial deposits (e.g. Shi, 1992; Lehmkuhl and Rost, 1993; Owen et al., 2008)[9], stalagmites (e.g. Wang et al., 2001; Yuan et al., 2004; Zhou et al., 2008) and lacustrine sediments (e.g. Fang, 1991; Herzschuh, 2006; Chen et al., 2008), of which the loess-paleosol sequences encompass the longest timeframe of several million years (An, 2000). These data express an alternation between the dominance of the cold-dry winter monsoon and the warm-humid summer monsoon and indicate in general a strengthened winter monsoon during glacial periods and an intensified summer monsoon during interglacial times.

The East Asian summer monsoon reached its strongest intensity (in terms of humidity and precipitation) during the Holocene. However, it is still debated if the maximum occurred during the early (Chen et al., 2008) or Mid-Holocene (Herzschuh, 2006) or asynchronous in different regions (An et al., 2000). The general monsoon trend is commonly related to north hemisphere insolation forcing (Xiao et al., 2006; Wang et al., 2008; Rohling et al., 2009; Peterse et al., 2011).

It has been also suggested that many of the East Asian paleoclimate proxy records show chronological correlations with north Atlantic climate records (Porter and An, 1995; Wang et al., 2001; Zhou et al., 2008), e.g. with the Greenland ice core record (Rasmussen et al., 2006; Vinther et al., 2006). This implies a profound influence of northern hemispheric westerly circulation on the monsoon variability, but an East Asian monsoon relationship to southern hemispherical circulation has been shown as well (Rohling et al., 2009).

[8] Cf. section 2.2 for an outline of present climate and atmospheric circulation

[9] Cf. chapter 8 for comprehensive review

Paleoclimatic information from the region is also available from the reconstruction of vegetation assemblages based on palynological data from both terrestrial and marine sources (Takahara et al., 2010; Xu et al., 2010). According to this data, northeastern China was occupied by grassland and steppe during the last glacial. Conifers were predominant in Japan and eastern China, followed further south by temperate and subtropical forest (Hope et al., 2004). However, the exposed continental shelf of the East China Sea, including the Taiwan Strait was covered by open grassland (Liew et al., 1998; Sun et al., 2000). Large parts of Southeast Asia including the northern part of the South China Sea shelf were Savannah or dry forest. Tropical and mangrove forest maintained in the lowlands of the (present) Malay Archipelago and colonized also large areas of the emerged southern South China Sea and Sunda shelves (Sun et al., 2000; Hope et al., 2004).

The paleoclimatic evolution in Taiwan is recorded in pollen assemblages at a subalpine site in the Toushe basin at 650 m (Liew et al., 1998; Kuo and Liew, 2000; Liew et al., 2006a; Liew et al., 2006b). They indicate an 8 – 10 °C lower annual temperature and a depression of the altitudinal vegetation belts of 1000 – 1500 m during the MIS 4 compared with the present, whereas the conditions during MIS 2 seem to have been less cold but dryer with a precipitation decrease of minimum 800 mm/ a (Liew et al., 1998). The palynological data also reflect the oscillating warming during the Lateglacial time and a strengthened summer monsoon during the Mid-Holocene (cf. discussions in chapters 4 and 6).

1.3 Previous research on former glaciations in Taiwan

Only little was known about Pleistocene glaciations in the Taiwanese mountain belt at the beginning of this project. Few field studies were undertaken in different mountain ranges by Japanese and German researchers in the first half of the 20th century. A cirque[10] is mentioned for the first time from „Mt. Tugitaka“ (Hsueh Shan) with a floor at 3818 m (Kano, 1932). Morphological traces of former glaciations like trough valleys, cirques, moraines, erratic boulders, roches moutonnées and striated rock surfaces down to 3000 m are described by Tanaka and Kano (1934) for the „Nankotaizan mountain group“ (Nanhuta Shan). However, sedimentological analyses were not made. Panzer (1935) reports glacial features like widened valley heads and a lateral moraine with smoothened and striated boulders

[10] For definition and terminology of glacial landforms and other geomorphological evidences cf. sections 3.3 and 3.4.

from “Niitakayama” (Yu Shan). He estimates the age of the moraine to be Rissian according to the Alpine classification and assumes a corresponding ELA at about 3500 m.

Basing on map and aerial photo interpretation, Böse (2000) identifies glacial landforms and reconstructs a last glacial snowline between 3100 m in Nanhuta Shan and 3300 m in Yu Shan and Hsueh Shan. Chu et al. (2000) report various glacial landforms from Nanhuta Shan in altitudes above 3400 m, but again without sediment analyses or dating.

Contemporaneous field studies alongside with the project reported here were undertaken by Chinese, Taiwanese and French colleagues. Detailed glacial evidence is reported from “Shesan“ (Hsueh Shan) (Yang et al., 1998; Cui et al., 2000; Yang, 2000; Cui et al., 2002). The glacial features include cirques, lateral and terminal moraines and polished surfaces. These authors classified three glacial stages for the last glacial cycle inferred from thermo-luminescence (TL)[11] dating of glacial sediments: The “Shanzhuang” stage at about 44 ka, the “Shuiyuan” stage at about 14 - 18 ka and the “Xueshan” stage at about 11 ka with respective ELAs at 3400 m, 3500 m and 3700 m. However, in which way the TL samples are related to the described moraines is not coherently explained in these publications (cf. section 7.1). Siame et al. (2007) dated glacial boulders and bedrock surfaces in Nanhuta Shan and confirmed the results of this work (Hebenstreit et al., 2006, chapter 4). Siame et al.’s results are discussed in much detail by Hebenstreit et al. (2011, chapter 6). Potential glacial phenomena have also been reported from Hohuan Shan (3416 m), and the Shangyang Shan (3602 m) – Sancha Shan (3496 m) massif in north-central and southern Taiwan, respectively (Chu, 2009). Nevertheless, despite early reported glacial landforms and deposits from various Taiwanese mountain ranges, the existence of former glaciations was not excepted without contradiction by e.g. Zhang (1960) and Xu (1990) (cited after Cui et al., 2002). Even recent publications ignore in their interpretation a possible contribution of glacial melt water for the development of alluvial fan terraces during the last glacial cycle (Hsieh and Chyi, 2010).

A number of publications show Pleistocene snowlines for Taiwan without own investigations. Shi (1992; 2002) indicates an ELA for the Yu Shan at 3600 m and for the northern part of the island at 3500 m. His maps of Pleistocene ELAs in East Asia are compiled from the available glacial record and from paleoclimatic proxy data in the region calculated with an atmospheric laps rate. However, the source of the data for Taiwan is not explicitly provided. Japanese authors show in a series of publications a more and more modified pattern of the

[11] Cf. section 3.6 for principles of luminescence dating

Pleistocene ELAs in East Asia and indicate the ELA for Taiwan at 3200 - 3400 m during MIS 4 and 3500 - 3700 m during MIS 2 (Ono, 1988; 1991; Ono and Naruse, 1997; Aoki and Hasegawa, 2003; Ono et al., 2003; Ono et al., 2004; Ono et al., 2005). Again, the given sources with information from Taiwan are quite intransparent. Subsequent assessments and reviews (Porter, 2001b; Mark et al., 2005; Zhang et al., 2006) refer to the former publications or to Cui et al. (2002) and show ELAs at 3400 - 3500 m for the last glaciation in Taiwan.

Both, the maps shown by Shi (1992, 2002) and by Ono (1988 and modified subsequently) show a characteristic course change of the ELA contour lines in Southeast Asia towards Taiwan. Ono even draws a pronounced "snowline trough" along the eastern margin of the Asian continent from Taiwan to Hokkaido inferred from the ELA gradient in the Japanese mountains. However, the ELA contour pattern appears to be created somewhat intuitively, since the contours continue virtually over the Pacific Ocean (cf. chapter 8). This ELA pattern would change considerably, when the ELA in Taiwan was much lower than 3500 m during the last glacial, which is intended to be shown by this work (fig. 1.1).

Pleistocene glaciations have been reported from various mountain areas in East Asia and the western Pacific like Japan, east and central China and the Malay Archipelago with a general ELA depression of about 1000 m. The extent of Pleistocene glaciers on the Tibetan plateau is discussed controversially. A comprehensive review on Pleistocene glaciations in the region is presented in Chapter 8 and compiled in figure 1.1).

-----> next page

Figure 1.1: Compilation of paleogeographic and paleoclimatic environmental features and the location of Taiwan in the East Asian and western Pacific region.

Last glacial mountain glaciations are compiled after various sources as given in table 1.1 and discussed in chapter 8. Different interpretations of the extent of the glaciation on the Tibetan plateau are shown according to Ehlers and Gibbard (2004, by using the provided shapefiles). Taiwanese Pleistocene mountain glaciations are: N – Nanhuta Shan, H – Hsueh Shan, Y – Yushan (cf. figure 2.1. for location of the black rectangle). The course of last glacial climatic snowlines is compiled by modification of the snowline maps of Shi (2002) and Ono et al. (2005) as well as by visual interpolation of the ELAs in the glaciated mountain ranges as reported in the respective reference given in table 1.1 (light blue). The dark blue snowlines represent the last glacial snowline course according to this work (Hebenstreit, 2006). Red spots indicate examples of deep sea drilling locations with the derived sea surface temperature decline after Thunnel et al. (1994), WPWP = western Pacific warm pool. Locations of Pleistocene vegetation zones follow Liew et al. (1998), Sun et al. (2000) and Hope et al. (2004). The topography bases on the 1 Arc-Minute global relief model ETOPO (compiled by Amante and Eakins, 2009), WGS 1984. The emerged sea shelves are shown as represented by the present 120 m and 160 m isobaths.

altitude above present sea level (m)

> 5000 | 3000 - 5000 | 2500 - 3000 | 2000 - 2500 | 1500 - 2000 | 1000 - 1500 | 500 - 1000 | 200 - 500 | 100 - 200 | 0 - 100

altitude below present sea level (m)

-120 | -160

3450 Last glacial mountain glaciaton with ELA (m)

Unconfirmed glaciations

Tibetan glaciaton

Tibetan ice sheet (after Kuhle)

Present rivers

Present lakes

1.5 Decline of Pleistocene sea surface temperatures (°C)

3500 Approx. last glacial climatc ELA (after various sources)

3500 Approx. last glacial climatic ELA according to this work (Hebenstreit, 2006)

Table 1.1: Examples of mountain ranges with Pleistocene glaciations in East Asia and the western Pacific region

Pleistocene snowline locality	Montain range	Region	lat (deg)	lon (deg)	Highest altitude (1) (m)	Terminus altitude (m)	lowest reported Pleistocene ELA (m)	Pleistocene ELA method (2)	Modern ELA (m)	Modern ELA Method	ΔELA (m)	References (main sources in bold)
Japan												
Mt. Tottabetsu	Hidaka Range	Hokkaido	42.75	142.70	1960	1175	**1500**	Max. discharge, AAR	2750	climate model	1250	Ono et al. (2005)
Mt. Poroshiri	Hidaka Range	Hokkaido	42.72	142.70	2052	1320	**1575**	Max. discharge, AAR	2680	climate model	1105	Ono et al. (2005)
Mt. Tateyama	Northern Japanese Alps (3)	Honshu	36.57	137.62	2999	2290	**1900**	AAR	2970	climate model	1070	Ono et al. (2005)
Mt. Kasagatake	Northern Japanese Alps (3)	Honshu	36.32	137.57	2860	2400	**2310**	THAR	3620	climate model	1310	Ono et al. (2005)
Mt. Kisokoma	Central Japanese Alps	Honshu	35.78	137.82	2931	2220	**2120**	AAR	3900	climate model	1780	Ono et al. (2005)
Mt. Ainodake	Southern Japanes Alps	Honshu	35.65	138.24	3130	2390	**2600**	AAR	4130	climate model	1530	Ono et al. (2005)
East and central China												
Changbai Shan		NE-China	42.00	128.00	2749	?	**2200**	CF	> 2800	?		**Lehmkuhl and Rost (1993)**, **Shi** (1992, **2002**) (4)
Wutai Shan		Central China	39.08	113.58	3062	1900	**2700**	TSAM, CF	> 3100	?		Lehmkuhl and Rost (1993), Rost (2000) (4)
Helan Shan		Central China	38.83	106.00	3556	2740	**3000**	TSAM, CF	4100	regional correlation	1100	Lehmkuhl and Rost (1993), **Hofmann (1993)**
Taibei Shan	Qingling Shan	Central China	33.95	107.77	3767	2850	**3300**	TSAM	4300	climate model	1000	**Lehmkuhl and Rost (1993), Rost (1994)**, Rost (2000)
Mt. Luoji		S-China	27.55	102.35	4359	?	**3700**	CF?	> 4400	?		**Shi (1992)** (4, 5, 6)
Gongwang Shan		S-China	26.15	102.95	4344	2950	**3650**	TSAM	4700	assumption	1050	**Zhang et al. (2006)** (7)
Diancang Shan	Hengduan Shan	S-China	25.67	100.12	4122	?	**3700**	CF	> 4200	?		Zheng et al. (2002), **Zhang et al. (2006)** (4, 8)
Tibetan plateau margin												
Mt. Xiabaoding	Min Shan	E-Tibet	32.65	103.85	5588	2600	**4000**	TSAM, CF	5000	assumption	1000	Lehmkuhl and Rost (1993), **Hövermann and Lehmkuhl (1994)**, Lehmkuhl et al. (1998) (5, 9)
Gongga Shan		SE-Tibet	29.62	101.90	7514	1750	**4150**	TSAM, CF	4970	TSAM	820	**Hövermann and Lehmkuhl (1994)**, Lehmkuhl et al. (1998), **Owen et al. (2005**) (10)
Yulongxue Shan		SE-Tibet	27.08	100.17	5596	2700	**4150**	TSAM	5000	TSAM	850	**Ives and Zhang (1993)**, Lehmkuhl et al. (1998), Lehmkuhl (1998), Zheng et al. (2002) (11)
Indonesia and Malaysia												
Mt. Kerinci		Sumatera	-1.70	101.27	3805	?	**3450**	?	?	?		Hope (2004)
Mt. Semuru		Java	-8.10	112.92	3676	?	**3450**	?	?	?		Hope (2004)
Mt. Rinjani		Lombok	-8.23	116.47	3726	?	**3450**	?	?	?		Hope (2004)
Mt. Lesuer (12)		Aceh	3.55	97.47	3381	?	**3100**	?	?	?		Hope (2004)
Mt Kinabalu		Borneo	6.08	116.60	4101	3230	**3665**	TSAM	4570	assumption	905	**Porter (2001b)**, Hope (2004) (13)
New Guinea												
Mt. Jaya	Maoke Range	Papua	-4.08	137.17	4884	1700	**3550**	MELM, CF	4580	assumption	1030	Hope et al. (1976), **Petersen et al. (2002**) (14)
Mt. Jaya	Maoke Range	Papua	-4.08	137.07	5000	3545	**3900**	AABR	4650	assumption	750	Prentice et al. (2005)
Mt. Trikora	Maoke Range	Papua	-4.30	138.67	4730	?	**3525**	CF	4580	assumption	1055	Petersen et al. (2002), Prentice et al. (2005) (15)
Mt. Mandala	Snow mountains	Papua	-4.71	140.27	6480	?	**3525**	CF	4580	assumption	1055	Petersen et al. (2002), Prentice et al. (2005) (15)
Mt. Giluwe		PNG	-6.05	143.88	4368	2750	**3500**	THAR, CF	4600	regional correlation	1100	**Löffler (1972),** Porter (2001b), Petersen et al. (2002), Prentice et al. (2005) (16)
Mt. Wilhelm		PNG	-5.79	145.02	4509	3300	**3500**	THAR, CF	4600	regional correlation	1100	**Löffler (1972),** Porter (2001b), Petersen et al. (2002), Prentice et al. (2005) (16)
Mt. Bantega (12)	Saruwaget Mts.	PNG	-6.23	147.10	4121	3300	**3650**	THAR, CF	4600	regional correlation	950	**Löffler (1972),** Porter (2001b), Petersen et al. (2002), Prentice et al. (2005) (16)
Mt. Albert Edward (12)	Owen Stanley Range	PNG	-8.40	147.50	3990	3400	**3600**	THAR, CF	4600	regional correlation	1000	**Löffler (1972),** Porter (2001b), Petersen et al. (2002), Prentice et al. (2005) (16)
Mt. Victoria (12)	Owen Stanley Range	PNG (18)	-8.90	147.53	4036	3200	**3650**	THAR, CF	4600	regional correlation	950	**Löffler (1972),** Porter (2001b), Mark et al. (2005) (17)
Taiwan												
Nanhuta Shan	Backbone Range	Taiwan	24.36	121.44	3742	2250	**2900**	TSAM	3950	climate model	1050	Hebenstreit, 2006
Hsueh Shan	Huseh Shan Range	Taiwan	24.38	121.23	3884	?	**2800**	MELM	3900	climate model	1100	Hebenstreit, 2006
Yushan	Yushan Range	Taiwan	23.47	120.96	3952	?	**< 3400**	TSAM	4000	climate model	> 600	Hebenstreit, 2006

(1) highest summit or headwall
(2) cf. section 3.8 for ELA methods
(3) mts. Yari-Hotaka in NJA reach 3175 m
(4) modern ELA higher than summit
(5) location of summit adapted with Google Earth
(6) ELA not provided in reference, here given as regionial correlation
(7) ELA calculated from map presented in Zhang et al. (2006)
(8) ELA averaged from reported cirque floor altitude in Zhang et al. (2006)
(9) modern ELA estimated after profile in L. et al. (1998)
(10) location and modern ELA after Owen et al. (2005), Pleist. ELA and lowest deposits from H & L (1994) after earlier sources
(11) Pleist. ELA calculated from reported altitudes
(12) not shown in map (fig. 1.1)
(13) data from Porter (2001b) after Koopmans and Stauffer (1967)
(14) location and terminus after Hope et al. (1976), ELAs after Petersen et al. (2002)
(15) location after Prentice et al. (2005), ELA after Petersen et al. (2002)
(16) location after Prentice et al. (2005), ELA after Löffler (1972), termini based on the maps and table of Löffler (1972)
(17) location after Mark et al. (2005), ELA and termini after Löffler (1972)
(18) PNG = Papua New Guinea

CHAPTER 2

The study area

2.1 Geographical units, topography and altitudinal zonation of Taiwan and the location of the study areas

Taiwan is a subtropical mountain island, situated in the western Pacific Ocean between the East China Sea (ECS) located in the north and the South China Sea (SCS) in the south. It is separated from the Chinese mainland by the Taiwan Strait. The island was discovered by Portuguese seafarers and named *„Ilha formosa"* – beautiful island.

The main island[12] (Taiwan proper) is located between 21° 53' 50" and 25° 18' 20" N latitude and between 120° 01' 00" and 121° 59' 15" E longitude. Its territory and the 85 offshore islands comprise around 36,000 km^2. One third of Taiwan proper is composed of alluvial coastal plains with altitudes below 100 m, which are mainly located in the western part of the island. Another third is build up of the so called western foothills and tablelands between 100 m and 1000 m altitude. The remaining third resembles high mountain area above 1000 m, referred to in a broader sense as the Central Mountain Range (CMR), which occupies the eastern part of the island at a length of 330 km and a width of 80 km (GIO, 2010).

There are 200 summits (GIO, 2010) or 20 massifs with 62 summits (Porter, 2001b) over 3000 m in Taiwan, depending on the category as a single summit. The topography of the CMR is characterized by extraordinary step relief with deep incised valleys and enormous relief energy at short distances (cf. section 2.3).

According to its altitude, relief and climatic hypsometrical zonation the CMR can be classified as "high mountains" (Böse, 2006) following the definition of Troll (1973). Fluvial processes causing effective backward erosion are dominant in altitudes up to *c.* 3000 - 3500 m, followed by a zone with weak geomorphological activity. The periglacial belt is limited to altitudes above 3600 - 3700 m (Klose, 2006).

[12] Except as noted otherwise, only the main island is referred to in this text in the following.

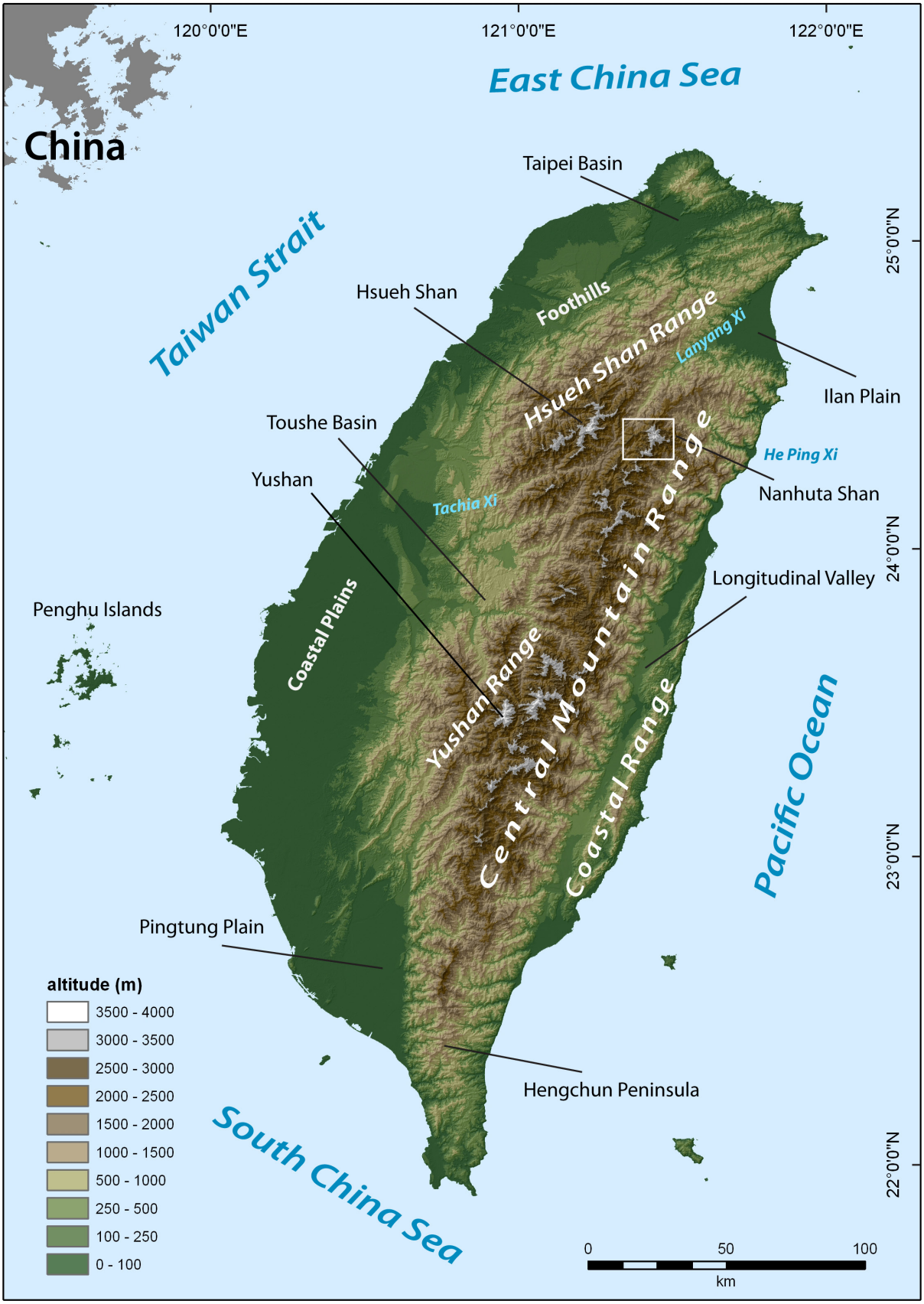

Figure 2.1: Topography, main geographical units of Taiwan and location of the study areas; information from GIO (2010). White rectangle shows the location of fig. 2.2. Map based on 90-m-resolution digital elevation model (DEM) derived from hole-filled seamless SRTM data, processed by Jarvis et al. (2006), UTM, WGS 1984.

The vegetation is characterized by lowland, sub-montane and montane evergreen broad-leaved forest in altitudinal zones up to 2500 m, followed by an upper montane and a sub-alpine coniferous forest locally up to 3600 m and finally alpine vegetation with some Juniperus (Liew et al., 2006a). The timberline is at about 3300 - 3500 m, depending on local climatic differences (Klose, 2006; Liew et al., 2006a).

The Central Mountain Range in a closer sense (Zhongyang Shanmai), also referred to as the backbone range, resembles the main water divide of the island as it spans longitudinal almost along the entire island. The main study area of this project, the Nanhuta Shan (3742 m), is located at the north-eastern edge of this mountain chain. This study covers an area of about 15 x 10 km in the central part of the Nanhuta Shan massif including parts of the west oriented valley Nanhu Xi[13] at *c*. 121° 21' - 121° 29' E and 24° 20' - 24° 25' N (fig. 2.2).

The topography of the central Nanhuta Shan is rather individual. Two parallel, north-south striking high valleys, named here the Upper (eastern) and the Lower (western) Valley resemble two widened basins with bottoms at 3420 m and 3375 m, respectively. A rock ridge named the "valley divide" separates the basins. They are surrounded by four summits and bounded by a sharp crest to the east. Both have a small tributary from the north and thus share a common outflow orthogonal to the west into the Nanhu Xi (fig. 2.2, cf. also figure 1 in chapter 4 and geomorphological maps in chapters 4 and 6). Their southern source is a several-hundred-square-meters wide flat area east of the Main Peak with an elevation of about 3550 m, which is called the "saddle" or the "plateau". Beside these two valleys the saddle represents the source of two additional valleys, the steep south trending Tao-Sai Xi and the south-east trending He Ping Nan Xi, of which the latter has a nearly flat section at about 3200 m. The massif is additionally eroded from the north by the steep He Ping Bei Xi and drained entirely in a more or less radial way.

Except the Nanhu Xi, whose discharge results via the Tachia Xi to the Taiwan Strait, the drainage from all other slopes and valleys results to the Pacific Ocean via various rivers. The He Ping Bei Xi and the He Ping Nan Xi combine with the discharge from the eastern slope to the river He Ping Xi. The drainage of the north-eastern slope results via the Lanyang Xi valley also to the Pacific Ocean. The Nanhuta Shan therefore represents a section of the main water divide of the island.

[13] Xi = Chinese for creek or river

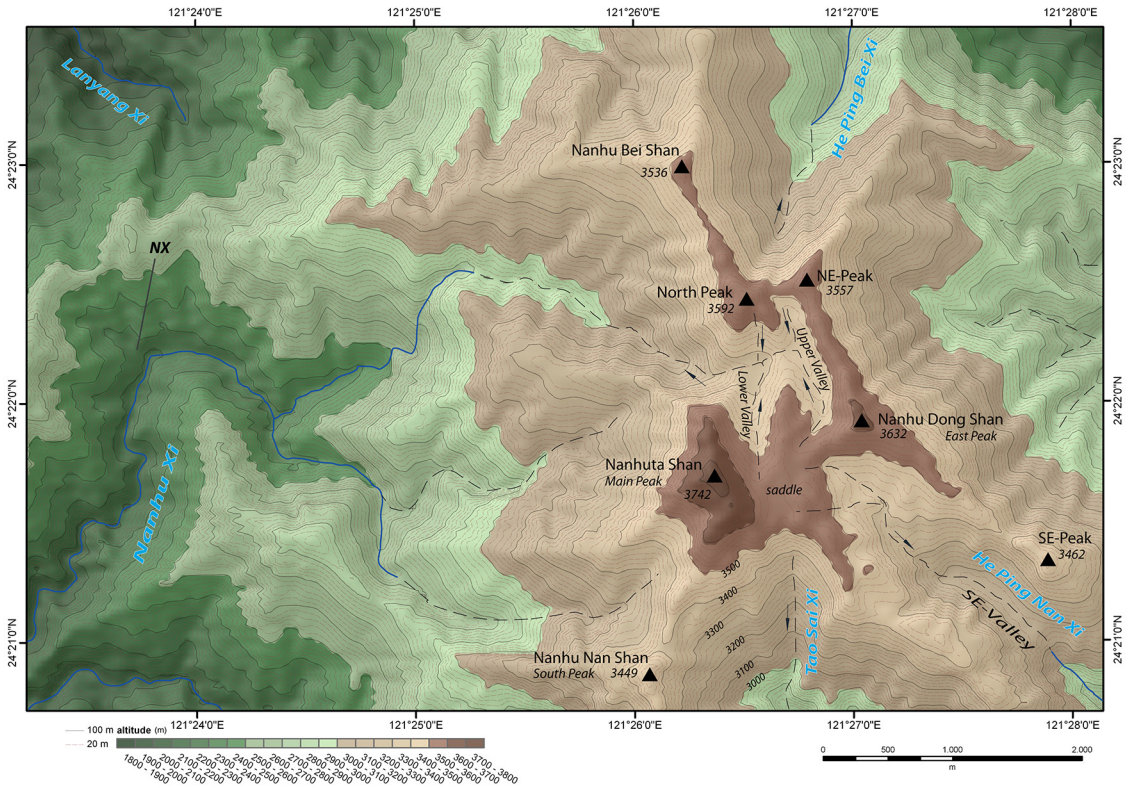

Figure 2.2: Topography of the central Nanhuta Shan, map based on a 40-m-resolution DEM, derived from stereoscopic air photo data, kindly provided by the National Taiwan University. For location *NX* cf. publication 1.

The two additional study areas Yushan[14] (Jade Mountains, Mt. Morrison) and the Hsueh Shan (Snow Mountains, Mt. Sylvia) are located in mountain ranges of the same name, which are located west and north-west of the central range, respectively. Both massifs discharge to the Taiwan Strait, except the very northern slope of Hsueh Shan. The Yushan (3952 m) - directly located at the tropic of cancer - is the highest elevation of Taiwan and in whole East Asia (GIO, 2010). Here, two valleys were studied, the west trending valley Qi Shan Xi and the northeast trending valley Laonong Xi including the pass Ba Tong Guan as well as the summit itself. The study area in Hsueh Shan is limited to the Main Peak (3886 m) and the northeast trending valley of the Chichiawan river (Qijiawan Xi) down to an altitude of *c*. 3000 m.

[14] Depending on the reference the spelling is *Yu Shan* or *Yushan*

2.2 Short outline of the present climate in Taiwan and the regional atmospheric circulation

2.2.1 Circulation and air masses

The atmospheric circulation in the Asian-Pacific region is composed of a number of components, which strongly control the climate in the region including Taiwan (Barry and Chorley, 1992). These atmospheric factors are complemented by the influence of the western Pacific warm pool and the associated warm Kuroshio current (Oba et al., 2009). The most striking factor is the East Asian monsoon system, which is traditionally attributed to seasonally alternating pressure systems over the Asian continent and the northern Pacific Ocean.

During the winter, a strong anticyclone is established over mid-Siberia and Mongolia counterparted by a strong cyclone centred over the Aleutian Islands. The resulting pressure gradient produces strong persistent winds from northerly directions, which bring dry continental and cold polar air masses into the region. They are commonly known as the East Asian “winter monsoon” (EAWM). On their way south they can be warmed and partly moistened as they reach the southern part of East Asia and Taiwan (Boyle and Chen, 1987; Domrös and Peng, 1988).

In summer, the pressure gradient is to the opposite direction, but weaker than in winter. A strong cyclone is located over the north-western Indian-Pakistan subcontinent accompanied by the dynamic Pacific high pressure anticyclone. As a result, warm and moist subtropical Pacific air masses and cross-equatorial tropical air masses stream into the region from southern directions, commonly called the East Asian “summer monsoon” (EASM). The influence of the tropical air is also forced by the Australian anticyclone during the (southern) winter. Therefore the summer monsoon in Southeast Asia is regarded to be composed of two branches: the tropical SW monsoon and the subtropical SE monsoon (Tao and Chen, 1987; Domrös and Peng, 1988).

Despite interannual variations, the average duration of both seasons is about 5 month in southern China and Taiwan. Due to the southern location, here, the onset of the winter monsoon takes place relatively late in early October. In contrast, the summer monsoon reaches the island initially already in early May (Tao and Chen, 1987; Kerns et al., 2010). The interannual variations in the duration and intensity of the East Asian monsoon are

associated with the El Niño Southern Oscillation (ENSO) as both systems are linked over the Australian monsoon system (Wang and Li, 2004).

Since the monsoon is a relatively shallow circulation system (Chan and Li, 2004), it decreases in altitudes above 2000 m and the westerly circulation keeps the prevailing influence (Domrös and Peng, 1988). Furthermore, it has been argued that the traditional model of the Asian monsoon (see above) as a reaction on thermal pressure systems does not adequately explain the working of this system. It rather constitutes the interaction of planetary and regional factors of the surface and the upper troposphere (Barry and Chorley, 1992). As the Tibetan plateau acts as an obstacle for the westerly jets, the wind splits into a northern and a southern branch during the winter and reunites over East Asia in the Tibetan lee convergence zone, which is associated with effective precipitation. (Murakami, 1987; Barry and Chorley, 1992; Benn and Owen, 1998; Ono and Irino, 2004).

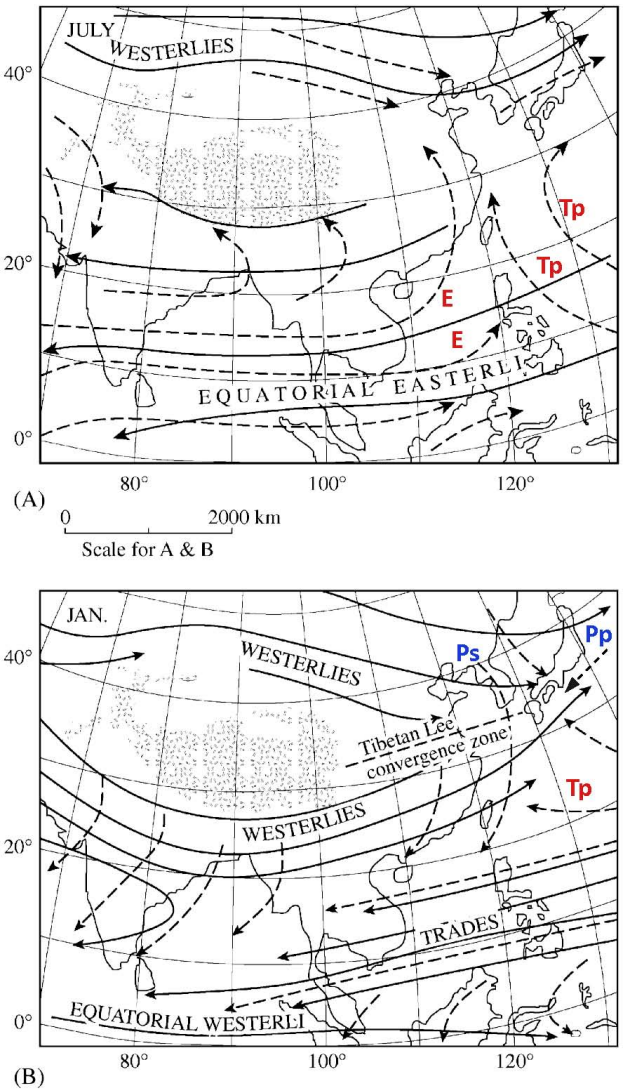

Figure 2.3: General circulation and dominating air masses in the Asian-Pacific region A) during summer and B) during winter. Solid lines indicate airflow at about 6000 m in (A) and 3000 m in (B), the dashed lines indicate aiflow at about 600 m (from Barry and Chorley, 1992; here modified after Owen and Benn, 2005). Air masses: Ps – polar Siberian, Pp – polar Pacific, Tp – tropical Pacific, E – equatorial, after Domrös and Peng (1988).

During the transition from the winter to the summer monsoon the northward migration of the polar front belt results in disturbances of the westerly circulation at the lee side of the Tibetan plateau (Tao and Chen, 1987; Wang and Li, 2004). These frontal disturbances are called Mei-Yu fronts, which are associated with heavy rainfalls that are known as the “plum

rains" in the Yangtze area and which are also responsible for the early summer rainy season in Taiwan during mid of May to mid June (Chen and Chen, 2003). Flohn (1957) showed that in summer the westerly circulation is an important source of moist over East Asia with a water vapour transport from the continent to the ocean. (For seasonal variations of the circulation over Taiwan see also Chen and Chen (2003)).

2.2.2 Precipitation

The existence and extent of glaciers depends crucially on the available amount and temporal distribution of precipitation. In Taiwan, precipitation data is derived from 25 conventional stations and 249 stations of an Automatic Rainfall and Meteorological Telemetry System (ARMTS) installed by the Central Weather Bureau (CWB) of Taiwan (Chen and Chen, 2003; Kerns et al., 2010). The annual mean precipitation amount over entire Taiwan is about 2500 mm but local means in Taiwan proper vary from 1347.7 mm in Wuqi (west coast) to 4863.1 mm in Anbu (Datun mountains) near the north coast (GIO, 2010; Central Weather Bureau, 2011) (fig. 2.5, appendix table A2).

Five sources for precipitation in the Taiwanese mountains can be summarised depending on the seasonal change of the prevailing air mass influence (Chen and Chen, 2003): (1) the monsoons, (2) the subtropical westerlies with (3) the passage of the tropic front (Mei-Yu), (4) tropical cyclones (typhoons), and (5) local convection. The monsoonal winter rainfalls are lighter and temporal more evenly distributed due to a higher stability of the atmosphere, while the summer rainfalls are caused by instable air masses resulting in heavy convective precipitation events. The two periods in southern China and Taiwan with the heaviest rainy events occur therefore in early summer (June) and mid/ late summer (August-September), caused by the passage of the Mei-Yu front and the influence of typhoons, respectively (Domrös and Peng, 1988).

The central mountain range influences the spatial distribution of the precipitation pattern during the seasons considerably as it acts as a barrier for air masses. Much higher rainfall occurs at the windward side of the respective air flow direction (Chen and Chen, 2003). This causes the relatively dry winter season in the southern part of Taiwan with a clear precipitation minimum, while the EAWM brings abundant rainfall in the northern and north-eastern part of the island (fig. 2.5) after warming and moistening over the China Seas and the Pacific (Domrös and Peng, 1988; Ono and Irino, 2004).

Figure 2.4: Three stories of air masses and clouds in the mountains of Taiwan, Nanhuta Shan, west ridge, *c.* 24° 22.5' N, 121° 23.5' E, 3000 m, facing NW. 17.10.2000. Lower level: Clouds of the beginning winter monsoon fill the Lanyang valley from the north. Middle level: Cumulus clouds from local convective systems, Upper level: alto-stratus clouds represent the westerly circulation.

Typhoons (tropical cyclones) hit the island frequently by an average of 3.7 events per year (Wu and Kuo, 1999). They produce the most effective precipitation rates on a short time scale with a high destructive potential. Typhoon “Herb”, for example, dumped heavy precipitation at the rate of 1748 mm in one day between 31 July and 1 August 1996 and caused severe damage in central Taiwan (Wu and Kuo, 1999; Chen, 2006).

The fact that the shallow monsoon circulation effects the higher parts of the mountains much reduced leads to the assumption that the precipitation decreases in altitudes above 3000 m (Böse, 2006). This idea is supported by the recorded precipitation data at mountain stations in Taiwan (fig. 2.6), which shows a slight decrease with altitude. However, there are only two official stations with continuous cumulative record and two available short time datasets (including our own measurements, cf. section 3.5.2) above 2000 m. Furthermore, orographic effects can lead to significant local variations in the productivity of rainfall events (Chen et al., 2005a). The mountainous terrain can affect the formation of non-frontal local convective precipitation systems as thermal forces influence the circulation in the mountains

(Jou, 1994; Lin and Chen, 2002) (fig. 2.4). A generalized horizontal and vertical distribution pattern for the annual precipitation in the central mountain range is therefore hard to establish. Nevertheless, all mountain stations show a clear winter minimum in the precipitation record, which implies that summer precipitation (monsoon, Mei-Yu and typhoons) contributes most to the annual total amount.

Only few data is available about snowfall and the duration of snow cover in the Taiwanese mountains. Observations from Yushan National Park show, that precipitation falls as snow above 2000 m usually from December to February and the snow cover can reach thicknesses well over 1 m and lasts until March in altitudes above 3500 m. This coincides with the occurrence of frost days (= T_{min} < 0 °C/ day), which are dominant in Yushan from December to March (Klose, 2007). Interpreting the circulation map of Barry and Chorley (1992), it has been suggested that the EAWM supplies the snow to the high mountain range of Taiwan like in Japan (Ono and Irino, 2004). However, the precipitation winter minimum in the central mountain range suggests a limited influence of the EAWM, which seems to be effective only in the northernmost coastal mountains of Taiwan. This should be due to the stable nature of this air mass with the tendency to sink. Therefore it can be assumed, that precipitation derived from disturbances in the subtropical westerlies contribute to snowfall in the Taiwanese mountains as it is the case for the Himalayas (Benn and Owen, 1998). The Taiwanese high mountain range is not glaciated at present. Considerations about the theoretical modern snowline are made in section 3.8.3 and publication 1, chapter 6.

-----> next page

Figure 2.5: Climate diagrams and respective locations of 21 lowland meteorological stations run by the Central Weather Bureau of Taiwan (blue). Green: locations of three highland met-stations of the CWB above 1000 m (SM – Sun-Moon-Lake, A – Alishan, Y – Yushan). Orange: mountain stations Nanhuta Shan (N) and Shaofenko (S). Cf. fig. 2.6 for diagrams and appendix table A2 for data.

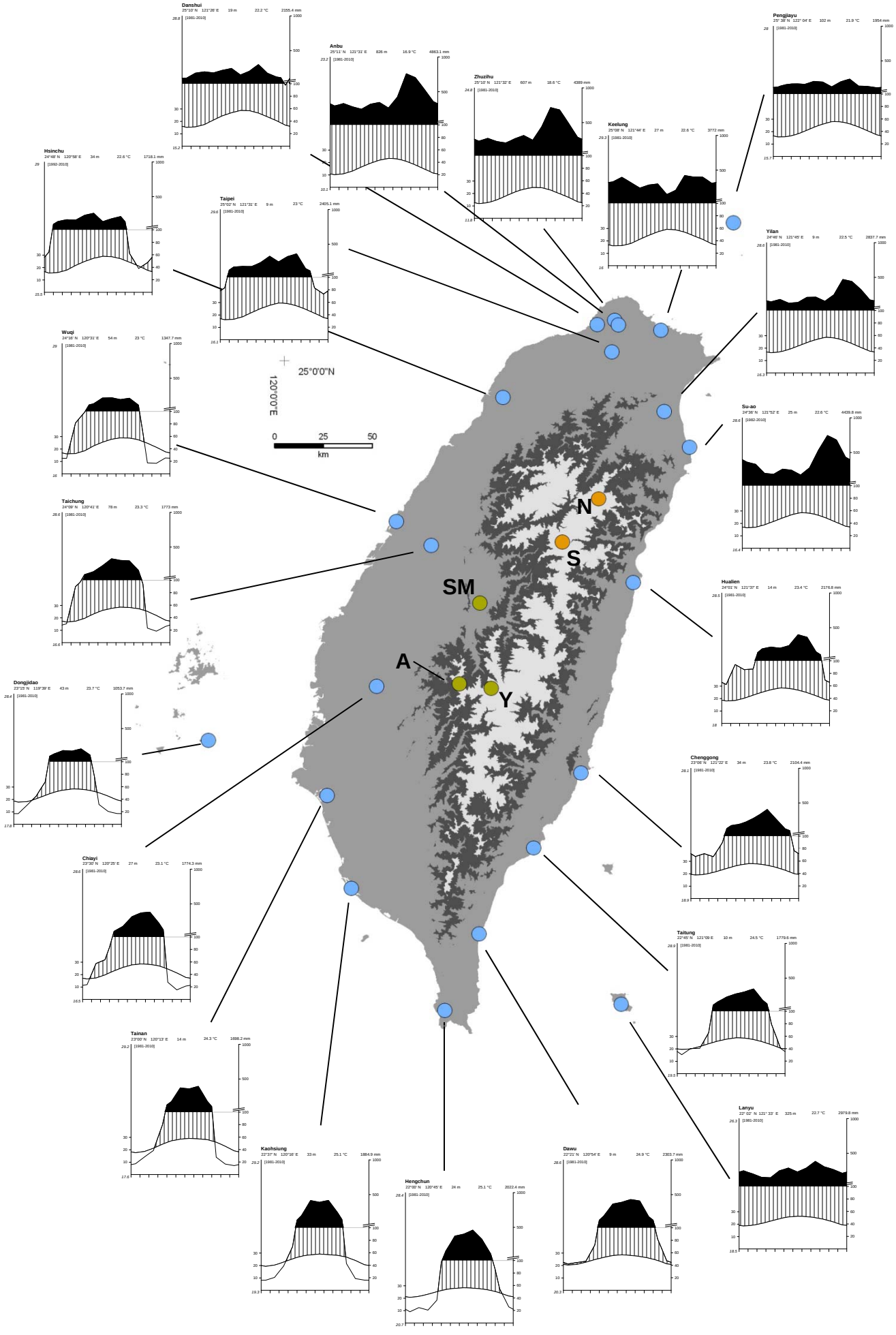
Danshui
Anbu
Zhuzihu
Pengjiayu
Keelung
Hsinchu
Taipei
Yilan
Wuqi
25°0'0"N
120°0'0"E
0
25
50
km
N
S
SM
A
Y
Su-ao
Taichung
Hualien
Donggidao
Chenggong
Chiayi
Taitung
Tainan
Kaohsiung
Hengchun
Dawu
Lanyu

2.2.3 Temperature

The temperature regime in Taiwan is rather balanced and the thermal seasonality is weak, which is partly caused by the maritime influence of the warm Kuroshio current. In the north, monthly means at sea level vary from 16 °C in January to 29 °C in July. The variation is somewhat less in the south with winter temperatures of 19/ 20 °C and summer temperatures of also 29 °C (fig. 2.5).

Mountain temperatures decrease with altitude but the data available from three stations of the CWB and from our own measurements in Nanhuta Shan exhibit an annual range of the monthly means of only about 9/ 10 °C (fig. 2.6).

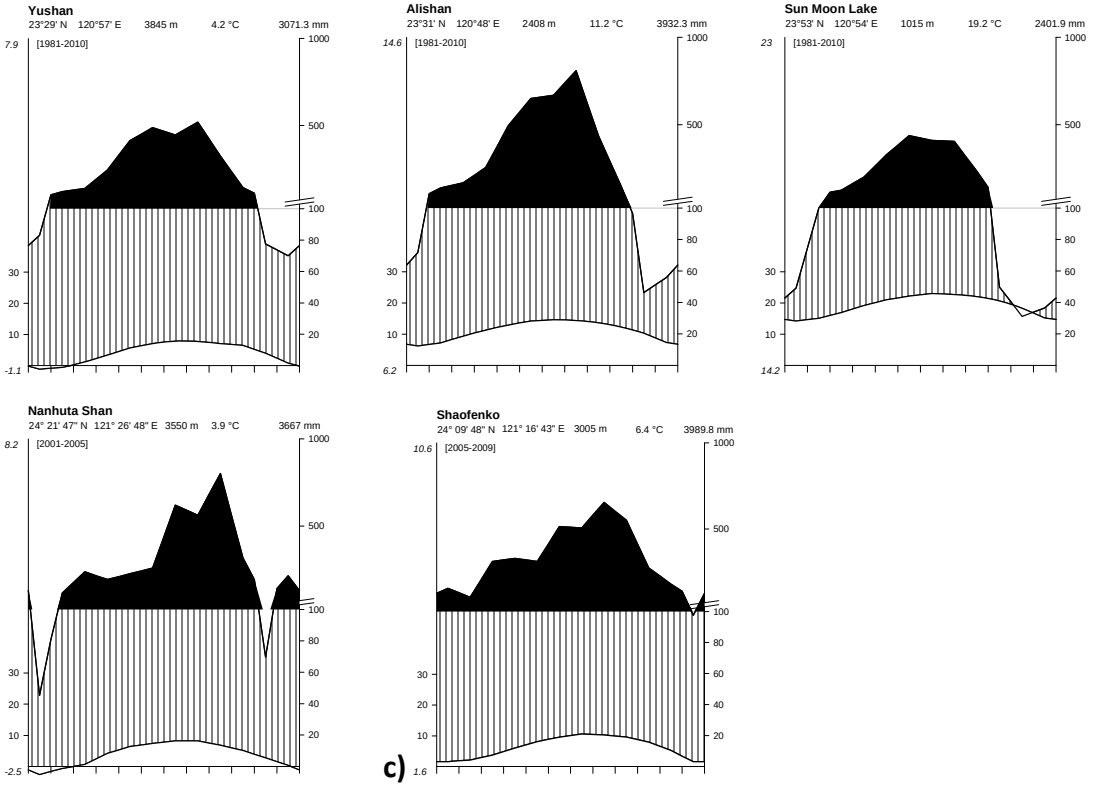

Figure 2.6: Climate diagrams of five highland and mountain stations above 1000 m. a) stations run by the Central Weather Bureau, b) our station, c) station run by Endemic Species Research Institute, Council of Agriculture. See figure 2.5 for location of the stations and appendix table A2 for data.

The climate of China and Taiwan has been subject to a variety of classifications. Most of them define the northern part of Taiwan as a humid subtropical climate and the southernmost part of the island – despite the dry winter season – as a humid peripheral tropical climate (Tietze and Domrös, 1987; Domrös and Peng, 1988).

2.2.4 Characteristics of annual and diurnal variations of air temperature in Nanhuta Shan

A four-year dataset on air temperature variation is available from Nanhuta Shan in northern Taiwan (Klose, 2007). Although the short measurement period does not allow interpretations in a climatological sense, the dataset exhibits some specific characteristics (fig. 2.7): The annual variation of the air temperature runs rather uniformly. None of the four years measured differs significantly from the others in the annual variation of the monthly means. Characteristically, the summers are thermally balanced, i.e. the temperature difference between the summer months is small, whereas the monthly means decrease rapidly in winter and rise likewise in spring. The annual mean is 3.9 °C. July and August are the warmest month each with 8.2 °C mean. The coldest month is January with -2.5 °C mean. The annual range is therefore 10.7 °C. The curve shows in total a weak decreasing trend, though it has no climatic significance, due to the short measured period.

The hourly and diurnal temperature variations exhibit a larger scatter in winter than in summer. However, both curves match in winter, which means that the temperature differences are between the individual days, while in summer the diurnal means compensate the hourly means, i.e. the temperature variations run within the individual days.

The highest and lowest diurnal means were found at 11.7 °C and -10.7 °C, respectively. The highest absolute temperature measured in the four year period was 16.1 °C and the lowest -13.8 °C. The mean diurnal range is 4.5 °C. The monthly means of the diurnal ranges are somewhat larger in late summer (5.4 °C) than in late winter (4.2 °C). Frost days (days with minimum temperature < 0 °C) occur regularly from November to early April.

The maximum diurnal ranges of individual days are found in March (9.8 °C). They coincide with strong frost nights, which occur annually in early March for a number of days. They might be related to cold surges, which are typical in eastern Asia (Boyle and Chen, 1987).

The graph exhibits also some distinctive singular features. October 2002, July 2004 and March 2005 were unusually cool. The largest temperature drop within a few days happened around New Year 2004/2005 with 15 °C in the diurnal mean. In October 2003, some days were exceptional warm. (cf. fig. 2.7 for the graph and Klose, 2006, 2007, for more discussion).

------> next page

Figure 2.7: Four-year air temperature variations in Nanhuta Shan. For interpretation cf. section 2.2.4

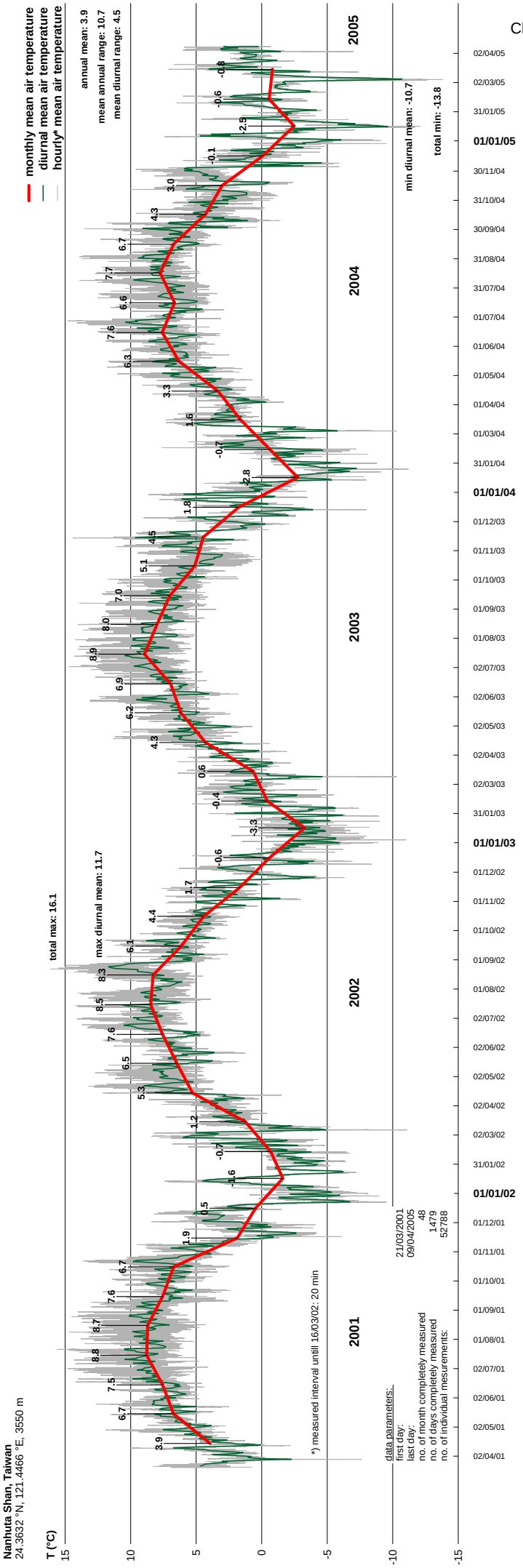

Nanhuta Shan, Taiwan
24.3632 °N, 121.4466 °E, 3550 m

2.3 Geologic-tectonical setting and morphodynamics in the Taiwanese orogen

2.3.1 Plate tectonics and geological provinces

The tectonic evolution of Taiwan is intensively studied and, although partly controversially discussed, usually taken as an ideal locality to investigate orogenic processes resulting in a vast number of publications (Byrne and Liu, 2002).

The island of Taiwan represents the subaerial part of an active thrust belt, which results from an oblique arc-continent collision between the Luzon island arc of the Philippine Sea Plate and the passive margin of the continental Eurasian Plate, of which the latter one is subducing eastward under the first along the Manila trench (Suppe, 1981; Ho, 1986; Teng, 1990; Chemenda et al., 2001; Lallemand et al., 2001). A second arc-trench system with opposite subduction polarity coexists northeast of the island, where the Ryukyu arc is created by northward underplating the Philippine Sea Plate under the Eurasian Plate combined with the widening of the Okinawa Trough and causing extension in the north-eastern part of Taiwan (Suppe, 1984; Teng, 1996; Hu et al., 2002; Hou et al., 2009). The Philippine Sea Plate is moving northwestward at approximately 70 km/ Ma performing an instantaneous clockwise rotation (Seno, 1977). GPS measurements indicate a current velocity of about 8 cm/ a (Yu et al., 1997).

The timing of the plate collision and therefore the beginning of the Cenozoic orogeny in Taiwan is not well determined yet. Radiometric data indicates, that the onset of the orogeny was at about 10 - 12 Ma, but the relevant collision may have begun at 5 Ma (e.g. Teng, 1990; summarised by Sibuet and Hsu, 2004). However, it started initially at the northern end of the island and propagates southward at about 90 km/ Ma due to the obliquity of both, the plate motion and the continent margin in relation to the deformation front (Suppe, 1984; Malavieille et al., 2002). During the collision, several hundred kilometres of crustal shortening were accomplished (Lin, 2000b; Sibuet and Hsu, 2004) resulting in the accretion of the sedimentary cover of the Chinese continental margin, which was partly metamorphosed, uplifted and exhumed (Byrne and Liu, 2002).

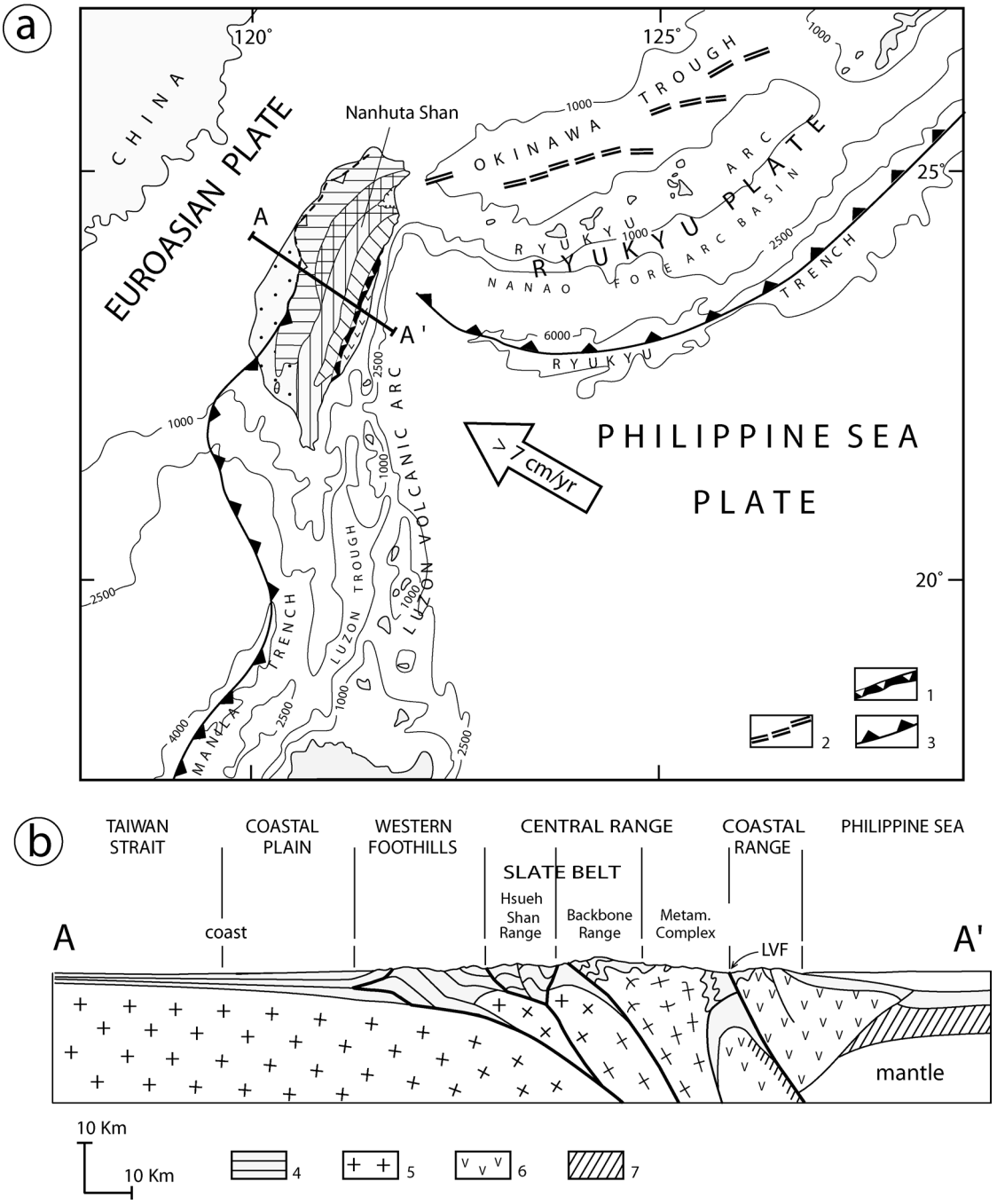

Figure 2.8: (a) Geodynamic setting of the Luzon–Taiwan–Ryukyu region (b) Geological cross-section AA' through central Taiwan (compiled and modified after various sources, here cited and modified after Chemenda et al. (2001). 1 - Longitudinal Valley with Longitudinal Valley Fault (LVF); 2 - axis of the Okinawa rift; 3 - subduction zone; 4 - sedimentary cover; 5 - continental crust; 6 - volcanic arc; 7 - oceanic crust; blank (cross-section), mantle. See figure 2.9 (b) for geological provinces.

Taiwan is divided into the following geological provinces, which are oriented more or less perpendicular to the convergence direction (Ho, 1986; Teng, 1990; Byrne and Liu, 2002). The Coastal Range is interpreted to represent the accreted northern extension of the Neogene

Luzon volcanic arc and the fore-arc basin of the North Luzon Trough and consists mainly of Miocene andesitic volcanic units. The eastern flank of the Central Range is composed of pre-Tertiary (Palaeozoic to Mesozoic) continental metamorphic basement, the so called Tananao schist complex and represents the oldest litho-tectonic unit in Taiwan. The central slate belt is composed of Eocene to Miocene shallow marine sediments, whose age and metamorphic grade decrease generally from East to West (Lee et al., 1997). It is divided into the so called Backbone Range, dominated by slate and phyllite and the Hsueh Shan Range, which is made up mostly of carbonaceous sandstones.

The Western Foothills represent the actively deforming fold-and-thrust belt comprised of Upper Oligocene to Pleistocene shallow marine and shelf units. The Coastal Plains are often not taken as an individual geological province since they are made up of young (Quaternary and modern) alluvium and clastic deposits from the interior mountain ranges (cf. fig. 2.9b).

2.3.2 Geologic setting in the Nanhuta Shan massif

The main study area in this work, the central Nanhuta Shan massif, is situated in the Eo-Oligocene Pilushan formation and only its north-western part belongs to the Miocene Lushan formation. Both are part of the northern Backbone Range, which is the least known geologic terrain in Taiwan, because of its bad accessibility. Unfortunately, the respective sheet of the geological map (1: 250,000) of this region is not yet published. Thus, only few geological information about the Nanhuta Shan is available (Chu, 1987) and had to be complemented by own observations (cf. section 3.5.3).

The Pilushan formation is mainly composed of slate and phyllite with alternating interbeds of quartzitic sandstone (meta-sandstone). In the south-eastern part, conglomerate and minor metamorphic crystalline limestone are also exposed (fig. 2.9). The local cleavage strike is 25 – 82 degree northeast with a dip of 20 – 80 degree to southeast.

--- > next page

Figure 2.9: Geological sketch map of central Nanhuta Shan. Information is derived from air photo interpretation, own field observations and personal communication with Dr. Hao-Tsu Chu as well as from Chu (1987). Contours base on topographical map 1:50,000. b) Simplified geological map of Taiwan basing on the Geological Map of Taiwan 1:500,000 (Wang and Lee, 2000), geological provinces after Ho (1986): CP – Coastal Plain, WF – Western Foothills, HSR – Hsueh Shan Range, BR – Backbone Range (Lu – Lushan Formation, Pi – Pilushan Formation), ECR – Eastern Central Range, Metamorphic Complex (= Tananao Schist), CR – Coastal Range, V – Quaternary volcanics.

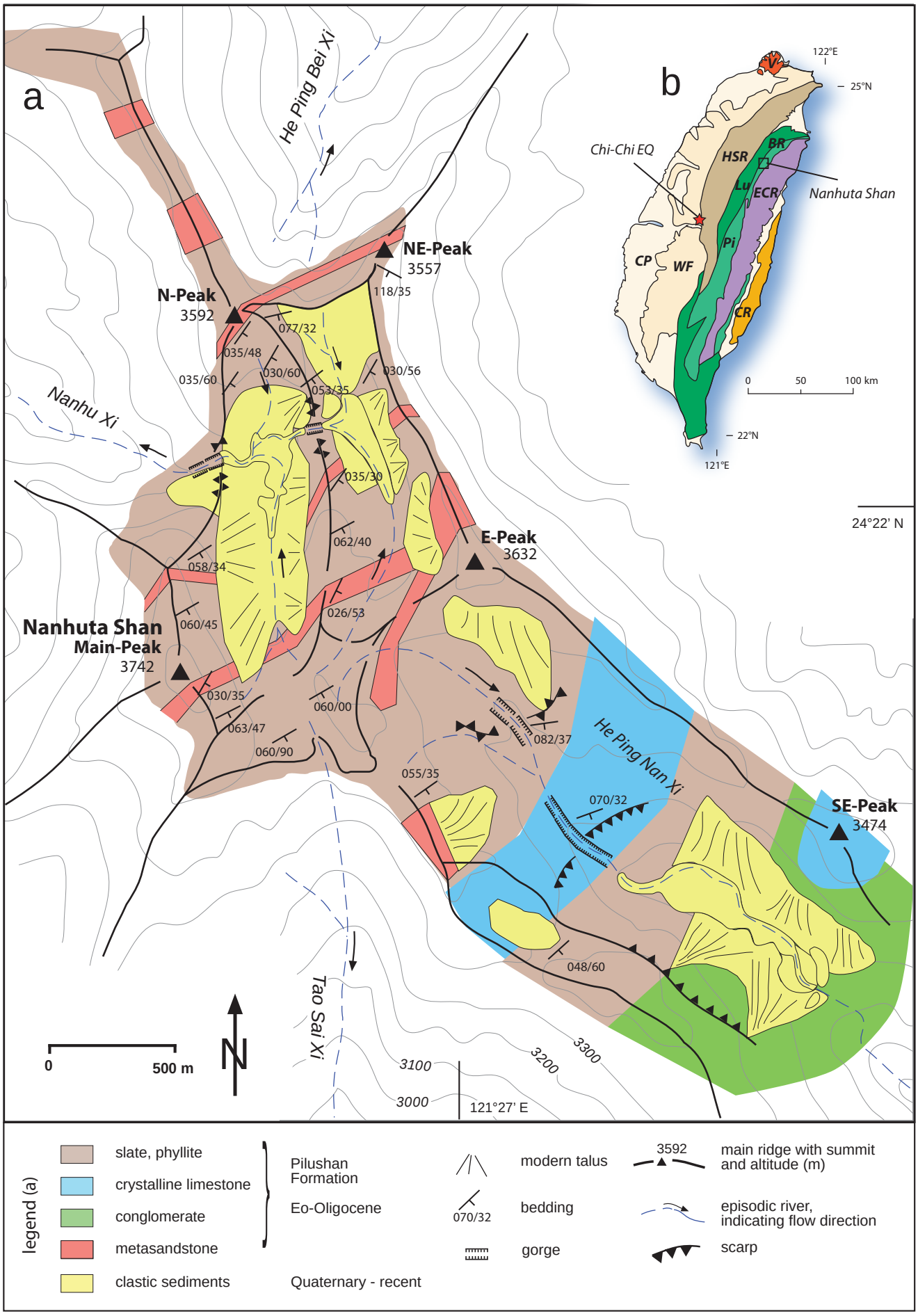
a
He Ping Bei Xi
NE-Peak
3557
118/35
N-Peak
3592
077/32
035/48
035/60
030/60
053/35
030/56
Nanhu Xi
035/30
062/40
E-Peak
3632
058/34
026/53
Nanhuta Shan
Main-Peak
3742
060/45
030/35
063/47
060/90
060/00
082/37
He Ping Nan Xi
055/35
070/32
SE-Peak
3474
048/60
Tao Sai Xi
3100
3000
3200
3300
121°27' E
24°22' N
0
500 m
b
122°E
25°N
22°N
121°E
Chi-Chi EQ
HSR
BR
Lu
ECR
Pi
CP
WF
CR
Nanhuta Shan
0
50
100 km
legend (a)
slate, phyllite
crystalline limestone
conglomerate
metasandstone
clastic sediments
Pilushan Formation
Eo-Oligocene
Quaternary - recent
modern talus
070/32
bedding
gorge
3592
main ridge with summit and altitude (m)
episodic river, indicating flow direction
scarp

2.3.3 Seismicity

As a result of the active tectonic movement, thousands of earthquakes occur in Taiwan each year with a distribution that mainly outlines the subducting crust slabs to a depth of 300 km (Lin, 2000a; Lin et al., 2010). The number of earthquakes with magnitudes (M_w) higher than 3 is about 1500 ($M_w > 3$), 220 ($M_w > 4$), 24 ($M_w > 5$) and 1.3 ($M_w > 6$) per year (Wang and Shin, 1998).

The most damaging earthquake in the younger history was the $M_w = 7.6$ Chi-Chi earthquake at September 21st 1999 killing approximately 2300 people. The co-seismic surface displacement during this event was up to 11.1 m horizontally and 7.5 m vertically (Lin et al., 2001), which implies a considerable contribution of surface ruptures to the topographic evolution of Taiwan (Chen et al., 2002).

2.3.4 Mountain uplift

Uplift rates in Taiwan are high in comparison with those elsewhere in the world (Lin, 1998; Lin, 2000b). However, reported uplift rates vary considerably depending on the respective geological time interval, the object of reconstruction, the dating method used and the location. Thus, they are not necessarily directly comparable.

Most records are available from coastal and lowland areas for a Holocene time period usually derived from uplifted shorelines and marine sediments. The eastern coast of Taiwan at the Coastal Range is the best studied area. Uplift rates reach 10 mm/ a in the southern part and decrease to less than 4 mm/ a in the northern Coastal Range (Hsieh et al., 2004), while the Ilan Plain is subject to subsiding at 6 - 10 mm/ a (Liew et al., 2004).

Holocene uplift rates at the Northern coast range between 2 and 5 mm/ a (Peng et al., 1977; Liew et al., 2004). Reported uplift rates for western and southern Taiwan are somewhat inconsistent. However, they are minor compared with the Coastal Range in east Taiwan. They reach 5 mm/ a in the Hengchun foothill area, while plains generally tend to subside (Liew et al., 2004).

Records from the Central Mountain Range are rare. Long-term uplift rates are derived from mineral cooling rates and fission track dating (Liu, 1982; Liu et al., 2001; Lee et al., 2006), suggesting to be in an order of magnitude of < 1 to 3 mm/ a for a Pliocene and early Pleistocene time range and 4 - 10 mm/ a for the last one million years. Recent geodetic measure-

ments yielded rates of 36 - 42 mm/ a (Liu, 1995). Information on late Pleistocene and Holocene uplift rates from the Central Range is completely lacking. Since most of the studied thrust and fold areas in coastal and lowland areas in Taiwan show uplift rates of 5 - 10 mm/ a, rates around 5 mm/ a are reasonable for the Central Range as well, as it is generally assumed in the literature (Lundberg and Dorsey, 1990).

Overall, it is assumed that the uplift of the Taiwanese orogene started around 5 million years ago (Sibuet and Hsu, 2004) with less than one millimetre per year in the Pliocene and accelerated dramatically up to several millimetres per year during the Pleistocene (Lin and Roecker, 1998; Lin, 2000b). Table 2.1 shows a selection of published uplifted rates in Taiwan, cf. also chapter 5 (= publication 2, there section 3.2).

2.3.5 Present morphodynamics and erosion in the Taiwanese mountain belt

Being one of the youngest orogenies in the world, the Taiwanese mountain belt is still subject to an actively growing and developing topography as a result of the intense interaction between mountain building and denudation determined by the tectonic dynamics of the island under the influence of the wet and stormy climate in the monsoonal-subtropical typhoon belt. It is characterized by the presence of extraordinarily active morphodynamic processes in a steep high-altitude relief with short-distant discharge (Lin, 2000b; Sibuet and Hsu, 2004). These processes are mainly triggered by the high seismicity and the availability of large scale precipitation events (typhoons), which both easily mobilize the weakly metamorphosed rock (Chang et al., 2007).

Modern erosion rates in Taiwan are among the highest worldwide and reach 2.2 – 8.3 mm/ a in the Eastern Central Range (Fuller et al., 2003) and 5.2 mm/ a averaged for entire Taiwan (Dadson et al., 2003) based on river sediment load measurements. The sediment flux into the surrounding seas is about 300 - 500 Mt/ a (Dadson et al., 2003; Liu et al., 2008), most of it delivered as hyperpycnal concentrations during typhoon events; for example the Choshui river (W-Taiwan) discharged 72 Mt of sediment[15] during typhoon Mindulle in early July 2004 (Milliman et al., 2007). Long-term erosion rates obtained from fission track thermochronometry range from 2.3 to 6 mm/ a (Dadson et al., 2003; Fuller et al., 2006), but in situ pro-

[15] For comparison, the annual average discharge of river Danube is about 52 Mt/ a (Giosan et al., 1999) and 500 Mt/ a of Yangtze river (Liu et al., 2009).

duced cosmogenic ^{10}Be concentrations in river-borne sands yielded only 2 mm/ a (Siame et al., 2011).

Linear incision rates vary considerably depending on the method of their determination and the time period regarded. Direct measurements of fluvial wear yielded 3 - 4 mm/ a (Hartshorn et al., 2002). Liew (1988, cited after Schaller et al., 2005) reported late Holocene incision rates of 6 - 11 mm/ a derived from radiocarbon dated uplifted terraces. Cosmogenic nuclide ages of gorge walls imply an incision rate of 26 mm/ a (Schaller et al., 2005).

The system of erosional and transportation processes is studied manifold in the mountain range of Taiwan (e.g. Jen et al., 2006). Emphasis is put on the understanding of the mechanisms of landslides, which represent one of the most destructive natural hazards in Taiwan (Lin et al., 2006; Chang et al., 2007) and are also an important factor of sediment supply to the river discharge in hillslope-channel coupled systems (Hovius et al., 2000; Wenske et al., in press). Further focus is put on the triggering function of the frequent earthquakes (Dadson et al., 2004; Chen et al., 2005b), typhoons (Lin and Jeng, 2000; Chen, 2006; Wu and Chen, 2009) or the combination of both (Lin et al., 2006; Chang et al., 2007; Chen, 2009).

In strong contrast to the rugged relief formed by the intense erosion in the mid-altitude mountain belt, the uppermost altitudes (> 3000 m) are characterized by a rather smooth relief and seem to be widely still unaffected by those processes. Accumulative processes including talus formation are predominant (Hebenstreit and Böse, 2003; Klose, 2006; Wenske et al., 2011) (cf. figs. 7.3 and 7.5). However, backward erosion of some valley heads reached these areas already locally, mainly from valleys that reach the water divide from the East and discharge into the Pacific Ocean, which is due to the shorter runoff distance. This implies that the uppermost geomorphologic belt represents a fossil surface, which is successively destroyed from below by modern erosion.

Table 2.1: Examples of published uplift and subsiding rates in different Taiwanese regions

area	uplift rate (mm/ a)	time period	reconstruction criterion	dating method	reference
Central Taiwan					
Central Range	5.5	< 5 Ma	assumption from denudation	n. a.	(Li, 1976)
Central Range	8.9 ± 1.9	0.6 Ma	mineral cooling and exhumation	fission track	(Liu, 1982)
Central Range	4 - 5	1.4 Ma	uplifted sediments	stratigraphic	(Dorsey, 1988)
Central Range	0.3 - 2.9	Pliocene	mineral cooling and exhumation	Rb-Sr	(Lan et al., 1990)
Central Range	36 - 42	recent	geodetic	n. a.	(Liu, 1995)
Central Range	7 - 16	< 1.5 Ma	mineral cooling and exhumation	fission track	(Lin and Roecker, 1998)
Central Range	4 - 7	> 1.5 Ma	mineral cooling and exhumation	fission track	(Lin and Roecker, 1998)
Central Range	5 - 10	< 5 Ma	summary	summary	(Lin, 1998)
Central Range	< 1	6 - 1 Ma	mineral cooling and exhumation	fission track	(Lee et al., 2006)
Central Range	4 - 10	< 1 Ma	mineral cooling and exhumation	fission track	(Lee et al., 2006)
East Taiwan					
Coastal Range	6.0 - 9.7	Holocene	uplifted corals	U/Th, radiocarbon	(Konishi et al., 1968)
Coastal Range	5.0 ± 0.4	Holocene	uplifted corals	radiocarbon	(Peng et al., 1977)
Longitudinal Valley	35	recent	geodetic	n. a.	(Yu and Liu, 1989)
Coastal Range	5.9 - 7.5	1 Ma	uplifted sediments	stratigraphic	(Lundberg and Dorsey, 1990)
Coastal Range	4.7 ± 1.0 to 5.3 ± 0.8	Holocene	uplifted corals	U/Th, radiocarbon	(Wang and Burnett, 1990)
Coastal Range	2.5 - 8	Holocene	shorelines	radiocarbon	(Liew et al., 1993)
Coastal Range	5.0 ± 0.4	Holocene	summary [(1)]	summary	(Lin, 1994)
Coastal Range	3 - 5	Holocene	shorelines	radiocarbon	(Vita-Finzi and Lin, 1998)
Longitudinal Valley	24	recent	GPS measurements	n. a.	(Yu and Kuo, 2001)
Coastal Range	4 - 10	Holocene	uplifted marine terraces	radiocarbon	(Hsieh et al., 2004)
Ilan Plain	- (6-10)	Holocene	summary [(1)]	summary	(Liew et al., 2004)
Coastal Range	5.1	Holocene	uplifted marine platforms	radiocarbon	(Hsieh and Rau, 2009)
Coastal Range	3.5 - 7.3	1 ka	uplifted shells	radiocarbon	(Hsieh and Rau, 2009)
North Taiwan					
Northern coast	5.3	early Holocene	uplifted corals	radiocarbon	(Peng et al., 1977)
Northern coast	2	late Holocene	uplifted corals	radiocarbon	(Peng et al., 1977)
Northern coast	2-5	Holocene	summary [(1)]	summary	(Liew et al., 2004)
South and West Taiwan					
Hengchun	1.8 - 4.8	Holocene	uplifted corals	U/Th, radiocarbon	(Konishi et al., 1968)
Hengchun	5.3 ± 0.2	Holocene	uplifted corals	radiocarbon	(Peng et al., 1977)
Western Foothills	1	3 Ma	uplifted sediments	stratigraphic	(Lee, 1977)
Western Foothills	5 - 10	0.7 Ma	uplifted sediments	stratigraphic	(Lee, 1977)
Tainan area	4.3 ± 0.4	Holocene	uplifted corals	radiocarbon	(Peng et al., 1977)
Hengchun	(10 - 20 m)	Holocene	reef terraces	assumption	(Liew and Lin, 1987)
Hengchun	3.3 ± 0.4 to 3.5 ± 0.3	Holocene	uplifted corals	U/Th, radiocarbon	(Wang and Burnett, 1990)
Tainan Plain	5 - 7	Holocene	terrace uplift	radiocarbon	(Chen and Liu, 2000)
Coastal Plain	4.3 - 5.4	Holocene	uplifted marine sediments	radiocarbon	(Hsieh and Knuepfer, 2001)
Coastal Plain (mountain front)	5.9 - 7.7	Holocene	uplifted marine sediments	radiocarbon	(Hsieh and Knuepfer, 2001)
Western coast (foothill area)	1 - 1.5	Holocene	summary [(1)]	summary	(Liew et al., 2004)
Western coast (Plains)	- (2-3)	Holocene	summary [(1)]	summary	(Liew et al., 2004)
Pingtung Plain	- (6-8)	Holocene	summary [(1)]	summary	(Liew et al., 2004)
Southern coast	0 - 5	Holocene	summary [(1)]	summary	(Liew et al., 2004)
Western Foothills	2.5 - 7	50 ka	uplifted river terraces	OSL	(Lai et al., 2006)
Pingtung Plain	-25 - 13	recent	GPS measurements	n. a.	(Hu et al., 2006)
Tainan Tableland	14	recent	SAR interferometry	n. a.	(Huang et al., 2006; Huang et al., 2009)

n. a. = not applied

[(1)] summary includes data from unpublished Ph.D. or M.Sc. thesis or from conference contributions

CHAPTER 3

Methods

3.1 Methodical framework and strategic approach of this work

To achieve the research aims of this work, a number of methods and techniques were applied. However, this geomorphological study does not define itself as a methodological approach and the focus lies on the application and combination of multiple methods. Its strategic concept can be outlined in a summarised way as follows:

1. Glacial landforms and deposits as well as their morphostratigraphical correlation were described, documented and mapped in the Taiwanese high mountain range (cf. sections 3.2 – 3.4).
2. Sediment characteristics of potentially glacigenic deposits were analysed with field and laboratory techniques to verify their glacial origin (cf. section 3.5).
3. For an absolute dating of glacigenic deposits, optically stimulated luminescence (OSL, cf. section 3.6) and rock surface exposure dating (SED) with terrestrial in situ produced cosmogenic nuclides (TCN, cf. section 3.7) were applied, which allows an independent temporal correlation of different geomorphologic evidences.
4. The mapping and dating of glacial indicators results in the reconstruction of the former glacier extent at different stages and the calculation of the respective equilibrium line altitude (ELA) and the ELA depression (ΔELA, cf. section 3.8).
5. This offers the possibility for a comparison with regional and interregional paleoclimatic evidences (cf. chapters 4 to 6).
6. This study was undertaken in three mountain areas. The Nanhuta Shan in north-east Taiwan was the main study area, because it came out with the best preserved glacial landforms and thus studies were focused there. Supplementary observations were made in Hsueh Shan in central-north Taiwan and in Yushan in central Taiwan to obtain comparative evidence (cf. chapter 2).

Nevertheless, a number of unalterable factors limited the practicability of the study. Since little was known about the natural environment in the study area at the beginning of the investigations due to bad topographic and geologic map coverage and rare climatological information, a basic inventory of the natural framework, the geological and geomorphological setting in particular had to be established (Klose, 2006; 2007).

Moreover, the physical accessibility of key locations in all study areas had to be explored. Thus, the project had the character of a pathfinder expedition. It turned out that large parts of the area, in particular the lower valley sections, were inaccessible due to the steepness of the terrain and temporally unsuitable weather conditions. The visibility of landforms and sediments in the field and in remote sensing data is additionally limited by the vegetation cover.

3.2 Some principles and theoretical aspects of glacio-geomorphological analyses

This study follows a classical geomorphological approach in terms of a historic-genetic landscape analysis (Ahnert, 1996) and the system of the climatic geomorphology on the basis of landscape diagnosis (Hövermann, 1985). The empirical base for this purpose is a morphographic documentation of landforms and deposits in the study area regarding their geometry, dimensions and spatial distribution as well as the analysis of the physical composition of the deposits.

The identification of geomorphologic indicators for a former presence of glaciers in a presently non-glaciated terrain was carried out by comparison with landforms, which are generated by present glacial activity elsewhere (*uniformitarianism*) and which are regarded as key landforms of glacial geomorphology (Kuhle, 1991a). This allows a genetic classification of the landforms as “glacial evidences” (*Gletscherzeugen*). In this context, a number of additional criteria must be fulfilled to prove the former presence of glacier ice:

1. It must be clarified that the considered landforms are real fossil and inactive (*Vorzeitformen*), i.e. their origin is in contrast with the present geomorphologic processes and the landforms, which are presently generated by those processes.
2. A possible alternative (non-glacial) origin of the landforms and deposits (converging phenomena) by neotectonic, mass movement, periglacial or fluvial processes has to be excluded.

3. The influence of the bedrock structure on the glacial landforms and the composition of the deposits must be taken into account (cf. section 2.3.2).
4. The combination of potential complementary glacial landforms and sediment associations in the respective area as well as the specific spatially correlation of geomorphological and sedimentological indicators in terms of the "*glaziale Serie",* (Penk and Brückner, 1901-1909) had to be achieved.

However, the identification of glacial landforms is limited as subsequent processes reshape or even destroy glacial landforms and deposits. This is in particular true in steep high mountain areas like Taiwan, were effective postglacial morphodynamic processes often leave only relictic glacial evidence caused by the high relief energy of the terrain.

3.3 Key landforms of glacial erosion

Glacial erosion has a profound effect on the scenery of mountainous landscapes. It comprises a number of processes like rock abrasion, fracture, extraction and exfoliation as well as the erosional influence of subglacial meltwater and causes the generation of characteristic landform and sediment associations in mountain areas (Klebelsberg, 1948; Embleton and King, 1975; Sudgen and John, 1976; Kuhle, 1991a). The mechanisms of glacial erosion are described and discussed in detail by Benn and Evens (1998).

3.3.1 Glacial valleys and associated key features

The classical and most spectacular feature of glacial erosion are U-shaped valleys or alpine troughs as known from Pleistocene and modern glacial landscapes e.g. in the European Alps, the Scottish Highlands, the Himalayas and the Western Cordillera of North America (Klebelsberg, 1949; Embleton and King, 1975; Hambrey, 1994). The typical transverse profiles of these valleys are generated through the combination of vertical and horizontal bedrock abrasion and rock extraction by the moving glacier ice and unlike fluvial erosion, which mainly generates vertical incision with typical resulting V-shaped valley cross-profiles (Klebelsberg, 1948). However, formerly and presently glaciated valleys are not necessarily U-shaped, but they can be shaped in a more complex way, depending on the pre-glacial valley topography, the thermal characteristics of the glacier ice (temperate or cold glaciers in terms of the classification of Ahlmann (1935), e.g. the presence of subglacial meltwater) and the bedrock characteristics (e.g. the hardness of the rock, asymmetric sediment rock layers)

(Sudgen and John, 1976; Benn and Evans, 1998). Thus, glacial valley cross-profiles range from wide, nearly parabolic shape to trough shape with steep flanks and nearly vertical cliffs (Hambrey, 1994). Glacial valleys may even have a V-shape cross-profile as shown for valleys in the European Alps, the Karakoram and the Himalaya (Embleton and King, 1975; Kuhle, 1991a).

The upper limit of glacial abrasion on a valley flank is often marked by a distinct change of the rock surface structure. This trimline (Benn and Evans, 1998; Florineth, 1998) describes the boundary between an ice-moulded downslope area, where the rock is smoothened and sometimes polished by the moving ice, and an upslope zone, where frost weathering generates a rough and jagged rock surface. The common German term for this line is *Schliffgrenze* or, with focus on a concave shape of the slope, *Schliffkehle* (Klebelsberg, 1948).

Glacial valleys are often over-deepened. That means, they trend with a reverse gradient in some sections of their longitudinal profiles towards their mouths (Sudgen and John, 1976). The over-deepening occurs when the ice motion is deflected in a valley section with a less steep inclination, while the pressure vector of the pushing ice is still in the steeper direction (Louis and Fischer, 1979). As a result, basins and steps are common characteristics of glacial valleys. Basins may host a lake or be subsequently filled with alluvium, while steps may occur in the form of rock bars (riegels), which are often subglacially or subsequently fluvial incised in form of a gorge (Embleton and King, 1975; Sudgen and John, 1976; Kuhle, 1991a).

If the ice thickness in a valley continues to increase, the glacier surface will eventually reach the highest parts of the valley flanks and rise above the lowest cols on the ridge. Then, the surplus will escape into the neighbouring valley causing a transfluence of the ice with a breaching of the watershed (Embleton and King, 1975).

Other characteristic features in glaciated mountains are hanging valleys, which end abruptly against the steep side flank of the main valley. They were occupied by tributary glaciers, which were not as effective at eroding as the (bigger) main glacier (Hambrey, 1994). However, the formation of hanging valleys and over-deepenings is not exclusively confined to glacial erosion. Neotectonic processes must be considered within the interpretation in tectonically active areas as Taiwan in particular.

3.3.2 Cirques and associated landforms

Among all landforms of glacial erosion cirques are regarded to be one of the surest indicators of past glacial activity (Hambrey, 1994). The main difference between a glacial trough and a cirque is the reduced longitudinal extension of the latter (Kuhle, 1991a). Although cirques are an extremely varied landform in terms of shape and size, they usually represent widened valley heads with flattened or even over-deepened floors and steepened head- and sidewalls. The erosional process on the cirque floor is, like under larger valley glaciers, abrasion, while the progressive back- and sideward widening is the result of rock shattering and headwall undercutting by freeze-thaw action (Embleton and King, 1975).

A large variety of cirque type classifications exists in the literature, describing the dimensions and geometry of the cirques. However, their shape strongly depends on the pre-glacial topography and the bedrock structure. Their size and morphology are therefore not a direct measure for the intensity of a former glaciation and the use of cirques floor altitudes as an indicator for the former altitude of the glacier equilibrium line (cf. section 3.8) is only meaningful under certain circumstances (Porter, 2001b). Nevertheless, the simple existence of a cirque indicates the former presence of glacier ice.

As valley flanks and headwalls are steepened and extended to the sides and backwards by glacial erosion and frost-shattering, the rock ridges between two valleys are sharpened and produce narrow and serrated arêtes as a characteristic feature in high mountain areas (Hambrey, 1994).

3.3.3 Roches moutonnées

When a glacier overrides a rock obstruction, it abrades its surface leaving a smoothed rock knob, which is sometimes streamlined in a whaleback form. Most common are, however, asymmetric forms, which are only smoothed on the up-glacier or stoss side, while the downstream lee side usually appears abruptly plucked and fractured. This contrast can be used to indicate approximately the former ice flow direction. The formation of roches moutonnées is attributed to joint-block removal effected by freeze-thaw action in combination with pressure release in cavities on its lee side. Although the basic shape is rather characteristic, the detail morphology is strongly influenced by the bedrock structure (Embleton and King, 1975; Hambrey, 1994; Benn and Evans, 1998).

3.3.4 Small scale erosional features

When abrading and scratching a bedrock surface the ice may – depending on the bedrock structure – leave a variation of small (cm to m scale) erosional forms like striations, chatter marks and fractures. Striations are also typical on clasts. These features are usually taken as a clear indicator of former glacier presence (Benn and Evans, 1998).

3.4 Glacigenic depositions

As a glacier erodes rock at its bed and at the valley sides, the debris is transported by the glacier on (supraglacial), in (englacial) and below (subglacial) the ice towards the glacier ablation zone[16] at the snout, where it is released and deposited. The definite identification of glacial deposits is crucial for the reconstruction of the former glacier extent and for the dating of this extent with radiometric methods. Ice marginal deposits are the preferred objects of interest, because they mark a (temporary) equilibrium position of the glacier, from which it subsequently melted back and thus they indicate a change in the ice mass balance of the glacier, most probably induced by a climatic change in the area. In the following, some definitions and the main concepts of the identification of glacigenic deposits are shortly outlined.

3.4.1 Definitions

According to the complex range of glacigenic sediments, landforms and the depositional processes they have undergone, a variety of descriptions, classifications and terminologies is established in the literature (Goldthwait and Matsch, 1989; Benn and Evans, 1998). Furthermore, the terminology is far from being consistent in different languages. However, the ongoing discussion about it is not subject of this thesis, but a short definition of the terms as used in this work will be given here.

“Glacigenic sediment” is used for a deposit of glacial origin in a broad sense to embrace sediments with greater or lesser component derived from glacier ice, whereas “glacial” debris is material transported by a glacier in contact with glacier ice (Dreimanis, 1989; Hambrey, 1994). “Glaciofluvial” sediments are transported and deposited by glacial meltwater.

[16] cf. section 3.8 about glacier mass balance

The common term for a primary terrestrial glacigenic deposition in the English literature is "till" (Benn and Evans, 1998). Sudgen and John (1976) have stated that "till" is used in terms of a deposit that can be analysed by sedimentological techniques, whereas "moraine" is used in a geomorphological sense, expressing the surface morphology of the deposit. However, since the German term "Moräne" is used in both, a sedimentological and geomorphological sense (Klebelsberg, 1948; Kuhle, 1991a), "moraine" is also used for both in this text, the glacial sediment and the landform. Moraines as landforms are divided into terminal (end-) and lateral moraines according to their position relative to the glacier (Embleton and King, 1975). For a non-genetic description of non-sorted or poorly sorted sediment, that contains a wide range of particle sizes the term "diamict" is used (Dreimanis, 1989; Hambrey, 1994)[17].

3.4.2 Characteristics of glacial deposits and problems associated with their identification in high mountain environments

Sequences of potentially glacigenic sediments are examined approaching a facies analysis by describing the specific characteristics of a sediment unit as bedding, geometry and texture as well as the characteristics of the individual sedimentary components (Eyles et al., 1983; Benn and Owen, 2002). A facies is a distinctive rock (sediment body) that forms under certain conditions of sedimentation, reflecting a particular process or environment (Hambrey, 1994). Facies can be grouped in associations or assemblages that reflect a range of processes in that environment (Benn and Evans, 1998).

Contemporary high mountain glacial facies tend to have typical characteristics, which can be used to reconstruct former (Quaternary) glacier extents (Benn and Owen, 2002; Owen et al., 2003a). The following criteria were applied to discriminate glacigenic depositions from those with different origin:

Moraines tend to be massive in structure without lamination or bedding. They are commonly non or poorly sorted and contain clasts of many sizes (including large boulders) in a variable finer matrix, which discriminates them from fluvial deposits, which are typically better sorted and depleted of fines (Kuhle, 1991a). As the matrix grain size distribution varies

[17] The term embraces both, a consolidated and an unconsolidated sediment. However, only unconsolidated sediments are described in this work.

depending on a number of factors, like the transport distance, the path of the particles through the glacier, the lithology of the material and the occurrence of meltwater, its value as a glacial indicator is limited. However, bimodal or polymodal distributions point to glacial origin, the latter tending to reflect the longer distance of transport (Kuhle, 1991a; Owen et al., 2003a). Triangular plots (cf. appendix figure A1) show characteristic envelopes (Boulton, 1978; Hartge and Horn, 1992; Hambrey, 1994).

Moraines are typically composed of mixed minerals and rock types and contain often material, which is derived from the source of the valley, while mass movements, landslides and rock avalanches tend to be petrographically homogeneous with components derived from a certain part of a local valley flank (Hewitt, 1999).

Moraine components often have a common orientation (fabric) of elongated particles, and glacial clasts often show a characteristic morphology. The clast *roundness* is affected in opposite ways during the transport. Abrasion produces rounded edges and polished surfaces, while fracturing creates new sharp edges. This results in a predominant content of subrounded or sub-angular components in the moraine (Boulton, 1978; Hambrey, 1994; Benn and Evans, 1998), whereas fluvial clast are usually better rounded (Kuhle, 1991a). Rock weathering and mass movement material is predominantly angular (Hewitt, 1999) (cf. fig. 7.10).

The clast *shape* (i.e. the relative dimensions of the clast axes), however, strongly depends on the lithological structure (Benn and Evans, 1998) and tends to be slabby for many depositions in the Taiwanese slate belt. That can mimic a bedding of actually massive diamicts and influences the fabric of the particles, which is also known from glacial deposits in the Karakoram (Owen, 1991).

Apart from roundness and sphericity, glacial clasts often have a specific faceted or pentagonal form. Their surface texture is also very distinctive. Polish is common and striations on clasts are regarded as a strong indicator for glacial transport (Boulton, 1978; Benn and Evans, 1998) (cf. figs. 7.7 - 7.9).

Nevertheless, the distinct identification of glacial deposits in mountain areas – and in Taiwan in particular – is a most challenging objective. This is due to a number of major uncertainties in the analysis and the interpretation of a potential glacial deposit found in the field. These problems are discussed in detail for numerous locations in the Himalaya-Karakoram-Tibet

area (Derbyshire et al., 1991; Owen, 1991; Owen et al., 1998; Hewitt, 1999; Benn and Owen, 2002). Associated problems are:

1. Glacigenic facies vary in a wide range of different and highly complex occurrences. All characteristic sediment parameters referred to above depend on the individual situation during the deposition including factors such as transport distance, bedrock material, thermal characteristics of the glacier and the topography of the pre-glacial terrain (cf. the “slate problem”, section 3.5.4). Therefore, the composition of non-glacial depositions (e.g. mass-movements, fluvial deposits) may be similar and can mimic a glacial origin and vice versa (Hewitt, 1999).
2. Regularly, glacial, glaciofluvial and non-glacial materials are accumulated in spatial association, in alternating beds or simply mix as a final deposit, e.g. mass movement or rock fall material is often deposited on glacier surfaces or on moraines (Owen et al., 2003a). This was termed the “diamicton problem” (Owen et al., 1998; Owen et al., 2008).
3. In high mountain areas, glacial deposits are often considerably reshaped, degraded, partly destroyed by non-glacial processes after deposition and therefore incompletely preserved (Hallet and Putkonen, 1994; Ballantyne, 2002; Owen et al., 2008).

Consequently, only the topographical configuration of complementary glacial evidences and the logic reconstruction of their individual, historical qualitative context lead to meaningful interpretations of former glacier extents (Kuhle, 1991a).

3.4.3 Erratics

Erratics are eminently important for the reconstruction of former glaciations, because they provide unambiguous prove for the former presence of a glacier and a minimum mark of its extent (Kuhle, 1991a). The fact is simple: Erratics are dislocated, often far travelled boulders or glacial sediment, which include a petrographical component, which does not occur in the bedrock at the location, where they are found. Because of the topographical situation, they can have reached this location exclusively by glacial transport, but not by fluvial transport with a monotonic river inclination or gravitating in straight slope line from above. The reason is the ability of glaciers to flow uphill and to transport particles valley parallel far above the valley floor (Embleton and King, 1975). Positions on ridges or on valley flanks far above the

floors or on summits, which can never be reached by a river, even during flood events, are the preferred target locations for the proof of a former glacier presence (Kuhle, 1991a).

"They (the erratics), even when sparsely occurring, are defining for the proof" and for "a minimum level, which has been reached by the ice." (Klebelsberg, 1948: 283). Morphology, surface structure, size and amount are of minor importance, because „even the smallest pieces tell – in general – the same, sometimes one can exclude an artificial dislocation of tiny clasts with higher plausibility than for larger stones" (ibid.).

Furthermore, erratic material, regardless of its form as single boulders or as a sediment, also provides the possibility to reconstruct transport directions and distances of the ice motion.

3.5 Applied techniques and field work

3.5.1 Remote sensing, aerial photo and topographic map interpretation, positioning

Topographic maps in scale of 1:10,000 and 1:50,000 (Aerial Survey Office Forestry Bureau, 1982; Topographic Department Combined Logistics Command, 1995) as well as aerial photographs were analysed for field work planning, overview on the study areas, the identification of glacial landforms and pre-selection of key sites for sampling as well as for the final mapping.

All available topographic maps are limited in precision and accuracy and don't include topographic details, which a map of the respective resolution should show. The geomorphological sketch maps in publication 1 and 3 were complied on the base of the 1:10,000 aerial photo topographic map of Taiwan. Previous aerial photo based geomorphological mapping was done by Böse (2000).

Digital terrain models were available only after field work, unfortunately. Topographical overviews of this dissertation use the 1 Arc-Minute Global Relief Model ETOPO, (compiled by Amante and Eakins, 2009), a 90 m horizontal resolution DEM, derived from hole-filled seamless SRTM-3 data, processed by Jarvis et al. (2006) and a 40 m horizontal resolution DEM based on stereoscopic air photo data (kindly provided by the National Taiwan University).

Field sites were positioned by defining the geographical coordinates and the altitude above the sea level by means of the Global Positioning System (GPS). This was done for mapping the field evidence, to retrieve these sites, for the subsequent calculation of the glacier ELA and for scaling of the ^{10}Be production rate for rock surface exposure dating. Because GPS

derived altitudes showed little consistency, an aneroid altimeter was used additionally (Thommen Classic 6000). The altimeter was calibrated with the Taiwanese aerial photo map 1:10,000 at the Nanhu hut (3373.7 m) in Nanhuta Shan, the Chika hut (2463 m) in Hsueh Shan and the Paiyun hut (3402 m) in Yushan.

Locations and altitudes were cross-checked with the Taiwanese 40 m resolution DEM. The estimated horizontal error is < 0.0005°, the estimated vertical error ± 10 m. All altitudes presented in this work are directly measured or interpolated aneroid measurements and are given in metres above the sea level (a.s.l.) except as noted otherwise or evidently noted in the context as relative vertical changes. Locations for sampling and sediment analyses are listed in appendix table A4.

3.5.2 Setup of a meteorological station in Nanhuta Shan and the ascertainment of a four-year dataset of temperature and precipitation

Few meteorological data is available from the high mountain area in Taiwan. Only two stations are run by the Central Weather Bureau of Taiwan (CWB) in altitudes above 2000 m (fig. 2.6), in Alishan (2408 m) and Pei Shan (3845 m, north peak of Yushan). No data was available from high altitudes in the northern part of Taiwan at the beginning of this work.

For comparison, a meteorological station was set up in Nanhuta Shan at 3550 m in March 2001 to log hourly precipitation, air temperature and ground temperature from March 2001 to April 2005. A description of the setup specifications of the station as well as a detailed analysis and discussion of the obtained data are made by Klose (2007). For this dissertation, air temperature and precipitation data were reviewed in terms of validity for the establishing of the present theoretical ELA over Taiwan. Only recently, the station Shaofenko (3005 m) in the Hohuan Shan range run by the Endemic Species Research Institute, Council of Agriculture provided additional data (2005 – 2009, fig. 2.6).

3.5.3 Elementary geological mapping

The knowledge of the bedrock lithology is crucial for the determination of boulders as “erratic“ and for tracing back the origin of the petrographical components of moraines. Since the sheet of the geological map for Nanhuta Shan is not published yet, a rough sketch map of the petrographical bedrock base in the study area was compiled (fig. 2.9) basing on air photo interpretation, field observation and personal communication with Dr. Chu Hao-Tsu

(Central Geological Survey of Taiwan). The lithological and chronological classification follows Chu (1987) and the general geological map of Taiwan 1:500,000 (Wang and Lee, 2000). Bedding and cleaving was measured using a conventional geological compass (*Freiberger Präzisionsmechanik*).

To discriminate the various quartzite layers and to assign them to definite erratics, 35 thin sections of samples from the relevant layers and boulders were made. Unfortunately, all quartzite samples bear a substantial similarity, so that a detailed discrimination was not possible within the limited scope of this project.

3.5.4 Sedimentological analyses

Sediments were analysed and sampled at key locations in the field to determine their physical composition (cf. appendix table A4). The structure and texture of a sediment unit were visually described in terms of bedding and sorting (Benn and Evans, 1998). The sizes of the largest components were measured. The matrix content was evaluated according conventional comparison diagrams (Tucker, 1996). Other sediment properties were obtained partially by quantitative and partially by qualitative means and include (1) the petrographical variation of the sediment components, (2) the clast orientation inferred from the direction of the longitudinal clast axes (Hövermann and Poser, cited after Köster and Leser, 1967) and (3) the clast roundness with a 4-class roundness index (Reichelt, 1955 cited after Köster and Leser, 1967). Clasts (n = 30 - 100) of 3 – 50 cm length were counted for each parameter. Clast shape and clast surface features (striations, facets, polish) were described visually.

The grain size distribution of the sediment matrix was determined by applying conventional laboratory procedures, such as sieve and pipette methods according to German standards (DIN 19683, DIN 18123)[18]. Depending on the assumed fine material content, 60 – 1000 g sediment were collected from sediment components < 63 mm. If possible, a representative amount of the gravel fraction was sampled. However, in case of diamicts the gravel might be underrepresented in the sample. The gravel fraction was separated and sieved dry. Grain sizes of 0.063 - 2 mm were sieved wet to collect all fine material. The fine fractions < 0.063 mm were determined applying the pipette method according to “Stokes law” (Tucker, 1996). The graphical presentation of the sedimentological results and the lithofacies codes used in

[18] (Fachnormenausschuß Wasserwesen, 1973; Normenausschuß Bauwesen (NABau), 1983)

publication 1 (Hebenstreit et al., 2006) follows Tucker (1996), Benn and Evans (1998) and Horn (2010).

The results of all analyses described above are influenced and limited by the dominating occurrence of slate as bedrock in the study area resulting in a petrographical uniformity of the sediments. Moreover, shape, fabric and grain size of a particle are often predominated by its lithological structure as the slate tends to produce slabby clasts, which are easily breakable. However, typical glacial characteristics could be obtained from most analysed sediments of assumed glacial origin (for sedimentological results cf. chapter 4, additional data are presented in the appendix tables A4-A6 and fig. A1).

3.6 Sediment dating by means of optically stimulated luminescence (OSL)

3.6.1 Introduction

Optically stimulated luminescence (OSL) has been applied to date quaternary glacigenic sediments with sufficient success in many high mountain ranges worldwide during the last two decades (Fuchs and Owen, 2008). In contrast to conventional absolute dating with radiocarbon this technique provides the possibility to date glacigenic deposits (the time of their deposition) directly, in particular with regard to the general rareness of organic matter in high altitude glacial environments. It can therefore constrain glacial advances with more confidence.

It is far beyond the scope of this work to discuss all details and technical specifications of the application. Therefore, only the principles are shortly introduced and some geomorphological field considerations are discussed. The basics of the technique are described in monographs (Wagner, 1995; Aitken, 1998), comprehensive papers (Godfrey-Smith et al., 1988; Murray and Olley, 2002; Preusser et al., 2008) and in papers, with focus on mountainous glacial environments (Richards, 2000; Fuchs and Owen, 2008). The results of OSL dating within this study are presented and discussed in publication 1 (Hebenstreit et al., 2006).

3.6.2 Principles of luminescence dating

Luminescence dating is a radiometric dating method. It uses the time-depended accumulation of electrons (i.e. energy) at traps within the crystal lattices of minerals initiated by the natural ionizing radiation, which is derived from radioactive isotopes in the sediment and by

the cosmic radiation, as long as the minerals are buried and shielded from light. If sediment is exposed to light, the electrons are released and the signal is zeroed, i.e. the sediment particles are “bleached”. Subsequent burial initiates the accumulation of electrons again. Therefore, optically stimulated luminescence dates the last exposure to light of the sampled sediment. The amount of the accumulated energy (= the equivalent dose, D_e) depends on the rate of the ionizing radiation (= dose rate) and the duration of burial of the sediment (Wagner, 1995; Fuchs and Owen, 2008).

In the laboratory, the accumulated energy can be detected as a luminescence signal, when the electrons are released by stimulating the minerals artificially with light or heat (optically stimulated luminescence or thermoluminescence, respectively). The relationship between the intensity of the luminescence signal and the accumulated radiation energy during the time of burial is determined by comparison of the naturally emitted luminescence intensity of the sample and the intensity that results from a known amount of radiation given to the sample in the laboratory. Then, the burial age of the sample can be simply derived from the equation

$$\text{Age} = \text{equivalent dose} / \text{dose rate} \qquad (1).$$

The age range that can be detected by OSL depends on the dose rate and the properties of the targeted mineral. Quartz, which is used in this study, can be dated back to 100 - 150 ka (Wagner, 1995; Aitken, 1998; Fuchs and Owen, 2008) or even 500 ka (Murray and Wintle, 2003).

3.6.3 Sampling and applied measurement protocol

Because of the light sensitivity, samples must be collected without exposure to light and opened in the laboratory under controlled red light conditions. Eight samples were taken from glacigenic sediments and three samples from slope sediments for this study using plastic tubes for fine grained sediments and steel tubes for diamicts. Detailed sediment and sample characteristics, sample locations and results are described in detail in publication 1 (Hebenstreit et al., 2006). The samples were prepared in the Nordic Laboratory for Luminescence Dating in Aarhus, Denmark according to standard procedures, where in a series of physical and chemical treatments quartz grains of sand size are isolated.

For this study we applied the single-aliquot regenerative-dose protocol (SAR) for the dating of quartz as a means of determining the equivalent dose (Murray and Wintle, 2000). In this protocol all measurement steps for determination of D_e are performed using the same sub-sample (aliquot). This way, problems caused by individual luminescence properties of grains from different aliquots are avoided (Murray and Wintle, 2003; Wintle and Murray, 2006). Repeated measurements of a number of aliquots generate an equivalent dose distribution, which allows the determination of the equivalent dose for the whole sample on a statistical basis.

The grains are exposed to light with a wavelength of 470 ± 30 nm, which is blue in the visible spectrum, and the hereby stimulated luminescence signals are measured in a photomultiplier tube (Murray and Wintle, 2003; Preusser et al., 2008).

The dose rates were calculated using radioanalytical data from gamma spectrometry (Murray et al., 1987; Olley et al., 1996) with an assumed lifetime water content as given in Hebenstreit et al. (2006, table1). Cosmic ray dose rates were estimated from the geographical position and the burial depth of the sampled material following standard equations (Prescott and Hutton, 1994).

3.6.4 Application for glacial sediments and associated problems

Glacial sedimentary environments are highly complex and involve a wide range of processes, which affect the sediments such as erosion, meltout, deposition, reincorporation and transport of particles by the glacier ice and by meltwater (cf. section 3.4). The resulting lithofacies associations show therefore highly variable characteristics. Beside the problems of classification, it is most challenging to identify units, which represent a distinct process and are therefore meaningful for sampling. Three main problems are faced:

First, it is commonly assumed that the likelihood for sufficient bleaching in such glacial environments is generally low and therefore ages tend to be overestimated. However, some of the involved processes provide the chance for light exposure during the sedimentation. These are supraglacial meltout and transport as well as glaciofluvial processes in latero-frontal positions (Richards, 2000; Benn and Owen, 2002; Fuchs and Owen, 2008). It is assumed in this study that all sampled sediments are sufficiently bleached suggested by the young ages and the internal and morphological consistence (cf. discussion in publication 1, Hebenstreit et al., 2006). Furthermore, incomplete bleaching could be detected by a large scatter or

asymmetries within the obtained equivalent dose distributions, which seems, however, not to be the case (A. Murray, pers. comm., 2002).

A second problem is represented by a possible variability of the dose rate, which can be caused by the mineralogical inhomogeneity of glacial sediments and changes in the water content (Preusser et al., 2008). We conclude for this study that this subject is of minor importance due to the general uniform petrography of the sediments and the content of fine matrix in all sampled sediments, which stabilises the sediment moisture. Thus, the dose rate and the water content are assumed to be constant over the time of the burial as given in Hebenstreit et al. (2006, table1).

However, the uniform petrography of the sediments in the Taiwanese slate belt constitutes a – third – problem concerning the quartz content, which is indeed low and one sample did not contain enough quartz grains of the right size. All other samples had a sufficient quartz content, which is derived from the few quartzite layers in the bedrock, and were measured successfully.

With regard to these uncertainties, the application of OSL in this study is also a test for the functionality of this technique under less suitable conditions.

3.7 Rock surface exposure dating using in situ produced terrestrial cosmogenic nuclides (TCN)

The dating of rock surfaces provides the possibility to date glacial events more directly than with all other radiometric dating methods (Ivy-Ochs and Kober, 2008). In this study, the direct dating of the deposition of erratic boulders and boulders on terminal moraines are of particular interest, because they are inaccessible for luminescence or radiocarbon dating. Furthermore, their dating provides an independent age control of the luminescence dated sediments of the same morphostratigraphical age.

The technique of rock surface exposure dating (SED) with in situ produced cosmogenic nuclides (TCN) has developed intensively during the last two decades and has been applied in a vast number of studies to date glacial events in high mountains and foreland regions (Reuther et al., 2006). However, the application is only meaningful under certain geomorphological conditions, which lead – if not fulfilled – to inconsistent results as shown in many studies reported from high mountain regions (Owen et al., 2008).

The main concept of exposure dating is that so called cosmogenic isotopes are produced in situ by nuclear reactions in mineral lattices of rock surfaces (or in sediments), which are exposed to cosmic radiation. The accumulated isotopes are a measure of the duration of exposure, if the production rate is known and if the rock surface is freshly created (e.g. by glacial abrasion) or exhumed from sediment cover and one can therefore assume that the initial concentration of the isotope is zero or negligible. In this study we use ^{10}Be produced in quartz.

Although the principles are straightforward, the physical background is complex. Introductions to the method and its application in geomorphology and in the reconstruction of glacial events in particular are given in many publications (e.g. Gosse and Phillips, 2001; Gosse, 2005; Ivy-Ochs and Kober, 2008).

Like the use of OSL, the application of TCN dating is taken as a tool for constraining the age of glacial events in this study and all technical specifications are beyond the scope of this work. Since the sample analysis and age calculations follow more or less standard procedures, the main focus in this study is put on the sample selection, their geomorphological context and the sampling itself. The sample preparation was accomplished by Dr. Susan Ivy Ochs and the measurements of the accelerator mass spectrometry (AMS) by Dr. Peter W. Kubik at the Laboratory of Ion Beam Physics of the ETH Zurich, Switzerland.

All geomorphological considerations, sample descriptions and age calculations including the respective methodological references are presented in detail in publication 3 (Hebenstreit et al., 2011) and supplementary data is given in the appendix tables A7 and A8.

3.8 Calculations of equilibrium line altitudes

3.8.1 Principles and Definitions

Changes of terrestrial glaciations have been early attributed to climatic changes (J. Walcher, 1773, cited after Kuhle, 1988). Today, the extent of mountain glaciations is used as a sensitive proxy to infer the associated climatic conditions in the particular region. Modern glacier-climate models can provide temperature and precipitation estimates derived from the ice mass balance of the glacier, i.e. ratio of ice gain (= accumulation) and loss (= ablation) throughout its surface (Ohmura et al., 1992; Kaser and Osmaston, 2002; Kull et al., 2008).

The altitude of the glacier equilibrium line (ELA) and its fluctuations are used as an index for regional and interregional comparison of climate conditions. It is defined as the locus of points on a glacier, along which the ice mass balance is zero over the period of one year (Benn and Lehmkuhl, 2000; Porter, 2001b). The term “snowline”, often used as a synonym for ELA, is defined as the lower limit of perennial snow cover on a landscape (Kuhle, 1986; 1988a; Porter, 2001b) and is, strictly speaking, only equivalent with the ELA of a glacier, where the local topography allows the accumulated snow to metamorphose into glacier ice. The difference between the modern ELA and a paleo-ELA at a particular time in the past is the equilibrium line (snowline) depression (ΔELA). In the European Alps, the depression is usually referred to the glacier advance in 1850 (Little Ice Age, LIA), because this is a well distinctive reference level (Gross et al., 1977; Ivy-Ochs et al., 2009). Where LIA evidences are missing, the ΔELA is referred to a “modern” or “present” stage.

Commonly the areas above and below the ELA are referred to as the accumulation zone and the ablation zone, respectively, although this is only a rough simplification, because a glacier may gain and loose mass in all altitudes round the year depending on the local climatic conditions. There is, however, a systematic variation of annual accumulation and ablation with altitude. The rates at which they change are termed the ablation and accumulation gradient, respectively (Benn and Evans, 1998).

The annual mass balance regime of a glacier is controlled by the duration of the accumulation and ablation season and is different in the tropics and in mid-latitudes. Mid-latitude climates have a thermal seasonality resulting in a distinct glacier mass balance seasonality with an accumulation season (winter) and ablation season (summer), whereas in the tropics ablation occurs throughout the year and accumulation is related to precipitation seasons or events (Kaser et al., 1996; Kaser and Osmaston, 2002).

The ELA of an individual glacier is strongly influenced by orographic effects like the topography of the surrounding terrain, which controls the differentiated snow accumulation, e.g. by wind drift or avalanche input. Ablation is influenced by solar radiation and therefore by the geographic direction in which the glacier is orientated. Debris cover influences the glacier mass balance, too, since it reduces its surface ablation (Benn and Evans, 1998). These effects must be considered in the climatic interpretation of a local ELA.

3.8.2 Geometrical reconstruction of present and former ELAs and the ΔELAs

Mass balance observations are extremely complex and are only available for a small number of present glaciers and of course not applicable for the calculation of former ELAs. To estimate the ELA for these glaciers, a set of indices were implemented, which make use of the geometrical abstraction from glacier size, areal configuration and altitude. A list of papers review these methods (Gross et al., 1977; Meierding, 1982; Benn and Evans, 1998; Benn and Lehmkuhl, 2000; Porter, 2001b)

For glaciers, of which the exact shape can be reconstructed, areal methods with a typical accumulation area ratio (AAR) are commonly applied. Other methods combine area ratios and hypsometry of the glacier (Kuhle, 1986; 1988a) or include also mass balance gradient models (AABR) (Osmaston, 2005). However, where topographical maps are limited in precision and the detailed outline, the hypsometry and the mass balance gradient of a glacier are poorly known, simple altitude ratio methods and geomorphological features can be applied to approximate the ELA. This is done in most studies in the East Asian region (cf. table 1.1), although these methods are associated with considerable uncertainty. For the Taiwanese high mountain range the following methods are applied (Hebenstreit, 2006).

(1) The terminal to summit altitude method (TSAM) is the most applicable one in the field and in remote sensing, because only the altitude of the lowest glacier end and the highest summit must be known (Louis, 1955). The ELA is the arithmetical average of the altitude of the highest peak in the catchment and the altitude of the terminal moraine, following the equation

$$ELA = h_t + \frac{(h_s - h_t)}{2} \qquad (2),$$

where h_t is the altitude of the glacier terminus and h_s the summit altitude of the catchment area. However, in comparison with modern glaciers in the European Alps, this method gives values that are about 100 m too high, in particular for glaciers with very high headwalls (Gross et al., 1977). Values of the ΔELA are therefore taken as minimum. Since most East Asian ELA studies use this method (cf. table 1.1), a direct comparison is possible. Other studies apply the terminal to headwall method (THAR), which uses the base of the glacier headwall instead of the summit resulting in somewhat lower ELAs.

(2) The upvalley limit or maximum elevation of lateral moraines (MELM) provides also a rough estimation to constrain the ELA following the idea that moraines are deposited only

below the ELA as ice in the ablation zone of a glacier flows outward towards the ice margins with a consequent deposition of debris (Lichtenecker, 1936). Problems arise when post-depositional degradation or displacement of the moraine occurs. If the upper limits of the lateral moraines are not preserved, the MELM method yields too low ELA values.

(3) When the body of a glacier is restricted to the infill of a cirque, the ELA must lie approximately around the cirque floor (CF). Therefore, in studies of Pleistocene glaciations the cirque floor level in a particular mountain area is sometimes taken as a proxy for the climatic ELA (e.g. Schulz, 2002). However, cirque floor altitudes are strongly controlled by the pre-existing relief and develop cumulatively over multiple glacial cycles (Benn and Lehmkuhl, 2000) resulting in a progressive lowering of the cirque basin and the derived ELA might be too low (cf. 3.3.2). In contrast, if a paleo-glacier expanded beyond the cirque, the former ELA may have been well below the cirque floor (Porter, 2001b).

The results of the ELA calculations are described and discussed in publication 2 (chapter 5) and refined and revised after more detailed dating in publication 3 (chapter 6). Cf. also fig. 7.11 and table 7.1.

3.8.3 Calculation of the modern theoretical ELA in Taiwan and some theoretical climatological considerations

In mountain massifs without present glaciation, the modern theoretical (hypothetical/ virtual) ELA (ELA_t) in the free atmosphere must be determined from present climatic parameters, presuming a mountainous terrain high enough to glacierize. If they are not available, the summit altitude of a massif is often used as a minimum altitude for the modern ELA, assuming that it must lie some unknown distance above the highest summit (Porter, 2001b). Here we used datasets of air temperature and precipitation from four Taiwanese mountain stations above 2400 m (cf. appendix tables A2 and A3). Several glacier-climate models exist to describe the climatic conditions at the ELA (Kaser and Osmaston, 2002; Kull et al., 2008). Modern models need, however, a set of parameters, which are not available for Taiwan. Thus, four alternative models are tested here, which require only precipitation and air temperature. These are (1) the altitude of the annual 0 °C isotherm or the annual mean freezing level (Kaser and Osmaston, 2002; Hastenrath, 2009), (2) the 0 °C July isotherm (Porter, 2005), (3) an empirical model combining the annual total precipitation

and the summer (June-July-August) mean air temperature (Ohmura et al., 1992) and (4) the same model adapted for winter (December - March) precipitation only (Ono et al., 2003).
These methods give considerably different results (cf. appendix table A3). Nevertheless, Ohmura's model for mid-latitude mountain glaciers is preferred here with a 30-year (1971 - 2000) meteorological dataset available from Pei Shan (3845 m), the North Peak of Yu Shan in central Taiwan for the following reasons:

1. The meteorological dataset used is the only existing long term dataset for Taiwan from an altitude above 3000 m including the most recent record of a complete three-decade-period at the time of publication. It seems therefore the most reliable one closest to the presumed theoretical ELA.
2. Altitudes above 2000 m are assumed to be influenced mainly by the westerly circulation, i.e. by non-tropical conditions in Taiwan. Therefore, the July mean freezing level (which is the same as the annual freezing level in a tropical isothermal atmosphere) as used by Porter (2005) for Hawaii (latitude 20° N) is certainly too high for a non-isothermal atmosphere and much more humid conditions.
3. The annual 0 °C isotherm is originally applied for glaciers in the (wet) tropics as well (Kaser and Osmaston, 2002; Hastenrath, 2009). However, the method yields plausible results although no information about precipitation is included. This might be due to the abundant precipitation in Taiwan.
4. Ono (2003) applies Ohmura's model with only winter (snow) precipitation to fit it for the Japanese Alps[19] and for Taiwan (Ono et al., 2005). However, his meteorological data source in not transparent.
5. Furthermore, presuming a constant precipitation regime, a temperature decrease or (virtual) terrain uplift would lead to a progressive contribution of summer precipitation to the glacier mass balance in Taiwan with its clear summer precipitation maximum. This is also the case in other subtropical monsoonal mountain ranges like the southern Himalaya and SE-Tibet, where the summer is the main accumulation

[19] As glacial features are concentrated mainly on slopes in easterly directions in the Japanese mountains because of drifted snow induced by westerly winds (winter monsoon and west wind drift), the ELA, derived from Kuranosuke cirque in the Northern Japanese Alps may be related to orographic effects (Watanabe, 1988).

season (Benn and Owen, 1998). Therefore it is assumed here, that the total annual precipitation must be included in Ohmura's equation.

However, estimates of the modern ELA probably constitute the least-reliable factor in the ΔELA calculations, because the mass balance of modern glaciers changes considerably due to global and regional climate change, which can have caused an ELA fluctuation of several hundred meters during the last century (Gross et al., 1977) and snowline values measured several decades apart may differ in tens of meters (Porter, 2001b). The same must be assumed for the modern theoretical ELA in the free atmosphere. Within a 20-year period, the annual and summer temperatures rose for 0.3 °C at Pei Shan causing a virtual ELA rise of 88 m (cf. appendix table A3). Therefore, the determination of the ELA depression can only be a rough estimate in any case. Details of the application of Ohmura's model are presented and discussed in publication 2 (Hebenstreit, 2006).

3.8.4 Adjustment for postglacial uplift and sea level rise

In mountain regions with strong vertical epeirogenic terrain motion, the uplift rate must be considered in the ELA calculation, because the glacial evidences as well as the catchment altitudes of the former glacier are located higher at present than during the time of glaciation. A minimum Pleistocene and Holocene uplift rate of 5 mm/ a is commonly assumed for the Taiwanese high mountain range (cf. 2.3.4 for details) and is also used in this study (cf. publication 2) (Hebenstreit, 2006).

It has been argued that Pleistocene ELAs must be adjusted for sea level lowering, because the glacio-eustatic fall of the sea level during the glacial cycles had the effect of raising the altitude of mountain summit by the amount of sea-level drawdown (Porter, 2001b). That would be about 120 m for the global last glacial maximum (e.g. Fairbanks, 1989; Bard et al., 1990). However, sea level changes are not considered here, because the ELA represents a value that results from the interaction of atmosphere and terrain. Lowering the sea level only changes the reference base resulting in a numerical increase of the altitude. Furthermore, Osmaston (2006) argued that the air, which was displaced by the ice sheets approximately filled the space left by the depressed sea surface. Therefore, the troposphere as a whole did not fall to a lower level with the effect that temperatures were not significantly decreased at any given altitude due to sea level lowering.

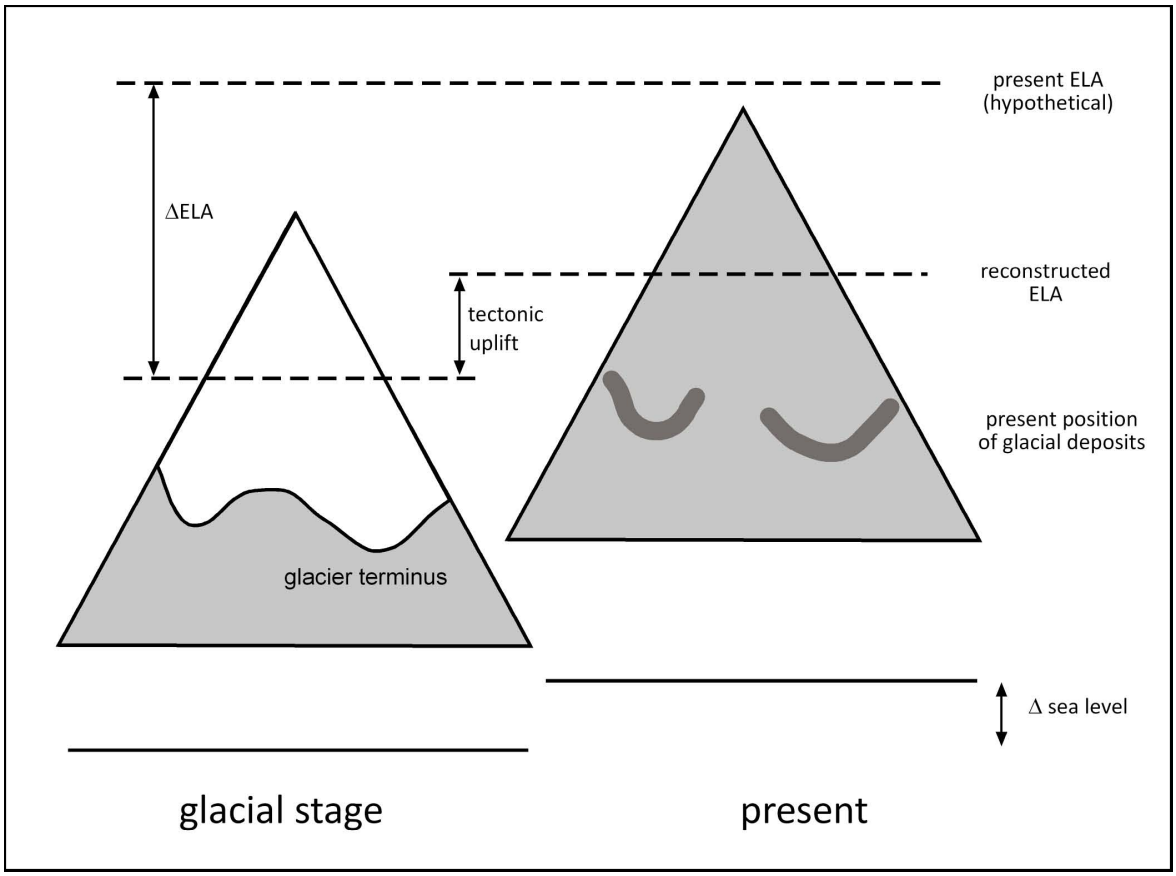

Figure 3.1: Schematic diagram showing ELA correction for vertical terrain uplift. Sea level adjustment is not applied.

CHAPTER 4

Sedimentological results and OSL dating

In this section, the results of the sedimentological analyses and of the OSL dating are presented. Geomorphological evidences are treated relatively short in the text. They have been published in a preliminary version before (Hebenstreit and Böse, 2003), which is not part of this thesis, because some of the results presented therein are out-dated by subsequent research. Please note therefore – when reading this paper - the supplementary figures and interpretations as well as additional references in chapter 7, which contains updated geomorphological evidences from Nanhuta Shan and Hsueh Shan. Additional tables and diagrams of the sedimentological results are provided in the appendix.

This section has been previously published in *Quaternary International*. For unknown reasons, which are not in the responsibility of the author, the proof corrections were unfortunately not included in the final print version of this article. Therefore, the author asks to excuse a minor number of orthographical errors.

Erratum concerning the content: table 1, sample 000901. The age must be **51** ± 10 ka.

Article information:

Citation:	Hebenstreit, R., Böse, M., Murray, A., 2006. Late Pleistocene and early Holocene glaciations in Taiwanese mountains. Quaternary International 147 (1), 76-88.
WWW:	www.sciencedirect.com/science/article/pii/S1040618205001540
PDF:	pdf (1440 K)
DOI:	doi:10.1016/j.quaint.2005.09.009

Available online 28 November 2005

CHAPTER 5

Present and former equilibrium line altitudes in the Taiwanese high mountain range

This section presents results of the equilibrium line altitude calculations from Nanhuta Shan, Hsueh Shan and Yushan. It has been previously published in *Quaternary International*.

Results of Lateglacial and early Holocene ELAs from Nanhuta Shan could be refined subsequently by new dating. Please note therefore the renewed result table (table 7.1) and the supplementary figure 7.11 in chapter 7. Results of alternative calculation methods for the modern theoretical ELA are presented in appendix table A3.

Article information:

Citation: Hebenstreit, R., 2006. Present and former equilibrium line altitudes in the Taiwanese high mountain range. Quaternary International 147 (1), 70-75.

Web-link: www.sciencedirect.com/science/article/pii/S1040618205001539

PDF: pdf (268 K)

DOI: doi:10.1016/j.quaint.2005.09.008

Available online 17 November 2005

CHAPTER 6

Application and results of the ^{10}Be surface exposure dating in Nanhuta Shan

In this section, the methods, sample descriptions and results from in situ produced cosmogenic ^{10}Be exposure dating in Nanhuta Shan are presented. Tables with supplementary data for alternative production rate scaling and age calculation are provided in the appendix. This section has been previously published in *Quaternary Science Reviews*.

Article information:

Citation: Hebenstreit, R., Ivy-Ochs, S., Kubik, P.W., Schlüchter, C., Böse, M., 2006. Lateglacial and early Holocene surface exposure ages of glacial boulders in the Taiwanese high mountain range. Quaternary Science Reviews 30 (3-4), 298-311.

Web-link: www.sciencedirect.com/science/article/pii/S0277379110003987

PDF: pdf (3174 K)

DOI: doi:10.1016/j.quascirev.2010.11.002

Received 26 April 2010

Revised 29 October 2010

Accepted 4 November 2010

Available online 15 December 2010

CHAPTER 7

Supplement to chapters 4 to 6

This section contains supplementary figures, results and comments to the previous three chapters, i.e. material which could not be included in the publications. Only figures 7.3 and 7.5 have been shown in chapter 6 before, but they are presented here with a more geomorphological focus and with more detailed information. Figures 7.2a, 7.3, 7.5 and 7.7 were also part of the publication with preliminary results in the *Zeitschrift für Geomorphologie*[20], which is not included in this dissertation. They are presented here in a modified way.

[20] (Hebenstreit and Böse, 2003)

7.1 Geomorphological evidence from Hsueh Shan

Figure 7.1: Overview on Main Peak, cirque and upper section of NE-Valley (Qi Jia Wan Xi) in Hsueh Shan (c. 24° 25' 30" N, 121° 16' 00" E), facing SW, oblique aerial photograph by C. H. Jen, 25.08.2006.

A classical cirque with widened flanks and steepened backwall occupies the NE side of the Hsueh Shan Main Peak (3884 m) and the upper section of the valley. The ridges surrounding the cirque are shaped as arête. The glacier filled the entire valley and terminated at an unknown location off the picture to the left during the maximum stage of glaciation. The rest of a lateral moraine at 3050 m (←) was dated with OSL to an age of 51 ± 10 / 56 ± 4 ka (cf. fig. 7.2 and chapter 4, section 3.2). Note, the bedrock outcrop seen above the moraine is orientated eastward (to the left in the picture) and is not related to the moraine ridge.

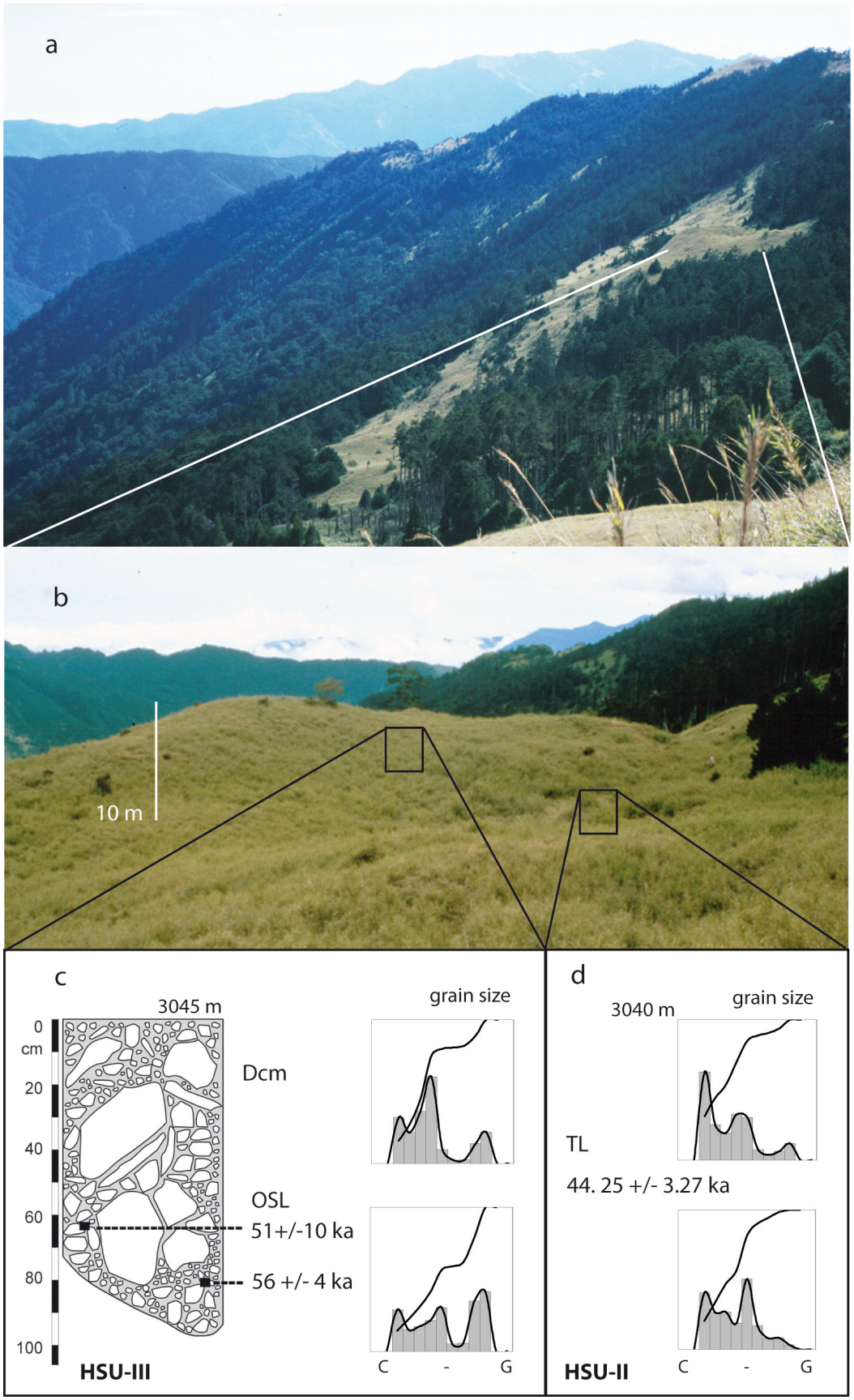

Figure 7.2: Right hand slope of a glacial valley and lateral moraine, Hsueh Shan, adapted from Hebenstreit and Böse (2003). **a – d ----- > *next page***

a) View along the NNW facing slope of the NE trending valley (Qi Jia Wan Xi). A 10-m-high rest of a lateral moraine is deposited about 500 m above the present valley floor. The ridge has a convex shape and is separated from the slope by a depression. The picture is facing E. The summit of Nanhuta Shan is visible in the background. Photograph taken by M. Böse, 4.3.2000.

b) Close up of the moraine ridge (24° 23' 28.3" N, 121° 15' 41.4" E), facing NE, moraine top at 3050 m. The picture indicates the location of the sections. Photograph taken by H. Martens, 4.3.2000.

c) Section Hsu-III is located at the distal side of the lateral moraine. The deposit is composed of a deeply brownish weathered clast supported diamict with a silty matrix. Boulders consist of slate and quartzite and measure up to 40 cm. They are dominantly subrounded and show often facetted and polished surfaces. Striations were not observed. Many clasts are secondarily broken resulting in a more angular shape or typical "turtle shape" with one rounded and one angular side. Two OSL samples were taken from matrix lenses.

d) Section Hsu-II in the depression behind the moraine shows similar composition, but with little finer matrix and more angular boulders, which is probably due to colluvium supply from the slope above. This fact could also explain the slightly younger TL age earlier obtained from a nearby site by Chinese and Taiwanese colleagues (Cui et al., 2002). However, it must be noted that TL ages are generally assumed to be less reliable in glacial environments (Godfrey-Smith et al., 1988; Fuchs and Owen, 2008) .

Evaluating all morphological and sedimentological characteristics, the ridge is interpreted as a weathered, potentially dislocated lateral glacier accumulation. Considering the steepness of the slope a pure landslide accumulation at the middle slope must be excluded. Cui et al. (2002) assumed this accumulation to represent a terminal position of the glacier, which has a distinct implication on the calculated ELA (Hebenstreit, 2006). However, the morphology and location of the sediment ridge is not consistent with this interpretation.

In summary, a distinct genesis of the sediment is hardly to infer in detail and the obtained ages must be handled with great care, in particular as they are the only available chronological information from potentially glacial sediments in whole Taiwan that constrains a glacier advance during the MIS 3/4.

7.2 Geomorphological evidence from Nanhuta Shan and updated ELA calculations

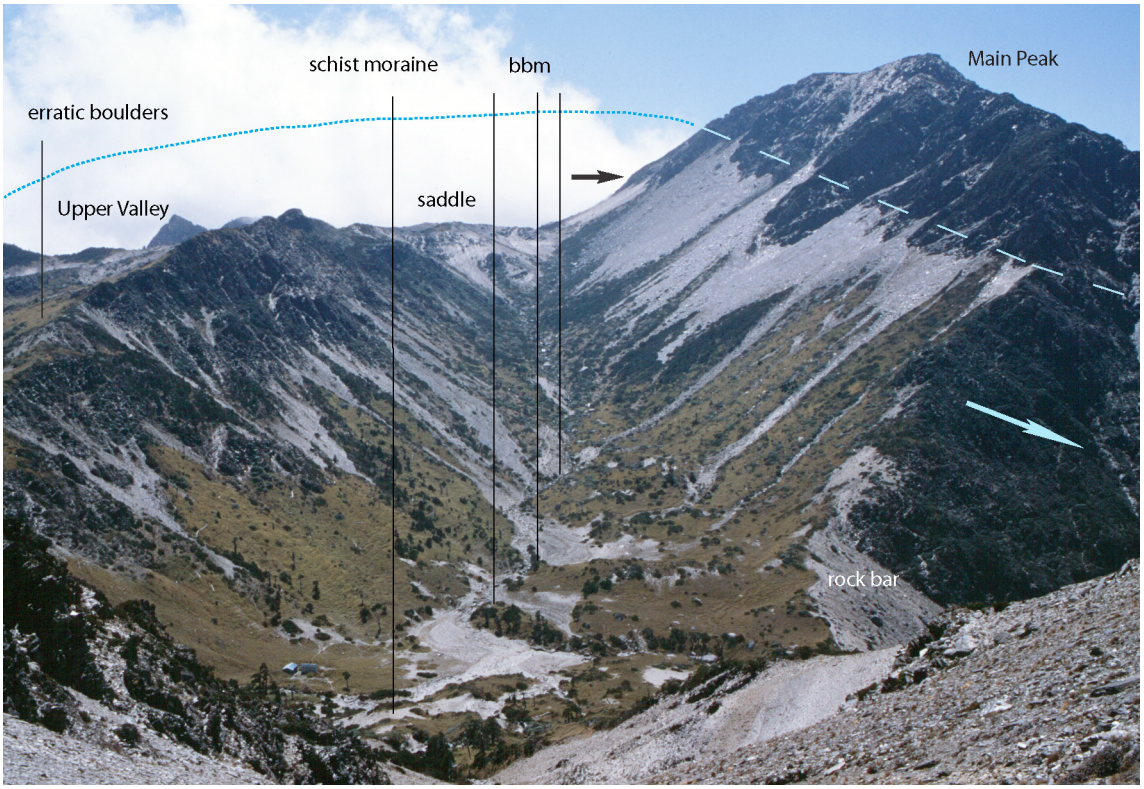

Figure 7.3: Lower Valley, Nanhuta Shan seen from North Peak (24° 22' 27.1" N, 121° 26' 30.4" E, 3592 m), facing S. 22.03.2000, modified from Hebenstreit and Böse (2003), cf. also chapter 6.

The flanks of this parabolic shaped trough valley have been abraded nearly up to the Main Peak (3742 m). The trimline at about 3600 m (- - -) is marked by a distinct difference in the rock surface structure (fig. 7.4). This indicates an almost complete ice infill in the valley of about 150 m. The valley itself is overdeepened. The ice outflow resulted rectangular over a several-meters-high bedrock bar (slate) to the W into the Nanhu XÏ). The present drainage flows through a deeply incised narrow gorge here. The bar is covered with debris, including boulders of slate and quartzite, several cubic meters in size. Similar boulders can be found on the right-hand (northern) shoulder of the outflow at about 3500 m in erratic positions (cf. chapter 4, fig. 6). They are mostly well rounded and up to 2 meters in diameter. Some show glacial striations on their lower sides.

The glacier originated on a small plateau called the saddle. An ice cap has developed here with an estimated thickness of 100 m during the maximum stage (·····). A secondary

trimline is marked by a distinct concave slope shape (*Schliffkehle,* →) above the saddle and resembles probably the early Holocene glacier stage (9.5 ka). Well preserved lateral and staggered end moraine ridges (schist moraine, big-boulder-moraines = bbm) at 3400 m did not longer reached as far as the rock bar and belong to this stage as well. Quartzitic erratic boulders of the same age are deposited on the ridge to the neighbouring Upper Valley (cf. chapter 6 for sampling sites and dating).

The present geomorphological activity is weak and characterized by a tendency to accumulation within this valley. Little frost weathering, which is limited mainly to the uppermost (> 3600 m) altitudes produces talus slopes below the Main Peak. Vegetation cover on the lower slopes indicates inactivity. Episodic discharge generates small fluvial gravel accumulation at the lowest part of the valley bottom.

Figure 7.4: Close-up of the rock surface at the trimline in the Lower Valley, Nanhuta Shan (24° 22' 07.2" N, 121° 25' 54.1" E, 3545 m), facing NNW. 26.10.2000.

The trimline is clearly recognizable between 3500 m and 3600 m on the left flank by a distinct difference in the bedrock shape (←). Below this line the slate bedrock is gently eroded. Even the outcropping slate layers are smoothly rounded. Above this zone the rock is weathered, producing a rough surface with out-splintering slate layers. Although striations are absent here, because they rarely preserve in slate (fig. 7.8), the variation in morphology between the upper and the lower parts of the slope is distinct.

Figure 7.5: SE-Valley (He Ping Nan Xi), Nanhuta Shan (24° 21' 25.2" N, 121° 27' 18.0" E, about 3300 m), facing SE. 21.03.2000, modified from Hebenstreit and Böse (2003).

This U-shaped valley trends from the saddle to SE and was almost completely ice-filled during the maximum stage of the glaciation (- - -), which is indicated by scoured flanks and nearly vertical rock cliffs. The ice thickness reached 150 m. The valley bottom is very flat here and nearly horizontal for a distance of about 1 km. With regard to the present fluvial sediment infill, the valley is certainly overdeepened by glacial erosion. The asymmetry of the valley cross section is due to the bedrock structure.

A younger glaciation stage at about 12 - 15 ka (cf. chapter 6 for exposure dating) is documented by an end moraine ridge (big-boulder-moraine, bbm), which crosses the valley at about 3200 m. Glaciofluvial sediments at its proximal side document the glacier retreat from this position (OSL age 11.1 ± 2.5 ka, cf. chapter 4).

The upper section of the valley (not visible in the vegetation covered foreground) is separated from the flat part by a steep scarp, where the bottom rock is shaped like a roche moutonnée. The river is deeply incised here forming a long and narrow gorge, which is typical for subglacial erosion (cf. geomorphological map in chapters 4 and 6).

Debris cones and talus slopes (O) indicate the dominant postglacial slope activity in this mountain area. Young slope downwash material at the left-hand side near the bottom was

dated with OSL to 3.1 ± 0.3 ka. Little present frost weathering occurs around the SE-Peak (3474 m). Modern fluvial discharge is minor and episodic in this upper valley section. It leads to gravel accumulation on the lowest part of the valley bottom.

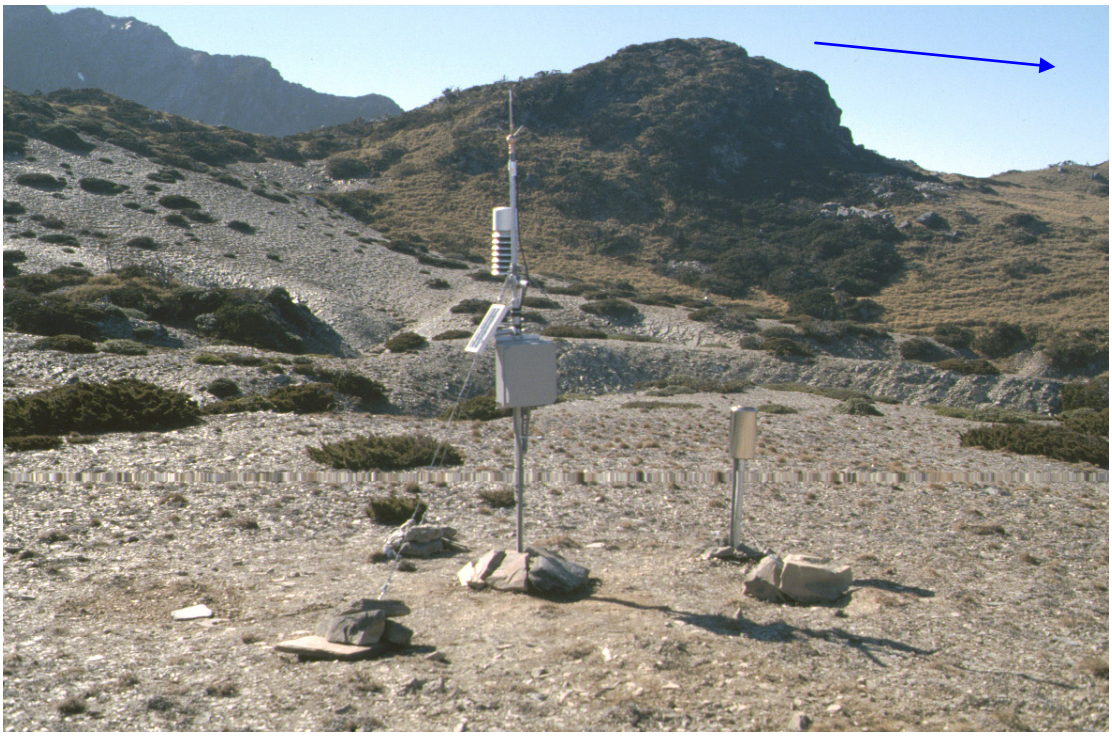

Figure 7.6: Roche moutonnée on the transition from the saddle to the ridge between the Upper and the Lower Valley and meteorological station, Nanhuta Shan (24° 21' 47.8" N, 121° 26' 48.0" E, 3550 m), facing NW. 21.03.2001.

The roche moutonnée consists of hard metamorphic sandstone (quartzite). Boulders from this site were presumably transported with the ice flow (→) to the lower parts of the valley divide, where they were deposited in erratic position (cf. fig. 7.7 and chapter 6: samples Expo1 and Expo2). The ice flow was to the right. In the foreground the meteorological station of the project is to be seen (cf. figs. 2.6 and 2.7, appendix table A2 for data and Klose, 2007 for setup).

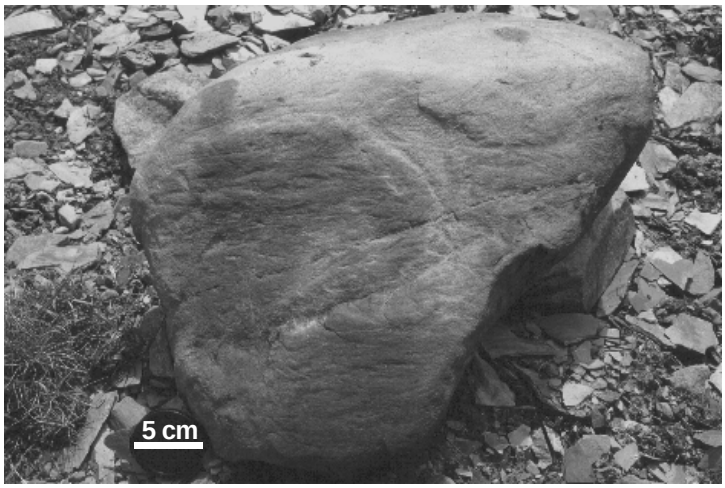

Figure 7.7: Erratic boulder. Nanhuta Shan, valley divide between Upper and Lower Valley (24° 22' 06.2" N, 121° 26' 42.8" E, about 3500 m), 20.03.2000. Modified from Hebenstreit and Böse (2003).

The rounded boulder shows typical glacial striations in various directions and a polished surface on its underside. It consists of hard quartzite, which occurs as bedrock some hundred meters from this location (cf. fig. 7.6), while the bedrock here is slate. Similar erratics are found at several locations in this area. They reach several meters in size. The boulder was turned over for the photo.

Glacial striations in slate are rarely present. Figure 7.8 shows that they can be generated indeed, but are only preserved in sheltered positions. The rock surface was uncovered from remnants of schist moraine by the author. The clasts were part of this sediment.

a) 

b) 

Figure 7.8: Glacial striations in the schist-moraine section of the Upper Valley, Nanhuta Shan (24° 22’ 24.7” N, 121° 26’ 43.9” E, 3485 m), 22.03.2001. a) striations in bedrock, b) striated schist clasts.

Figure 7.9: Shape comparison of a glacial clast from Findelen Glacier, Wallis, Switzerland (left, sampled on 11.09.2000) with a clast from the assumed glacial deposit at location Nan-NX in Nanhuta Shan (right, sampled on 24.03.2001).

The Findelen clast consists of serpentinite and was sampled from the inactive right hand lateral moraine near the glacier terminus. The Nanhu clast consists of quartzite and was directly taken from the outcrop 10 m above the present riverbed (cf. chapter 4, figs. 3 and 8, Nan-NX). The similarity of both clast shapes is notable. Both are typically sub-rounded, i.e. angular in general with faceted surfaces and rounded edges, and they are more pointed at one site (the lower end in the picture) than at the other, which is typical for glacial transport (Hambrey, 1994, p. 125). Both clasts do not show striations.

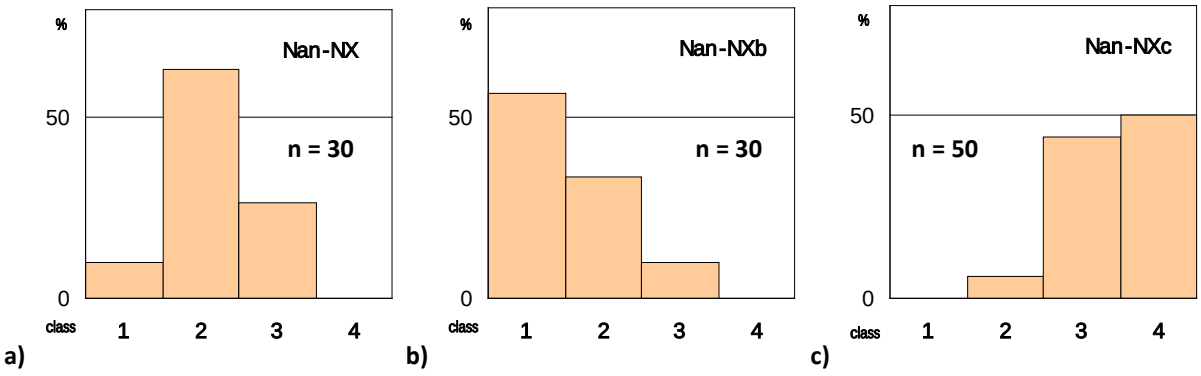

Figure 7.10: Clast roundness index of three sediment types in the Nanhu Xi in the four-class-system of Reichelt (1955, cited after Köster and Leser, 1967). a) assumed glacial deposit, b) freshly weathered slope deposit, c) fluvial clasts from the nearby river bank (cf. appendix table A6).

The assumed glacial deposit at location Nan-NX in the Nanhu Xi at 2250 m in Nanhuta Shan is clearly distinguishable from fluvial and in situ weathered material in the immediate vicinity when compared the clast roundness. Fluvial clasts are much more rounded, while

weathering material is more angular, which is not the case for glacial deposits. (cf. chapter 4, figs. 3 and 8 for picture of the sediment outcrop and fig. 2 for location).

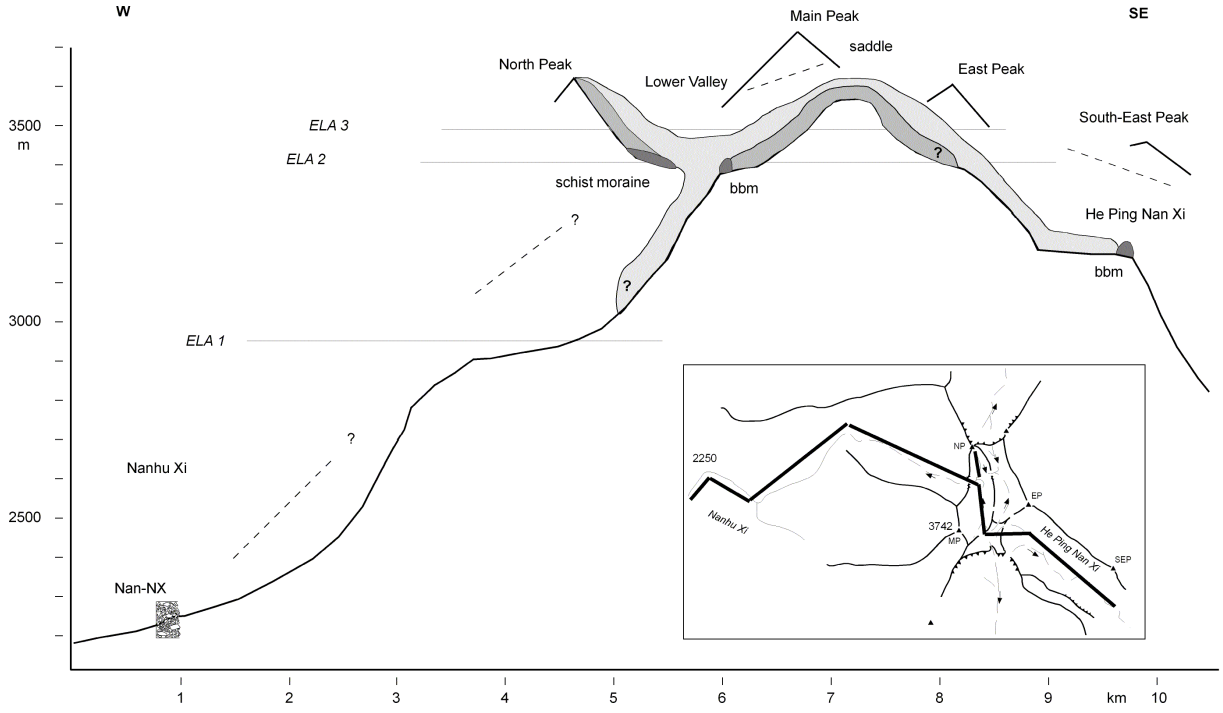

Figure 7.11: Schematic vertical profile of Nanhuta Shan with different stages of glaciation and respective equilibrium line altitudes.

Light gray shaded glaciers represent the Lateglacial stage at 12 - 15 ka (ELA 2), marked by the big-boulder-moraine (bbm) in the SE-Valley. Early Holocene glaciers (9.5 ka, ELA 3) are dark gray shaded and marked by the big-boulder-moraine and schist moraine in the Lower Valley. Broken lines below the Main and the SE-Peak indicate trimlines, which represent the glacier surface during the maximum stage of glaciation (ELA 1). Glacial deposits at location Nan-NX mark the minimum extent of the West exposed glacier in the Nanhu Xi (possibly MIS 3/4). Insert shows the course of the profile. All altitudes represent the present position, i.e. postglacial uplift is not considered in this figure.

Table 7.1: Calculation of the late Pleistocene and early Holocene equilibrium line altitudes in three Taiwanese mountain ranges (refinement of table 1, publication 2)

range	glacier	exposure	geomorph. evidence	location ID		age (1)	dating method	ELA method (2)	present theoretical ELA	summit	present summit altitude	present altitude of terminal deposits	recon-structed ELA without consi-dereing uplift	uplift since glaciation (3)	resulting ELA including uplift (4)	resulting ΔELA	chronological interpretation
						(ka)			(m)		(m)	(m)	(m)	(m)	(m)	(m)	
Nanhuta Shan																	
	Nanhu Xi	W	glacial deposits	Nan-NX	>	10	-	TSAM	3950	plateau (5)	3650	2250	2950	50	**2900**	**1050**	last glacial cycle
	SE-Valley	SE	bbm	Nan-V		13,1	^{10}Be	TSAM	3950	East peak	3630	3190	3410	65,5	**3340**	**610**	Lateglacial
	Lower Valley	N	bbm	Nan-IX		9,5	^{10}Be	TSAM	3950	plateau (6)	3600	3380	3490	47,5	**3440**	**510**	early Holocene
	Lower Valley	S	schist moraine	Nan-VII		9,5	OSL	TSAM	3950	North Peak	3590	3380	3485	47,5	**3440**	**510**	early Holocene
	Lower Valley	S	schist moraine	Nan-VII		9,5	OSL	CF	3950	North Peak	3590	-	3500	47,5	**3450**	**500**	early Holocene
	Upper Valley	S	schist moraine	Nan-II,-III		9,5	OSL	TSAM	3950	NE-Peak (7)	3560	3420	3490	47,5	**3440**	**510**	early Holocene
Yushan																	
	NE-Valley	NE/ E	boulder deposit (8)	Yu-II		?	-	TSAM	4000	Main Peak	3950	2850	3400		**3400**	**600**	min. for last gl. cycle
Hsueh Shan																	
	NE valley	NE	lateral moraine	HSU-III		55	OSL	MELM	3900	Main Peak	3890	?	3050	275	**2780**	**1120**	MIS 3/4
	NE valley	NE	lateral moraine (8)	HSU-III		55	OSL	TSAM	3900	Main Peak	3890	3050	3470	275	**3200**	**700**	MIS 3/4

(1) mean ages, cf. appendix table A8
(2) MELM – maximum elevation of lateral moraines; TSAM – terminal to summit altitudinal method; CF – cirque floor
(3) 5 mm/a, Lundberg and Dorsey (1990)
(4) rounded to 10 m
(5) plateau plus 100 m ice thickness
(6) plateau plus 50 m ice thickness
(7) estimated minimum, because of present erosion of the catchment area
(8) moraine taken as minimum glacier extent

CHAPTER 8

Concluding remarks

8.1 Excurse with a wider view: Pleistocene and Holocene glaciations and ELAs in the western Pacific and East Asian region

Japan

The Japanese mountains are not glaciated at present, but Quaternary glacial landforms and deposits are known from several high mountain ranges in central and northern Japan between 35° and 45° N latitude.

Evidence for multi-stage glaciation is reported from the Northern (3190 m), the Central (2956 m) and the Southern Japanese Alps (3192 m) in Honshu as well as from the Hidaka range (2052 m) in Hokkaido. Early research has been undertaken since the early 20th century and was summarised by Ono (1980; 1991). Recent summaries with younger results are also available (Aoki and Hasegawa, 2003; Ono et al., 2003; Sawagaki et al., 2003; Sawagaki et al., 2004; Ono et al., 2005).

Glacial evidences were also reported from mountains in northern Honshu island, but these are still controversial (Sawagaki et al., 2004). Reports on glacial evidence down to 500 m in the Northern Alps (Kerschner and Heuberger, 1997) are rejected by Japanese researchers (Ono et al., 2003). No information is found in the international literature, whether or not any glacial evidence was found on Mt. Fuji (3776 m).

Although numerous studies were undertaken in Japan, glacial deposits are still poorly known in detail, because of their limited distribution and poor preservation. Absolute (radiometric) dating is also still rare and chronologies are under debate. The classification of sub-stages reaches back to MIS 6 and is mainly based on relative correlations using morphostratigraphy in combination with tephra layers of Quaternary volcano eruptions (Sawagaki et al., 2004). However, it is generally accepted that glacier extent was larger during MIS 3/4 than during MIS 2 (Ono and Naruse, 1997; Sawagaki et al., 2004; Ono et al., 2005).

Estimates for Pleistocene ELAs in Japan are given by Ono and co-workers in several publications (Ono, 1991; Ono and Naruse, 1997; Ono et al., 2003; Ono et al., 2005). For the global

LGM they calculate around 1500 m in the Hidaka Range, 2500 m in the Northern Japanese Alps, 2700 m in the Central Japanese Alps, and 2800 m in the Southern Japanese Alps. This corresponds to an ELA depression between 1100 and 1300 m in all Japanese mountains except those located on the northern margin of the Northern Japanese Alps, where the depression is only 400 m. That phenomenon is explained with an extraordinarily low present theoretical ELA (2970 m), which is estimated at Kuranosuke Cirque at Mt. Tateyama, where a perennial snow patch exists. Here, abundant present snowfall is thought to be caused by humidity supply from the warm Tsushima current to the cold and dry winter monsoon air masses (Watanabe, 1988; Aoki and Hasegawa, 2003; Ono et al., 2005). However, the ELA was 1900 m at Mt. Tateyama during MIS 3/4 implying an ELA depression of about 1000 m. The publications referred to above also show maps with regional ELA (snowline) distribution in East Asia for the LGM with a steep ELA gradient from the Pacific Ocean to the Sea of Japan, which are, however, not comprehensible from the presented ELA data.

Since present meteorological data from high altitude stations in the Japanese Alps is lacking, Ono et al. (2005) used data from the nearest lowland weather station by using an atmospheric lapse rate to establish a present theoretical ELA. Problems associated with this method are discussed in chapter 3.8. Therefore the ELA depression values given in table 1.1 appear only as somewhat estimated.

There are also indications for a Lateglacial/ early Holocene glacial advance, which is dated with in situ produced cosmogenic ^{10}Be to 10 - 11 ka in three mountain massifs in the Northern Japanese Alps (Aoki, 2003).

Borneo/ Mt. Kinabalu (Kinabulu)

Traces of Pleistocene glaciations are reported from Mt. Kinabalu (4101 m) on the northern tip of Borneo island. Possible moraines down to 3230 m and 2835 m are identified on aerial photographs (Porter, 2001b). However, they have not been dated yet. If the higher moraines date to the LGM, the ELA would be at about 3665 m. Koopmans and Stauffer (1967) estimated a present ELA at about 4570 m, which would imply an ELA depression of 905 m. Hope (2004) noted that the ELA might have laid below 3600 m, suggested by the stripping of the summit plateau. The deglaciation of the mountain was probably completed by the end of Pleistocene as obtained from radiocarbon dated organic material near the summit (Hope, 2004).

Indonesian highlands and volcanoes

A number of volcanoes and highlands above 3000 m are situated on the Indonesian islands. Three of them (Mounts Kerinci, Semuru and Rinjani in Sumatera, Java and Lombok, respectively) exceed a possible snowline at 3450 m (Hope, 2004). However, field data is not reported. Evidence may not be preserved due to volcanic activity. Nevertheless, several of the active volcanoes might have gained or lost height during Holocene eruptions, which implies that they may have carried a smaller or larger ice cap than suggested by their present height. Reports of a more extensive glaciation with an ELA of 3100 m from the Leseur massif (3381 m) in Aceh, North Sumatera, must be treated with caution as noted by Hope (2004).

New Guinea

The mountains of New Guinea were extensively glaciated during the late Pleistocene. However, according to Prentice et al. (2005) the available glacial-geologic mapping in the highlands is at a reconnaissance level because of the remote location and the minimal aerial photo coverage. Today, small glaciers still remain on the highest mountains, mainly in the Maoke Range in the western part of the island (Papua, formerly Irian Jaya, Indonesia), including the highest peak in SE-Asia and Australia, the Puncak Jayakesuma (Mt. Jaya, Carstensz Pyramid, 4884 m, 5000 m, 5030 m)[21].

Field work at Mt. Jaya was undertaken by Hope et al. (1976). They mapped cirques and reported glacial valleys and moraines down to 1700 m giving a Pleistocene ELA at 3600 – 3700 m. Basing on their observations, a present (1972) ELA is assumed to be at 4580 m (Peterson et al., 2002). However, the present glaciers retreat considerably and the ELA rose to 4850 m in the second half of the last century (Allison and Peterson, 1976; Prentice et al., 2005). Prentice et al., (2005) argue that the Carstensz Glacier mass balance was closest to equilibrium around 1972 and the ELA of 4650 m should therefore be used for comparison with LGM conditions.

Due to its better accessibility, the eastern part of the island (Papua New Guinea, PNG) is studied in greater detail (Löffler, 1972; 1980; Porter, 2001b). Here, all glaciers vanished during the 20th century (Hope et al., 1976; Porter, 2001b; Peterson et al., 2004; Prentice et al., 2005). Löffler (1972) lists 20 mountains in PNG glaciated during the Pleistocene with a total

[21] The altitude information differs in the literature and the maps

glacier area of 600 km^2. Evidence is mainly inferred from air photos, own field work and few reports of earlier researchers. Recent reviews and assessments (Porter, 2001b; Peterson et al., 2002; Mark et al., 2005) cite this publication. Löffler calculates a Pleistocene ELA of 3500 - 3700 m for this region on the basis of the lowest position of terminal moraines and the altitude of lowest cirque floors. Adopting the value of the present ELA from the western ranges with modern glaciers (about 4600 m) and assuming some mountain uplift he concludes an ELA depression of 1000 - 1100 m.

It has been commonly assumed that the late Pleistocene maximum glaciation in New Guinea was contemporaneous with the global LGM (Porter, 2001b). However, Prentice et al. (2005) reviewed the available geological and chronological information in detail and compared it with own field observations. They noted that many moraines are build up sedimentological and morphostratigraphical more complex than previously reported, and that the earlier mapping bases on topographical information with an estimated uncertainty of ± 100 m. They also pointed, that there is very little age control of the moraine record since practically all available radiocarbon dates provide minimum-limiting ages and there is no ELA information from New Guinea that is well constrained to the LGM. Prentice et al. (2005) argue therefore ELAs during the maximum late Pleistocene glacier extent cannot be bracketed closer than 3400 - 3900 m. Since reliable dating of glacial advances is lacking, the age of the LGM in the region is estimated from the lowering of vegetation zones and treelines on the base of pollen record and radiocarbon dating (Bowler et al., 1976) at about 19 - 22 ka (Porter, 2001b; Prentice et al., 2005).

For Mt. Jaya, Prentice et al. (2005) recalculated the LGM ELA to 4050 ± 50 m using an area-altitude balance ratio model, which implies only 600 m of ELA depression. However, they do not explain the discrepancy with the lower ELA in the rest of New Guinea.

East China and Tibet

Pleistocene glacial areas on the Asian continent are reported from a small number of mountain ranges in eastern, central and southern China and from the Tibetan plateau with its eastern marginal mountain massifs.

The existence of Pleistocene glaciations East China has been explored and discussed intensively during the first half of the 20th century. However, most of the assumed glacial evidences have been refused and it is now generally assumed, that none of the mountain

ranges in SE-China south of the Yangtzekiang was glaciated (Lehmkuhl and Rost, 1993). Only four mountain ranges in central and north-eastern China have reliable glacial evidence. Detailed field mapping shows cirques and glacial deposits in the Wutai Shan (Rost, 2000), the Taibai Shan in the Qingling Shan range (Rost, 1994) and the Helan Shan (Hofmann, 1992; 1993) with ELAs at 2700 to 3300 m. Cirque floor altitudes at 2200 – 2300 m are reported from the volcanic area of Changbai Shan at the Korean border (Shi, 2002).

The closest mountain range – seen from Taiwan - with reported Pleistocene glaciations in southern China is the Gongwang Shan (Hulifang, 4344 m). This range is the most comparable one with the Taiwanese mountain ranges, because of the same latitude and similar monsoonal influence. Zhang et al. (2006) summarise Chinese reports about glacial landforms and deposits with four stages of glaciation. TL dating yielded ages for lateral and terminal moraines at around 100 ka, 41 ka, 26 - 18 ka and 12 ka. The authors also present an estimation for the modern ELA at 4700 m without giving more details. A Pleistocene ELA can be inferred at 3650 from the lowest mapped moraine (“early stage of last glaciation”). Zhang et al. (2006) also report multiple glacial successions from the nearby Diancang Shan at the transition from the Tibetan plateau to the low relief terrain in SE Asia with TL dated stages at prior about 57 ka, at 21 - 17 ka and at 11 ka. The Louji Shan in South China is mentioned as glaciated without giving any specific details neither of the evidence nor the former ELA (Shi, 1992). However, a regional correlation for the Pleistocene ELA is plausible (table 1.1).

A general trend of the Pleistocene ELA in the eastern part of China is obvious. It rose from NE (2200 m at Changbai Shan) to SW (3700 m at Diancang Shan) with decreasing latitude and increasing continental climate.

The extent of the Pleistocene glaciation on the Tibetan plateau and its bordering mountains has been discussed intensively during the last three decades. Based on a series of own field campaigns on and around the plateau, Kuhle (e.g. 1982; 1987; 1988b; 1991b; 1993; 1998; 2004; 2011) reconstructs an extensive ice sheet, which has covered the plateau nearly entirely with an implicit ELA depression of more than 1000 m in many of the bordering mountain ranges. However, numerous publications argue against an extensive ice sheet (e.g. Derbyshire et al., 1991; Shi, 1992; Hövermann et al., 1993; Lehmkuhl, 1998; Lehmkuhl et al., 1998; Zheng and Rutter, 1998; Shi, 2002), and it is stated in many available publications that this opinion is generally accepted now (e.g. Lehmkuhl and Owen, 2005; Owen et al., 2008). Chinese workers have compiled a number of maps with the probable extent of the former

glaciations across the Tibetan plateau (cited in Owen et al., 2008). Lehmkuhl and Owen (2005) and Owen et al. (2008) point out, that it is, however, unlikely that all glaciers reached their maximum extent at the same time. It is far beyond the frame of this work to evaluate in detail the data given in those publications. Therefore both versions are shown in figure 1.1, following Ehlers and Gibbard (2004).

According to ELA maps and regional cross sections (Shi, 1992; Lehmkuhl, 1998; Lehmkuhl et al., 1998; Shi, 2002; Owen and Benn, 2005) the Pleistocene ELA rose from the eastern margin of the Tibetan plateau at about 4000 m in the Minshan area towards its centre reaching 5200 m in the Tangula Shan. The ELA depression decreased from the margin (1000 m) to the centre (300 m), which is a steepening of the ELA gradient compared with the present. Kuhle (e.g. 2004) shows also an ELA at 4000 m in East Tibet, but without a significant gradient. Examples of individual mountain ranges at the eastern margin of the Tibetan plateau with published field evidence are listed in table 1.1 (Ives and Zhang, 1993; Hövermann and Lehmkuhl, 1994; Owen et al., 2005).

Beside the dispute about the maximum extent of the Tibetan glaciers, there is much discussion about the chronological correlation between local glacier advances throughout Tibet and the Himalaya. Many studies focus on some classic geographic (and relatively well accessible) areas, while others mountain ranges are much less known. Relative chronologies with local terminology base on the morphostratigraphy in individual mountain ranges and are often supported by the stage of moraine weathering, the degree of vegetation cover or the soil development (e.g. Hövermann and Lehmkuhl, 1994), but a common classification is not yet established (Lehmkuhl, 1997; Lehmkuhl and Owen, 2005). Lacking absolute dating or using radiocarbon ages from stratigraphically younger units as minimum-limiting ages, the most prominent moraines are often simply considered to be deposited during the LGM, which is not necessarily the case (see discussions in Owen et al., 2008 and Owen, 2009).

The Chinese Pleistocene stratigraphy often follows the classical Alpine classification of Penck and Brückner and is divided into four Pleistocene glaciations (Lehmkuhl and Rost, 1993). The last glacial cycle is commonly divided into two main stages, which are thought to represent the MIS 2 and 4 (summarized in Lehmkuhl and Owen, 2005). It has been suggested, that mountain glacier advances may have been asynchronous with each other and with the global LGM (Gillespie and Molnar, 1995). Furthermore, Lehmkuhl and Owen (2005) argue for

an increasing evidence that during the MIS 2 (LGM) glacier advances were limited and the ELA depression small, which confirms the results from Japan (Ono and Naruse, 1997).

Only few information is available about the extent of Lateglacial and early Holocene glacier fluctuations, mostly due to a lack of reliable dating and discontinuous moraine preservation. (Owen, 2009) reviews the available data for the entire Tibetan and Himalaya region, but information about eastern Tibet is rare.

Four Holocene glacier advances in China and Tibet are commonly classified, named "Neoglaciacion I-IV" in the earlier Chinese literature (summarised by Lehmkuhl, 1997). However, Lehmkuhl emphasizes that the chronology for this classification basing on radiocarbon ages is not well established, in particular for the early Holocene stage Neoglacial-I. Yi et al. (2008) present a compilation of recalibrated Holocene radiocarbon ages from Tibet and surrounding mountains and identify an early Holocene glacial advance at 9.4 - 8.8 ka. However, this stage is inferred from only 4 (!) individual ages at 3 sites in West Kunlun Shan, in Qilian Shan and in Hengduan Shan, which are all as far from each other as 1000 - 2000 km.

Lateglacial moraines are present in many Tibetan valleys as inferred from recent surface exposure dating. TCN ages cluster around 16 - 15 ka (Owen and Benn, 2005; Owen, 2009) including individual studies in eastern Tibet (Schäfer et al., 2002; Owen et al., 2003b; Owen et al., 2003c; Owen et al., 2003d; Owen et al., 2005). However, these authors stress the uncertainty of the dating. The same studies show examples of early Holocene glacier advances in eastern Tibet. Again, the obtained ages scatter as much as 20.3 to 7.6 ka or 17.5 to 9.0 ka on individual moraines in Qilian Shan and Laji Shan (both NE-Tibet), respectively (Owen et al., 2003c; Owen et al., 2003d). Therefore, many of the included Holocene and Lateglacial ages should be attributed to postglacial moraine degradation. Only one example with consistent early Holocene moraine ages (9.2 - 7.6 ka) is reported from Gongga Shan (Owen et al., 2005). A Younger Dryas glacial advance has never been identified in the Tibetan-Himalaya region (Owen, 2009).

The Lateglacial and early Holocene glacier extent and ELA depressions are thought to be considerably variable in different mountain areas throughout the Tibetan region. In the dryer western part the ΔELA was less than 200 m, while in the monsoonal influenced areas the ΔELA was more than 500 m (Owen, 2009). Owen et al. (2005) suggested for the Gongga Shan that Holocene glaciers may have had the same extent as the Pleistocene glaciers.

8.2 Some concluding paleoclimatic implications of the results or: Where did the snow come from?

Discussion on the data and on the results obtained in this work as well as paleoclimatic correlations are already presented in much detail in the discussion sections of the three papers. Here, the main conclusions can be summarised in a rough way as follows:

1. The high mountains of Taiwan were subject to repeated glaciations during the last glacial cycle.
2. Large scale glacio-erosional landforms indicate a last glacial ELA below 3000 m with an ELA depression of about 1000 m and a possible glacier extent down to 2000 m probably during the MIS 4.
3. No reliable glacial evidence from Taiwan can be clearly attributed to the global LGM.
4. Small scale glacial sediments yielded independently derived and reliable OSL and ^{10}Be exposure ages in Nanhuta Shan from a Lateglacial to Holocene stage with two possible sub-stages at 12 - 15 ka and 9.5 ka and ELA depressions of 610 m and 510 m, respectively.

These results correspond widely with the paleoclimatic proxies (Liew et al., 2006a) and other glacial records (Ono et al., 2004; Owen et al., 2008) from the region and confirm the picture that the maximum extent of mountain glaciation during the last glacial cycle occurred presumably asynchronous with the global LGM, rather during the MIS 4 with very cold and medium dry conditions, while during the MIS 2 the glacier extent was reduced reflecting less cold but dry conditions. Glaciers advanced in several East Asian mountains - including Taiwan - during the Lateglacial/ early Holocene, reflecting moist conditions.

This overall pattern of paleoclimatic conditions during the last glacial cycle leads to **some assorted more or less intuitive considerations** concerning the change of atmospheric circulation over Taiwan and the source of sufficient snow precipitation:

1. The present winter monsoon does not effectively contribute to precipitation in the central mountain range (cf. section 2.2). During glacial times it was reasonably colder and dryer and could not absorb moist over the exposed Asian shelves and was therefore even less effective.
2. Since the monsoon is a shallow circulation, the precipitation regime in high altitudes reflects the influence of the planetary westerly circulation, during the winter in particular.

3. During glacial times the planetary circulation belts migrated equator-wards with a general increase of the planetary and altitudinal temperature and pressure gradient, which strengthened the westerly circulation (Ono and Irino, 2004).
4. The position of its southern branch was permanently south of Tibet resulting in a persistence of the Tibetan lee convergence zone, which is today a source of effective winter precipitation in East Asia (cf. fig. 2.3) (Barry and Chorley, 1992). Its associated southern shift must have led to an all year westerly influence over Taiwan with significantly increased precipitation.
5. Therefore, the main source of snow in Taiwan during glacial times was most probably by westerly circulation transported moist, which originated somewhere over the Eurasian continent.
6. The Lateglacial to mid Holocene glacier advances in many monsoonal influenced Asian mountain ranges including Taiwan are usually attributed to the increase of insolation with an associated increase of precipitation, which resulted in snow accumulation in high altitudes and glacier advance (Owen et al., 2005) with an implicit summer accumulation regime, which is typical for present monsoonal glacier mass balance regimes (Benn and Owen, 1998).
7. Summarizing these assumptions, the atmospheric circulation over Taiwan must have changed fundamentally during glacial times. That means the climatic conditions did not change only gradually and one cannot derive a simple temperature decrease from the ELA depression in Taiwan because the precipitation pattern changed considerably in space and time.

8.3 Critical remarks on paleoclimate estimations in mountain areas inferred from ELA reconstructions and comments on future research

As stated at the beginning, the reconstruction of former glacier equilibrium lines altitudes promises a valuable tool for the comparison of climatic conditions on an interregional scale. However, summarizing the experiences of this work and reviewing the available information about Pleistocene and Holocene glaciations in the East Asian and western Pacific region, it must be stated that the knowledge about former (and present) ELAs is still associated with enormous uncertainties, although the bulk of data and the number of publications increased

during the last years. This is related to four major reasons (in modification to Owen et al., 2008):

1. The immense size of the area and the remote location of most study sites led to a patchy spatial pattern of information with spots, where rather dens data is available from and vast areas of terra incognita, into which this information is extrapolated lacking strong geological evidence. Much of the information about former glaciations is therefore derived from remote sensing data or only visual field observation. Although recently available remote sensing information has improved considerably, which enables an instant personal impression and assessment, it turned out that many of the reported evidences are hard to relocate due to inconsistent localization and terminology in the literature. So the difficulty arises to find out, which mountain range is actually referred to. Many maps from Asian mountains don't provide geographical coordinates for their localities. Altitude information and transcriptions of local names differ often considerably (cf. appendix A1 for Taiwanese transcriptions).

2. The misinterpretation of sediments and landforms is another reason. This is often due to the similarity of glacial and non-glacial deposits (cf. section 3.4 and discussion in publication 1) and their poor preservation in high mountain environments, which constitutes a major problem in humid monsoonal regions (Hövermann and Lehmkuhl, 1994; Owen et al., 2005) and in Taiwan in particular. Here it must be added, that much of the field evidence presented in the literature is not quite transparent and much of the available information is actually more interpretation than empirical data. Chinese maps are compiled from the work of scientists, who usually reported in Chinese. International available reviews often simply refer to their interpretations without giving any details of the methodology (geomorphologic, dating or ELA calculation) or the field evidence. Many recent reviews refer subsequently to the Chinese maps uncritically.

3. Although the availability of new applications like OSL and surface exposure dating has increased the number of numerical dating considerably, detailed age control of glacial evidence is still poor. Furthermore, the derived data show often substantial inconsistence and the numerical dating confuses a clear morphostratigraphical correlation in many studies as

shown e.g. for the available ages in the Himalaya and Tibet (Owen et al., 2005; Owen et al., 2008).
Again, the published data is not transparent in many cases. This concerns in particular the relationship between the sampling and the geomorphological setting, which makes it extremely difficult to assess the validity of the derived ages.

4. The ELA estimations themselves constitute an additional and probably the main source of uncertainties in paleoclimatic reconstructions as shown for the Taiwanese mountains in particular. They arise from a number of factors (Porter, 2001b): Unreliable topographical information, methodological uncertainties of reconstruction, unknown mountain uplift or subsidence, unknown orographic effects, the lack of a consistent and rigorous method of determining the modern theoretical ELA, lacking present high altitude climatological data.

Consequently, the combined topographical, geological, glaciological, chronological and climatological uncertainties in the calculation of a former ELA depression at a specific location may exceed the depression value itself by far. Reported depressions are in many (most) cases highly interpretative. Therefore, all information derived from paleo- equilibrium line studies must be evaluated and handled with great care, when used in global climate models and for the prediction of future climate change.
In agreement with Owen et al. (2008), the author wishes to state, that accurate reconstructions of former glacier extents need a framework of sedimentological and geomorphological criteria for a careful analysis and discrimination of glacial evidence. But moreover, besides a required larger **quantity** of (numerical) information it is crucial to improve the **quality** of this data by a more detailed mapping, standardized sampling protocols and a greater transparency of the derived data, which include the evaluation of all (!) relevant parameters (numerical and non-numerical) of a sample and its geomorphological and sedimentological environment.

Overall bibliography

Aerial Survey Office Forestry Bureau, 1982. Orthophoto Base Map of Taiwan 1:10,000. Topographic Department, Combined Logistics Command, Taipei City. (Chinese)

Ahlmann, H.W., 1935. Contribution to the physics of glaciers. Geographical Journal 86, 97-113.

Ahnert, F., 1996. Einführung in die Geomorphologie. Ulmer, Stuttgart, 440 pp.

Aitken, M.J., 1998. An Introduction to Optical Dating. The Dating of Quaternary Sediments by the Use of Photon-stimulated Luminescence. Oxford University Press, Oxford, 267 pp.

Alley, R.B., Meese, D.A., Shuman, C.A., Gow, A.J., Taylor, K.C., Grootes, P.M., White, J.W.C., Ram, M., Waddington, E.D., Mayewski, P.A., Zielinski, G.A., 1993. Abrupt increase in Greenland snow accumulation at the end of the Younger Dryas event. Nature 362, 527-529.

Alley, R.B., Mayewski, P.A., Sowers, T., Stuiver, M., Taylor, K.C., Clark, P.U., 1997. Holocene climatic instability: A prominent, widespread event 8200 yr ago. Geology 25 (6), 483-486.

Allison, I., Peterson, J.A., 1976. Ice areas on Mt. Jaya: Their extent and recent history. In: Hope, G.S., Peterson, J.A., Radok, U. and Allison, I. (Eds.), The equatorial glaciers of New Guinea - Results of the 1971-1973 Australian Universities' Expeditions to Irian Jaya: survey, glaciology, meteorology, biology and palaeoenvironments. A.A.Balkema, Rotterdam, pp. 27-38.

Amante, C., Eakins, B.W., 2009. ETOPO1 1 Arc-Minute Global Relief Model: Procedures, Data Sources and Analysis, NOAA Technical Memorandum NESDIS NGDC-24. National Oceanic and Atmospheric Administration, pp. 1-19.

An, Z., 2000. The history and variability of the East Asian paleomonsoon climate. Quaternary Science Reviews 19 (1-5), 171-187.

An, Z., Porter, S.C., Kutzbach, J.E., Wu, X., Wang, S., Liu, X., Li, X., Zhou, W., 2000. Asynchronos Holocene optimum of the East Asia monsoon. Quaternary Science Reviews 19 (8), 743-762.

Aoki, T., 2003. Younger Dryas Glacial Advances in Japan Dated with in situ Produced Cosmogenic Radionuclides. Transactions, Japanese Geomorphological Union 24 (1), 27-39.

Aoki, T., Hasegawa, H., 2003. Late Quaternary glaciations in the Japanese Alps controlled by sea level changes, monsoon oscillations and topography. Zeitschrift für Geomorphologie, N.F. Suppl.-Vol. 130, 195-215.

Balco, G., Stone, J.O., Lifton, N.A., Dunai, T.J., 2008. A complete and easily accessible means of calculating surface exposure ages or erosion rates from ^{10}Be and ^{26}Al measurements. Quaternary Geochronology 3 (3), 174-195.

Ballantyne, C.K., 2002. Paraglacial geomorphology. Quaternary Science Reviews 21 (18-19), 1935-2017.

Bard, E., Hamelin, B., Fairbanks, R.G., 1990. U-Th ages obtained by mass spectrometry in corals from Barbados: sea level during the past 130,000 years. Nature 346, 456 - 458.

Bard, E., 1999. Ice Age Temperatures and Geochemistry. Science 284 (5417), 1133-1134.

Barry, R.G., Chorley, R.J., 1992. Atmosphere, weather and climate. Routledge, London and New York, 392 pp.

Benn, D.I., Evans, D.J.A., 1998. Glaciers and Glaciation. Arnold, London, 760 pp.

Benn, D.I., Owen, L.A., 1998. The role of the Indian summer monsoon and the mid-latitude westerlies in Himalayan glaciation: review and speculative discussion. Journal of the Geological Society 155 (2), 353-363.

Benn, D.I., Lehmkuhl, F., 2000. Mass balance and equilibrium-line altitudes of glaciers in high-mountain environments. Quaternary International 65-66, 15-29.

Benn, D.I., Owen, L.A., 2002. Himalayan glacial sedimentary environments: a framework for reconstructing and dating the former extent of glaciers in high mountains. Quaternary International 97-98, 3-25.

Berger, A., 1988. Milankovitch Theory and climate. Reviews of Geophysics 26 (4), 624-657.

Bevington, P.R., Robinson, D.K., 1992. Data reduction and error analysis for the physical sciences. McGraw-Hill, New York, 328 pp.

Böse, M., 2000. Glacial Landforms in Taiwan and a Reinterpretation of the Last Glacial Snowline Depression. In: Slaymaker, O. (Ed.), Geomorphology, Human Activity and Global Environmental Change. Wiley, Chichester, pp. 25-41.

Böse, M., 2006. Geomorphic altitudinal zonation of the high mountains of Taiwan. Quaternary International 147 (1), 55-61.

Boulton, G.S., 1978. Boulder shapes and grain-size distributions of debris as indicators of transport paths through a glacier and till genesis. Sedimentology 25, 773–799.

Bowler, J.M., Hope, G.S., Jennings, J.N., Singh, G., Walker, D., 1976. Late Quaternary climates of Australia and New Guinea. Quaternary Research 6 (3), 359-394.

Boyle, J.S., Chen, T.-J., 1987. Synoptic aspects of the wintertime East Asian monsoon. In: Chang, C.-P. and Krishnamurti, T.N. (Eds.), Monsoon Meteorology. Oxford Monographs on Geology and Geophysics. Oxford University Press, pp. 125-160.

Bradley, R.S., 2000. Past global changes and their significance for the future. Quaternary Science Reviews 19 (1-5), 391-402.

Brown, I.M., 1990. Quaternary glaciations of New Guinea. Quaternary Science Reviews 9 (2), 273-280.

Büdel, J., 1982. Climatic geomorphology. Princeton University Press, Princeton; Guildford, 443 pp.

Byrne, T.B., Liu, C.-S., 2002. Preface: Introduction to the geology and geophysics of Taiwan. In: Byrne, T.B. and Liu, C.-S. (Eds.), Geology and Geophysics of an Arc-Continent Collision, Taiwan. Geological Society of America Special Papers, 358. The Geological Society of America, Boulder, Colorado, pp. v-vii.

Catt, J.A., 1992. Angewandte Quartärgeologie. Enke, Stuttgart, 358 pp.

Central Weather Bureau, 2011. Climate statistics, Taipei.

Chan, J.C.L., Li, C., 2004. The East Asia winter monsoon. In: Chang, C.-P. (Ed.), East Asian Monsoon. World Scientific Series on Meteorology of East Asia. World Scientific, New Jersey, pp. 54-106.

Chang, K.-T., Chiang, S.-H., Hsu, M.-L., 2007. Modeling typhoon- and earthquake-induced landslides in a mountainous watershed using logistic regression. Geomorphology 89 (3-4), 335-347.

Chemenda, A.I., Yang, R.-K., Stephan, J.-F., Konstantinovskaya, E.A., Ivanov, G.M., 2001. New results from physical modelling of arc-continent collision in Taiwan: evolutionary model. Tectonophysics 333 (1-2), 159-178.

Chen, C.-S., Chen, Y.-L., 2003. The Rainfall Characteristics of Taiwan. Monthly Weather Review 131 (7), 1323-1341.

Chen, C.-S., Chen, W.-C., Chen, Y.-L., Lin, P.-L., Lai, H.-C., 2005a. Investigation of orographic effects on two heavy rainfall events over southwestern Taiwan during the Mei-yu season. Atmospheric Research 73 (1-2), 101-130.

Chen, C.-Y., 2009. Sedimentary impacts from landslides in the Tachia River Basin, Taiwan. Geomorphology 105 (3-4), 355-365.

Chen, F., Li, J., W., Z., 1991. Loess Stratigraphy of the Lanzhou Profile and its Comparison with Deep-Sea Sediment and Ice Core Record. GeoJournal 24 (2), 201-209.

Chen, F., Yu, Z., Yang, M., Ito, E., Wang, S., Madsen, D.B., Huang, X., Zhao, Y., Sato, T., John B. Birks, H., Boomer, I., Chen, J., An, C., Wünnemann, B., 2008. Holocene moisture evolution in arid central Asia and its out-of-phase relationship with Asian monsoon history. Quaternary Science Reviews 27 (3-4), 351-364.

Chen, H., 2006. Controlling factors of hazardous debris flow in Taiwan. Quaternary International 147 (1), 3-15.

Chen, R.-F., Chan, Y.-C., Angelier, J., Hu, J.-C., Huang, C., Chang, K.-J., Shih, T.-Y., 2005b. Large earthquake-triggered landslides and mountain belt erosion: The Tsaoling case, Taiwan. Comptes Rendus Geosciences 337 (13), 1164-1172.

Chen, Y.-G., Liu, T.-K., 2000. Holocene uplift and subsidence along an active tectonic margin southwestern Taiwan. Quaternary Science Reviews 19 (9), 923-930.

Chen, Y.-G., Chen, W.-S., Wang, Y., Lo, P.-W., Liu, T.-K., Lee, J.-C., 2002. Geomorphic evidence for prior earthquakes: Lessons from the 1999 Chichi earthquake in central Taiwan. Geology 30 (2), 171-174.

Chmeleff, J., von Blanckenburg, F., Kossert, K., Jakob, D., 2010. Determination of the ^{10}Be half-life by multicollector ICP-MS and liquid scintillation counting. Nuclear Instruments and Methods in Physics Research Section B: Beam Interactions with Materials and Atoms 268 (2), 192-199.

Chu, H.T., 1987. Investigations on the Pilushan Formation in the Nanhutashan and the Chungyangchienshan area, In commemoration of Dr V.-K. Ting for his hundredth birthday. Annual Meeting of the Geological Society of China, pp. 63.

Chu, H.T., Sonic, W.L., Kuo, Y.C., 2000. New evidences of late Quaternary glacial relicts in the Nanhutashan area, Taiwan. The Symposium on Taiwan Quaternary & Workshop of the Asia Paleoenvironmental Change Project, Keelung, p. 18.

Chu, H.T., 2009. Glacial landforms and relicts in the high mountains of Taiwan. European Geosciences Union General Assembly 2009. Geophysical Research Abstracts, Vienna, p. 7083.

Clapperton, C.M., 1997. Fluctuations of local glaciers 30-8 ka BP: Overview. Quaternary International 38-39, 3-6.

Cui, Z., Yang, J., Liu, G., Wang, X., Song, G., 2000. Discovery of Quaternary glacial evidence of Snow Mountain in Taiwan, China. Chinese Science Bulletin 45 (6), 566-571.

Cui, Z., Yang, C., Liu, G., Zhang, W., Wang, S., Sung, Q., 2002. The Quaternary glaciation of Shesan Mountain in Taiwan and glacial classification in monsoon areas. Quaternary International 97-98, 147-153.

Dadson, S.J., Hovius, N., Chen, H., Dade, W.B., Hsieh, M.-L., Willett, S.D., Hu, J.-C., Horng, M.-J., Chen, M.-C., Stark, C.P., Lague, D., Lin, J.-C., 2003. Links between erosion, runoff variability and seismicity in the Taiwan orogen. Nature 426 (6967), 648-651.

Dadson, S.J., Hovius, N., Chen, H., Dade, W.B., Lin, J.-C., Hsu, M.-L., Lin, C.-W., Horng, M.-J., Chen, T.-C., Milliman, J., Stark, C.P., 2004. Earthquake-triggered increase in sediment delivery from an active mountain belt. Geology 32 (8), 733-736.

Derbyshire, E., Shi, Y., Li, J., Zheng, B., Li, S., Wang, J., 1991. Quaternary Glaciation of Tibet: The Geological Evidence. Quaternary Science Reviews 10 (6), 485-510.

Diaz, H.F., Graham, N.E., 1996. Recent changes in tropical freezing heights and the role of sea surface temperature. Nature 383 (6596), 152-155.

Domrös, M., Peng, G., 1988. The Climate of China. Springer, Berlin, Heidelberg, New York, London, 360 pp.

Dorsey, R.J., 1988. Provenance evolution and unroofing history of a modern arc-continent collision; evidence from petrography of Plio-Pleistocene sandstones, eastern Taiwan. Journal of Sedimentary Research 58 (2), 208-218.

Dreimanis, A., 1989. Tills: Their genetic terminology and classification. In: Goldthwait, R.P. and Matsch, C.L. (Eds.), Genetic Classification of Glacial Deposits. Final report of the commission on genesis and lithology of glacial Quaternary deposits of the International Union for Quaternary Research (INQUA). A.A.Balkema, Rotterdam, pp. 17-83.

Dunne, J., Elmore, D., Muzikar, P., 1999. Scaling factors for the rates of production of cosmogenic nuclides for geometric shielding and attenuation at depth on sloped surfaces. Geomorphology 27 (1-2), 3-11.

Ehlers, J., Gibbard, P.L. (Eds.), 2004. Quaternary Glaciations - Extent and Chronology, Part III: Southamerica, Asia, Africa, Australia, Antarctica. Developments in Quaternary Science, 2. Elsevier, Amsterdam, 380 pp.

Ehlers, J., Gibbard, P.L., 2007. The extent and chronology of Cenozoic Global Glaciation. Quaternary International 164-165, 6-20.

Embleton, C., King, C.A.M., 1975. Glacial geomorphology. Arnold, London, 573 pp.

Emiliani, C., 1955. Pleistocene temperatures. Journal of Geology 63, 538-578.

Eyles, N., Eyles, C.H., Miall, A.D., 1983. Lithofacies types and vertical profile models; an alternative approach to the description and environmental interpretation of glacial diamict and diamictite sequences. Sedimentology 30, 393–410.

Fachnormenausschuß Wasserwesen, 1973. Physikalische Laboruntersuchungen. DIN 19 683. Deutscher Normenausschuß (DNA), Beuth. Blatt 1-3.

Fairbanks, R.G., 1989. A 17,000-year glacio-eustatic sea level record: influence of glacial melting rates on the Younger Dryas event and deep-ocean circulation. Nature 342, 637 - 642.

Fang, J.-Q., 1991. Lake Evolution during the Past 30,000 Years in China and Its Implications for Environmental Change. Quaternary Research 36, 37-60.

Farr, T.G., Rosen, P.A., Caro, E., Crippen, R., Duren, R., Hensley, S., Kobrick, M., Paller, M., Rodriguez, E., Roth, L., Seal, D., Shaffer, S., Shimada, J., Umland, J., Werner, M., Oskin, M., Burbank, D., Alsdorf, D., 2007. The Shuttle Radar Topography Mission. Reviews of Geophysics 45, 1-33.

Fitzsimons, S.J., 1997. Late-glacial and early Holocene glacier activity in the Southern Alps, New Zealand. Quaternary International 38-39, 69-76.

Flint, R.F., 1971. Glacial and Quaternary Geology. Wiley & Sons, New York, 892 pp.

Flohn, H., 1957. Zur Kenntnis des "Monsuns" in Ostasien. Stuttgarter Geographische Studien 69, 263-275.

Florineth, D., 1998. Surface geometry of the Last Glacial Maximum (LGM) in the southeastern Swiss Alps (Graubünden) and its paleoclimatological significance. Eiszeitalter und Gegenwart 48 (1), 23-37.

Frenzel, B., Boulton, G.S., Gläser, B., Huckriede, U. (Eds.), 1997. Glacier fluctuations during the Holocene. Paläoklimaforschung, Palaeoclimate Research (Special Issue: ESF Project "European palaeoclimate and Man" 16, European Science Foundation und Akademie der Wissenschaften und der Literatur, Mainz), 24. G. Fischer, Stuttgart, 182 pp.

Fuchs, M., Owen, L.A., 2008. Luminescence dating of glacial and associated sediments: review, recommendations and future directions. Boreas 37 (4), 636-659.

Fuller, C.W., Willett, S.D., Hovius, N., Slingerland, R., 2003. Erosion Rates for Taiwan Mountain Basins: New Determinations from Suspended Sediment Records and a Stochastic Model of Their Temporal Variation. The Journal of Geology 111, 71–87.

Fuller, C.W., Willett, S.D., Fisher, D., Lu, C.Y., 2006. A thermomechanical wedge model of Taiwan constrained by fission-track thermochronometry. Tectonophysics 425 (1-4), 1-24.

Gagan, M.K., Hendy, E.J., Haberle, S.G., Hantoro, W.S., 2004. Post-glacial evolution of the Indo-Pacific Warm Pool and El Niño-Southern oscillation. Quaternary International 118-119, 127-143.

Gibbard, P.L., West, R.G., 2000. Quaternary chronostratigraphy: the nomenclature of terrestrial sequences. Boreas 29, 329-336.

Gibbard, P.L., Head, M.J., Walker, M.J.C., 2010. Formal ratification of the Quaternary System/Period and the Pleistocene Series/Epoch with a base at 2.58 Ma. Journal of Quaternary Science 25 (2), 96-102.

Gillespie, A., Molnar, P., 1995. Asynchronos Maximum advances of mountain and continental glaciers. Reviews of Geophysics 33 (3), 311-364.

GIO (Ed.), 2010. 2010 - The Republic of China Yearbook. Republic of China Government Information Office, Taipei, 553 pp.

Giosan, L., Bokuniewicz, H., Panin, N., Postolache, I., 1999. Longshore Sediment Transport Pattern along the Romanian Danube Delta Coast. Journal of Coastal Research 15 (4), 859-871.

Godfrey-Smith, D.I., Huntley, D.J., Chen, W.H., 1988. Optical dating studies of quartz and feldspar sediment extracts. Quaternary Science Reviews 7 (3-4), 373-380.

Goldthwait, R.P., Matsch, C.L. (Eds.), 1989. Genetic Classification of Glacial Deposits. Final report of the commission on genesis and lithology of glacial Quaternary deposits of the International Union for Quaternary Research (INQUA). A.A.Balkema, Rotterdam, 294 pp.

Gosse, J.C., Phillips, F.M., 2001. Terrestrial in situ cosmogenic nuclides: theory and application. Quaternary Science Reviews 20 (14), 1475-1560.

Gosse, J.C., 2005. The Contribution of Cosmogenic Nuclides to Unraveling Alpine Paleoclimate Histories. In: Huber, U.M., Bugmann, H.K.M. and Reasoner, M.A. (Eds.), Global Change and Mountain Regions - An Overview of Current Knowledge. Advances in Global Change Research, 23. Springer, Dordrecht, pp. 39-49.

Grootes, P.M., Stuiver, M., White, J.W.C., Johnsen, S., Jouzel, J., 1993. Comparison of oxygen isotope records from the GISP2 and GRIP Greenland ice cores. Nature 366, 552-554.

Gross, G., Kerschner, H., Patzelt, G., 1977. Methodische Untersuchungen über die Schneegrenze in alpinen Gletschergebieten. Zeitschrift für Gletscherkunde und Glazialgeologie 12 (2), 223-251.

Hallet, B., Putkonen, J., 1994. Surface Dating of Dynamic Landforms: Young Boulders on Aging Moraines. Science 265, 937-940.

Hambrey, M.J., 1994. Glacial environments. UCL Press, London, 296 pp.

Hanebuth, T., Stattegger, K., Grootes, P.M., 2000. Rapid Flooding of the Sunda Shelf: A Late-Glacial Sea-Level Record. Science 288 (5468), 1033-1035.

Hartge, K.H., Horn, R., 1992. Die physikalische Untersuchung von Böden. Enke, Stuttgart, 177 pp.

Hartshorn, K., Hovius, N., Dade, B.W., Slingerland, R.L., 2002. Climate-driven bedrock incision in an active mountain belt. Science 297, 2036-2038.

Hastenrath, S., 2009. Past glaciation in the tropics. Quaternary Science Reviews 28 (9-10), 790-798.

Hays, J.D., Imbrie, J., Shackleton, N.J., 1976. Variations in the Earth's Orbit: Pacemaker of the Ice Ages. Science 194 (4270), 1121-1132.

Hebenstreit, R., Böse, M., 2003. Geomorphological evidence for a Late Pleistocene glaciation in the high mountains of Taiwan dated with age estimates by optically stimulated luminescence (OSL). Zeitschrift für Geomorphologie, N.F. Suppl.-Vol. 130, 31-49.

Hebenstreit, R., 2006. Present and former equilibrium line altitudes in the Taiwanese high mountain range. Quaternary International 147 (1), 70-75.

Hebenstreit, R., Böse, M., Murray, A., 2006. Late Pleistocene and early Holocene glaciations in Taiwanese mountains. Quaternary International 147 (1), 76-88.

Hebenstreit, R., Ivy-Ochs, S., Kubik, P.W., Schlüchter, C., Böse, M., 2011. Lateglacial and early Holocene surface exposure ages of glacial boulders in the Taiwanese high mountain range. Quaternary Science Reviews 30 (3-4), 298-311.

Heisinger, B., Lal, D., Jull, A.J.T., Kubik, P., Ivy-Ochs, S., Knie, K., Nolte, E., 2002. Production of selected cosmogenic radionuclides by muons: 2. Capture of negative muons. Earth and Planetary Science Letters 200 (3-4), 357-369.

Herzschuh, U., 2006. Palaeo-moisture evolution in monsoonal Central Asia during the last 50,000 years. Quaternary Science Reviews 25 (1-2), 163-178.

Heuberger, H., 1980. Die Schneegrenze als Leithorizont in der Geomorphologie. In: Jentsch, C. (Ed.), Höhengrenzen in Hochgebirgen. Arbeiten aus dem Geographischen Institut der Universität des Saarlandes, 29, Saarbrücken, pp. 35-48.

Hewitt, K., 1999. Quaternary Moraines vs Catastrophic Rock Avalanches in the Karakoram Himalaya, Northern Pakistan. Quaternary Research 51 (3), 220-237.

Ho, C.S., 1986. A synthesis of the geologic evolution of Taiwan. Tectonophysics 125 (1-3), 1-16.

Hofmann, J., 1992. Investigations on the present and former periglacial and glacial features in Central Helan Shan (Inner Mongolia/ PR China). Zeitschrift für Geomorphologie, N.F. Suppl.-Bd. 86, 139-154.

Hofmann, J., 1993. Geomorphologische Untersuchungen zur jungquartären Klimageschichte des Helan Shan und seines westlichen Vorlandes (Autonomes Gebiet Innere Mongolei, VR China). Berliner Geographische Abhandlungen, 57, Berlin, 187 pp.

Hope, G., Kershaw, A.P., Kaars, S.v.d., Xiangjun, S., Liew, P.-M., Heusser, L.E., Takahara, H., McGlone, M., Miyoshi, N., Moss, P.T., 2004. History of vegetation and habitat change in the Austral-Asian region. Quaternary International 118-119, 103-126.

Hope, G.S., Peterson, J.A., Radok, U., Allison, I. (Eds.), 1976. The equatorial glaciers of New Guinea - Results of the 1971-1973 Australian Universities' Expeditions to Irian Jaya: survey, glaciology, meteorology, biology and palaeoenvironments. A.A.Balkema, Rotterdam, 244 pp.

Hope, G.S., 2004. Glaciation of Malaysia and Indonesia, excluding New Guinea. In: Ehlers, J. and Gibbard, P.L. (Eds.), Quaternary Glaciations - Extent and Chronology - Part III: South America, Asia, Africa, Australasia, Antarctica. Developments in Quaternary Science, Volume 2, Part 3. Elsevier, Amsterdam, pp. 211-214.

Horn, R., 2010. Physikalische Eigenschaften und Prozesse. In: Blume, H.-P. et al. (Eds.), Scheffer/ Schachtschabel: Lehrbuch der Bodenkunde. Spektrum Akademischer Verlag, Heidelberg, Berlin, pp. 171-271.

Hou, C.-S., Hu, J.-C., Ching, K.-E., Chen, Y.-G., Chen, C.-L., Cheng, L.-W., Tang, C.-L., Huang, S.-H., Lo, C.-H., 2009. The crustal deformation of the Ilan Plain acted as a westernmost extension of the Okinawa Trough. Tectonophysics 466 (3-4), 344-355.

Hövermann, J., 1985. Das System der klimatischen Geomorphologie auf landschaftskundlicher Grundlage. Zeitschrift für Geomorphologie, N.F. Suppl.-Bd. 56, 143-153.

Hövermann, J., Lehmkuhl, F., Pörtge, K.-H., 1993. Pleistocene glaciations in Eastern and Central Tibet - preliminary results of Chinese-German joint expeditions. Zeitschrift für Geomorphologie, N.F. Suppl.-Bd. 92, 85-96.

Hövermann, J., Lehmkuhl, F., 1994. Die vorzeitlichen Vergletscherungen in Ost- und Zentraltibet. Göttinger Geographische Abhandlungen 95, 71-114.

Hovius, N., Stark, C.P., Chu, H.-T., Lin, J.-C., 2000. Supply and removal of sediment in a landslide-dominated mountain belt: Central Range, Taiwan. Journal of Geology 108 (1), 73-89.

Hsieh, M.-L., Knuepfer, P.L.K., 2001. Middle-late Holocene river terraces in the Erhjen River Basin, southwestern Taiwan--implications of river response to climate change and active tectonic uplift. Geomorphology 38 (3-4), 337-372.

Hsieh, M.-L., Liew, P.-M., Hsu, M.-Y., 2004. Holocene tectonic uplift on the Hua-tung coast, eastern Taiwan. Quaternary International 115-116, 47-70.

Hsieh, M.-L., Rau, R.-J., 2009. Late Holocene coseismic uplift on the Hua-tung coast, eastern Taiwan: Evidence from mass mortality of intertidal organisms. Tectonophysics 474 (3-4), 595-609.

Hsieh, M.-L., Chyi, S.-J., 2010. Late Quaternary mass-wasting records and formation of fan terraces in the Chen-yeo-lan and Lao-nung catchments, central-southern Taiwan. Quaternary Science Reviews 29 (11-12), 1399-1418.

Hu, J.-C., Yu, S.-B., Chu, H.-T., Angelier, J., 2002. Transition tectonics of northern Taiwan induced by convergence and trench retreat. In: Byrne, T.B. and Liu, C.-S. (Eds.), Geology and Geophysics of an Arc-Continent Collision, Taiwan. Geological Society of America Special Papers, 358. The Geological Society of America, Boulder, Colorado, pp. 147-160.

Hu, J.-C., Chu, H.-T., Hou, C.-S., Lai, T.-H., Chen, R.-F., Nien, P.-F., 2006. The contribution to tectonic subsidence by groundwater abstraction in the Pingtung area, southwestern Taiwan as determined by GPS measurements. Quaternary International 147 - Morphodynamics and climate in Taiwan since the Late Pleistocene (1), 62-69.

Huang, C.-Y., Liew, P.-M., Meixun, Z., Chang, T.-C., Kuo, C.-M., Chen, M.-T., Wang, C.-H., Zheng, L.-F., 1997. Deep sea and lake records of the Southeast Asian paleomonsoons for the last 25 thousand years. Earth and Planetary Science Letters 146 (1-2), 59-72.

Huang, M.-H., Hu, J.-C., Hsieh, C.-S., Ching, K.-E., Rau, R.-J., Pathier, E., Fruneau, B., Deffontaines, B., 2006. A growing structure near the deformation front in SW Taiwan as deduced from SAR interferometry and geodetic observation. Geophysical Research Letters 33 (12), L12305.

Huang, M.-H., Hu, J.-C., Ching, K.-E., Rau, R.-J., Hsieh, C.-S., Pathier, E., Fruneau, B., Deffontaines, B., 2009. Active deformation of Tainan tableland of southwestern Taiwan based on geodetic measurements and SAR interferometry. Tectonophysics 466 (3-4), 322-334.

Ijiri, A., Wang, L., Oba, T., Kawahata, H., Huang, C.-Y., Huang, C.-Y., 2005. Paleoenvironmental changes in the northern area of the East China Sea during the past 42,000 years. Palaeogeography, Palaeoclimatology, Palaeoecology 219 (3-4), 239-261.

IPCC, 2007. Climate Change 2007: Synthesis Report. Contribution of Working Groups I, II and III to the Fourth Assessment Report of the Intergovernmental Panel on Climate Change, Intergovernmental Panel on Climate Change, Geneva, Switzerland.104 pp.

Ives, J.D., Zhang, Y., 1993. Glaciation of the Yulongxue Shan, Northwestern Yunnan province, People's Republic of China. Erdkunde 47 (3), 165-176.

Ivy-Ochs, S., 1996. The dating of rock surfaces using in situ produced ^{10}Be, ^{26}Al and ^{36}Cl, with examples from Antarctica and the Swiss Alps. Diss. ETH No. 11763 Thesis, Swiss Federal Institute of Technology, Zürich, 197 pp.

Ivy-Ochs, S., Kerschner, H., Schlüchter, C., 2007. Cosmogenic nuclides and the dating of Lateglacial and Early Holocene glacier variations: The Alpine perspective. Quaternary International 164-165, 53-63.

Ivy-Ochs, S., Kober, F., 2008. Surface exposure dating with cosmogenic nuclides. Eiszeitalter und Gegenwart 57 (1-2), 179-209.

Ivy-Ochs, S., Kerschner, H., Maisch, M., Christl, M., Kubik, P.W., Schlüchter, C., 2009. Latest Pleistocene and Holocene glacier variations in the European Alps. Quaternary Science Reviews 28 (21-22), 2137-2149.

Jarvis, A., Reuter, H.I., Nelson, A., Guevara, E., 2006. Hole-filled seamless SRTM data V3, International Centre for Tropical Agriculture (CIAT). available from http://srtm.csi.cgiar.org

Jen, C.-H., Lin, J.-C., Hsu, M.-L., Petley, D.N., 2006. Fluvial transportation and sedimentation of the Fu-shan small experimental catchments. Quaternary International 147 (1), 34-43.

Jian, Z., Wang, P., Saito, Y., Wang, J., Pflaumann, U., Oba, T., Cheng, X., 2000. Holocene variability of the Kuroshio Current in the Okinawa Trough, northwestern Pacific Ocean. Earth and Planetary Science Letters 184 (1), 305-319.

Johnsen, S.J., Clausen, H.B., Dansgaard, W., Fuhrer, K., Gundestrup, N., Hammer, C.U., Iversen, P., Jouzel, J., Stauffer, B., Steffensen, J.P., 1992. Irregular glacial interstadials recorded in a new Greenland ice core. Nature 359, 311-313.

Jou, B.J.-D., 1994. Mountain-Originated Mesoscale Precipitation System in Northern Taiwan: A Case Study 21 June 1991. Terrestrial, Atmospheric and Oceanic Sciences 5 (2), 169-197.

Kano, T., 1932. Preliminary Notes on the Morphology of the High Mountain Lands of Formosa. The Geographical Review of Japan 8 (3 & 6), 196-202, 505-520. (Japanese with English abstract)

Kaser, G., Hastenrath, S., Ames, A., 1996. Mass balance profiles on tropical glaciers. Zeitschrift für Gletscherkunde und Glazialgeologie 32, 75-81.

Kaser, G., Osmaston, H., 2002. Tropical glaciers. International hydrology series. Cambridge University Press, Cambridge; New York, 209 pp.

Kato, M., Fukusawa, H., Yasuda, Y., 2003. Varved lacustrine sediments of Lake Tougou-ike, Western Japan, with reference to Holocene sea-level changes in Japan. Quaternary International 105 (1), 33-37.

Keigwin, L.D., Boyle, E.A., 2000. Detecting Holocene changes in thermohaline circulation. Proceedings of the National Academy of Sciences of the United States of America 97 (4), 1343-1346.

Kerns, J., Wesley, B., Chen, Y.-L., Chang, M.-Y., 2010. The Diurnal Cycle of Winds, Rain, and Clouds over Taiwan during the Mei-Yu, Summer, and Autumn Rainfall Regimes. Monthly Weather Review 138 (2), 497-516.

Kerschner, H., Heuberger, H., 1997. New results on the Pleistocene Glaciation of the Japanese alps (Honshu) and the "Hettner Stein" problem - a preliminary report. Zeitschrift für Gletscherkunde und Glazialgeologie 33 (1), 1-14.

Kerschner, H., Ivy-Ochs, S., 2008. Palaeoclimate from glaciers: Examples from the Eastern Alps during the Alpine Lateglacial and early Holocene. Global and Planetary Change 60 (1-2), 58-71.

Kiefer, T., Kienast, M., 2005. Patterns of deglacial warming in the Pacific Ocean: a review with emphasis on the time interval of Heinrich event 1. Quaternary Science Reviews 24 (7-9), 1063-1081.

Kienast, M., Steinke, S., Stattegger, K., Calvert, S.E., 2001. Synchronous Tropical South China Sea SST Change and Greenland Warming During Deglaciation. Science 291 (5511), 2132-2134.

Klebelsberg, R.v., 1948. Handbuch der Gletscherkunde und Glazialgeologie, Erster Band: Allgemeiner Teil. Springer, Wien, 403 pp.

Klebelsberg, R.v., 1949. Handbuch der Gletscherkunde und Glazialgeologie, Zweiter Band: Historisch-Regionaler Teil. Springer, Wien, 408 -1028 pp.

Klose, C., 2006. Climate and geomorphology in the uppermost geomorphic belts of the Central Mountain Range, Taiwan. Quaternary International 147 (1), 89-102.

Klose, C., 2007. Rezente und vorzeitliche geomorphologische Formungs- und Prozessregionen und ihre klimatischen Rahmenbedingungen in den obersten Höhenstufen des Hochgebirges von Taiwan. Dissertation Thesis, Freie Universität, Berlin, 241 pp.

Kohl, C.P., Nishiizumi, K., 1992. Chemical isolation of quartz for measurement of in situ-produced cosmogenic nuclides. Geochimica et Cosmochimica Acta 56 (9), 3583-3587.

Konishi, K., Omura, A., Kimura, T., 1968. ^{234}U-^{230}Th Daing of Some Late Quaternary Coralline Limestones from Southern Taiwan (Formosa). Geology and Palaeontology of Southeast Asia 5, 211-224.

Koopmans, B.N., Stauffer, P.H., 1967. Glacial phenomena on Mount Kinabulu, Sabah. Malaysia Geological Survey (Borneo Region) Bulletin 8, 25-35.

Korschinek, G., Bergmaier, A., Faestermann, T., Gerstmann, U.C., Knie, K., Rugel, G., Wallner, A., Dillmann, I., Dollinger, G., von Gostomski, C.L., Kossert, K., Maiti, M., Poutivtsev, M., Remmert, A., 2010. A new value for the half-life of ^{10}Be by Heavy-Ion Elastic Recoil Detection and liquid scintillation counting. Nuclear Instruments and Methods in Physics Research Section B: Beam Interactions with Materials and Atoms 268 (2), 187-191.

Köster, E., Leser, H., 1967. Geomorphologie I. Das Geographische Seminar - Praktische Arbeitsweisen. Westermann, Braunschweig, 131 pp.

Kubik, P.W., Christl, M., 2010. ^{10}Be and ^{26}Al measurements at the Zurich 6 MV Tandem AMS facility. Nuclear Instruments and Methods in Physics Research Section B: Beam Interactions with Materials and Atoms 268 (7-8), 880-883.

Kuhle, M., 1982. Was spricht für eine pleistozäne Inlandvereisung Hochtibets? Sitzungsberichte und Mitteilungen der Braunschweigischen Wissenschaftlichen Gesellschaft Sonderheft 6 (Die 1. Chinesisch-deutsche Tibet-Expedition 1981. Braunschweig-Symposium 14.-16.4. 1982), 68-77.

Kuhle, M., 1986. Schneegrenzberechnungen und typologische Klassifikation von Gletschern anhand spezifischer Reliefparameter. Petermanns Geographische Mitteilungen 130, 41-51.

Kuhle, M., 1987. The Problem of a Pleistocene Inland Glaciation of the Northeastern Qinghai-Xizang Plateau. In: Hövermann, J. and Wang, W. (Eds.), Reports on the Northeastern Part of the Qinghai-Xizang (Tibet) Plateau by Sino- W. German Scientific Expedition, Beijing, pp. 250-315.

Kuhle, M., 1988a. Topography as a fundamental element of glacial systems. GeoJournal 17 (4), 545-568.

Kuhle, M., 1988b. Geomorphological Findings on the build-up of Pleistocene glaciation in southern Tibet and the problem of inland Ice. Results of the Shisha Pangma and Mt. Everest Expedition 1984. GeoJournal 17 (4), 457-512.

Kuhle, M., 1991a. Glazialgeomorphologie. Wissenschaftliche Buchgesellschaft, Darmstadt, 213 pp.

Kuhle, M., 1991b. Observations supporting the Pleistocene inland glaciation of High Asia. GeoJournal 25 (2-3), 133-231.

Kuhle, M., 1993. Eine Autozyklentheorie zur Entstehung und Abfolge der quartären Kalt- und Warmzeiten auf der Grundlage epirogener und glazialisostatischer Bewegungsinterferenzen im Bereich des tibetischen Hochlandes. Petermanns Geographische Mitteilungen 137, 133-152.

Kuhle, M., 1998. Reconstruction of the 2.4 million km^2 late Pleistocene ice sheet on the Tibetan Plateau and its impact on the global climate. Quaternary International 45-46, 71-108.

Kuhle, M., 2004. The High Glacial (Last Ice Age and LGM) ice cover in High and Central Asia. In: Ehlers, J. and Gibbard, P.L. (Eds.), Developments in Quaternary Science, Volume 2, Part 3. Elsevier, pp. 175-199.

Kuhle, M., 2011. The High Glacial (Last Ice Age and Last Glacial Maximum) Ice Cover of High and Central Asia, with a Critical Review of Some Recent OSL and TCN Dates. In: Ehlers, J., Gibbard, P.L. and Hughes, P.D. (Eds.), Developments in Quaternary Sciences, Volume 15. Elsevier, Amsterdam, pp. 943-965.

Kull, C., Imhof, S., Grosjean, M., Zech, R., Veit, H., 2008. Late Pleistocene glaciation in the Central Andes: Temperature versus humidity control -- A case study from the eastern Bolivian Andes (17°S) and regional synthesis. Global and Planetary Change 60 (1-2), 148-164.

Kuo, C.M., Liew, P.M., 2000. Vegetational History and Climatic Fluctuations based on Pollen Analysis of the Toushe Peat Bog, Central Taiwan Since the Last Glacial Maximum. Journal of the Geological Society of China 43 (3), 379-392.

Lai, K.-Y., Chen, Y.-G., Hung, J.-H., Suppe, J., Yue, L.-F., Chen, Y.-W., 2006. Surface deformation related to kink-folding above an active fault: Evidence from geomorphic features and co-seismic slips. Quaternary International 147 - Morphodynamics and climate in Taiwan since the Late Pleistocene (1), 44-54.

Lallemand, S., Font, Y., Bijwaard, H., Kao, H., 2001. New insights on 3-D plates interaction near Taiwan from tomography and tectonic implications. Tectonophysics 335 (3-4), 229-253.

Lan, C.-Y., Lee, T., Lee, C.W., 1990. The Rb-Sr isotopic record in Taiwan gneisses and its tectonic implication. Tectonophysics 183 (1-4), 129-143.

Lea, D.W., Pak, D.K., Spero, H.J., 2000. Climate Impact of Late Quaternary Equatorial Pacific Sea Surface Temperature Variations. Science 289 (5485), 1719-1724.

Lee, J.-C., Angelier, J., Chu, H.-T., 1997. Polyphase history and kinematics of a complex major fault zone in the northern Taiwan mountain belt: the Lishan Fault. Tectonophysics 274 (1-3), 97-115.

Lee, P.Y., 1977. Rate of the Early Pleistocene uplift in Taiwan. Memoir of the Geological Society of China 2, 71-76.

Lee, Y.-H., Chen, C.-C., Liu, T.-K., Ho, H.-C., Lu, H.-Y., Lo, W., 2006. Mountain building mechanisms in the Southern Central Range of the Taiwan Orogenic Belt -- From accretionary wedge deformation to arc-continental collision. Earth and Planetary Science Letters 252 (3-4), 413-422.

Lehmkuhl, F., Rost, K.T., 1993. Zur pleistozänen Vergletscherung Ostchinas und Nordosttibets. Petermanns Geographische Mitteilungen 137, 67-78.

Lehmkuhl, F., 1997. Late Pleistocene, Late-glacial and Holocene glacier advances on the Tibetan Plateau. Quaternary International 38-39, 77-83.

Lehmkuhl, F., 1998. Extent and spatial distribution of Pleistocene glaciations in Eastern Tibet. Quaternary International 45-46 (1), 123-134.

Lehmkuhl, F., Owen, L.A., Derbyshire, E., 1998. Late Quaternary Glacial History of Northeast Tibet. In: Owen, L.A. (Ed.), Mountain Glaciation. Quaternary Proceedings, 6. John Wiley & Sons, Chichester, pp. 121-142.

Lehmkuhl, F., Haselein, F., 2000. Quaternary paleoenvironmental change on the Tibetan Plateau and adjacent areas (Western China and Western Mongolia). Quaternary International 65-66, 121-145.

Lehmkuhl, F., Owen, L.A., 2005. Late Quaternary glaciation of Tibet and the bordering mountains: a review. Boreas 34 (2), 87-100.

Li, Y.-H., 1976. Denudation of Taiwan Island since the Pliocene Epoch. Geology 4, 105-107.

Licciardi, J.M., Schaefer, J.M., Taggart, J.R., Lund, D.C., 2009. Holocene Glacier Fluctuations in the Peruvian Andes Indicate Northern Climate Linkages. Science 325 (5948), 1677-1679.

Lichtenecker, N., 1936. Die gegenwärtige und die eiszeitliche Schneegrenze in den Ostalpen. Verhandlungen der III. Internationalen Quartär-Konferenz, Wien, pp. 141-147.

Liew, P.M., Lin, C.F., 1987. Holocene Tectonic Activity of the Hengchun Peninsula as Evidenced by the Deformation of Marine Terraces. Memoir of the Geological Society of China 9, 241-259.

Liew, P.M., Pirazzoli, P.A., Hsieh, M.L., Arnold, M., Barusseau, J.P., Fontugne, M., Giresse, P., 1993. Holocene tectonic uplift deduced from elevated shorelines, eastern Coastal Range of Taiwan. Tectonophysics 222 (1), 55-68.

Liew, P.M., Huang, S.Y., 1994. A 5000-Year Pollen Record from Chitsai Lake, Central Taiwan. Terrestrial, Atmospheric and Oceanic Sciences 5 (3), 411-419.

Liew, P.M., Kuo, C.M., Huang, S.Y., Tseng, M.H., 1998. Vegetation change and terrestrial carbon storage in eastern Asia during the Last Glacial Maximum as indicated by a new pollen record from central Taiwan. Global and Planetary Change 16-17 (1-4), 85-94.

Liew, P.M., Hsieh, M.L., Shyu, B.H., 2004. An overview of coastal development in a Young Mountain Belt-Taiwan. Quaternary International 115-116, 39-45.

Liew, P.M., Huang, S.Y., Kuo, C.M., 2006a. Pollen stratigraphy, vegetation and environment of the last glacial and Holocene--A record from Toushe Basin, central Taiwan. Quaternary International 147 (1), 16-33.

Liew, P.M., Lee, C.Y., Kuo, C.M., 2006b. Holocene thermal optimal and climate variability of East Asian monsoon inferred from forest reconstruction of a subalpine pollen sequence, Taiwan. Earth and Planetary Science Letters 250 (3-4), 596-605.

Lifton, N.A., Bieber, J.W., Clem, J.M., Duldig, M.L., Evenson, P., Humble, J.E., Pyle, R., 2005. Addressing solar modulation and long-term uncertainties in scaling secondary cosmic rays for in situ cosmogenic nuclide applications. Earth and Planetary Science Letters 239 (1-2), 140-161.

Lin, A., Ouchi, T., Chen, A., Maruyama, T., 2001. Co-seismic displacements, folding and shortening structures along the Chelungpu surface rupture zone occurred during the 1999 Chi-Chi (Taiwan) earthquake. Tectonophysics 330, 225–244.

Lin, C.-H., 1998. Tectonic implications of an aseismic belt beneath the eastern central range of Taiwan: crustal subduction and exhumation. Journal of the Geological Society of China 41 (3), 441-460.

Lin, C.-H., Roecker, S.W., 1998. Active Crustal Subduction and exhumation in Taiwan. In: Hacker, B. and Liou, J.G. (Eds.), When Continents Collide: Geodynamics and Geochemistry of Ultrhigh-Pressure Rocks. Kluwer, Dortrecht, pp. 2-16.

Lin, C.-H., 2000a. Thermal modeling of continental subduction and exhumation constrained by heat flow and seismicity in Taiwan. Tectonophysics 324 (3), 189-201.

Lin, C.-Y., Chen, C.-S., 2002. A study of orographic effects on mountain-generated precipitation systems under weak synoptic forcing. Meteorology and Atmospheric Physics 81 (1), 1-25.

Lin, J.-C., 2000b. Morphotectonic evolution of Taiwan. In: Summerfield, M.A. (Ed.), Geomorphology and Global Tectonics. Wiley, Chichester, pp. 135-146.

Lin, J.-C., Petley, D., Jen, C.-H., Koh, A., Hsu, M.-L., 2006. Slope movements in a dynamic environment - A case study of Tachia River, Central Taiwan. Quaternary International 147 - Morphodynamics and climate in Taiwan since the Late Pleistocene (1), 103-112.

Lin, J.C., 1994. An Evolutionary Model for the Coastal Range, Eastern Taiwan. In: Kirkby, M.J. (Ed.), Process Models and Theoretical Geomorphology. John Wiley & Sons, London, pp. 97-112.

Lin, K.-C., Hu, J.-C., Ching, K.-E., Angelier, J., Rau, R.-J., Yu, S.-B., Tsai, C.-H., Shin, T.-C., Huang, M.-H., 2010. GPS crustal deformation, strain rate, and seismic activity after the 1999 Chi-Chi earthquake in Taiwan. Journal of Geophysical Research 115 (B7), B07404.

Lin, M.L., Jeng, F.S., 2000. Characteristics of hazards induced by extremely heavy rainfall in Central Taiwan -- Typhoon Herb. Engineering Geology 58 (2), 191-207.

Liu, C.C., 1995. Geodetic Monitoriing of Mountain Building in Taiwan. Eos transactions, American Geophysical Union 76 (46-Suppl.), F636.

Liu, J.P., Milliman, J.D., Gao, S., Cheng, P., 2004. Holocene development of the Yellow River's subaqueous delta, North Yellow Sea. Marine Geology 209 (1-4), 45-67.

Liu, J.P., Liu, C.S., Xu, K.H., Milliman, J.D., Chiu, J.K., Kao, S.J., Lin, S.W., 2008. Flux and fate of small mountainous rivers derived sediments into the Taiwan Strait. Marine Geology 256 (1-4), 65-76.

Liu, J.P., Xue, Z., Ross, K., Wang, H.J., Yang, Z.S., Li, A.C., Gao, S., 2009. Fate of sediments delivered to the sea by Asian large rivers: Long-distance transport and formation of remote alongshore clinothems. The Sedimentary Record 7 (4), 4-9.

Liu, K.-B., Sun, S., Jiang, X., 1992. Environmental change in the Yangtze River delta since 12,000 years B.P. Quaternary Research 38 (1), 32-45.

Liu, T.-K., Hsieh, S., Chen, Y.-G., Chen, W.-S., 2001. Thermo-kinematic evolution of the Taiwan oblique-collision mountain belt as revealed by zircon fission track dating. Earth and Planetary Science Letters 186 (1), 45-56.

Liu, T.K., 1982. Tectonic implications of fission track ages from the Central Range, Taiwan. Proceedings of the Geological Society of China 25, 22-37.

Löffler, E., 1972. Pleistocene Glaciation in Papua and New Guinea. Zeitschrift für Geomorphologie, N.F. Suppl.-Bd. 13, 32-58.

Löffler, E., 1980. Neuester Stand der Quartärforschung in Neuguinea. Eiszeitalter und Gegenwart 30, 109-123.

Louis, H., 1955. Schneegrenze und Schneegrenzbestimmung. Geographisches Taschenbuch 1954/55, 414-418.

Louis, H., Fischer, K., 1979. Allgemeine Geomorphologie. Lehrbuch der allgemeinen Geographie. de Gruyter, Berlin, 814 pp.

Lundberg, N., Dorsey, R.J., 1990. Rapid Quaternary emergence, uplift, and denudation of the Coastal Range, eastern Taiwan. Geology 18 (7), 638-641.

Magny, M., Schoellammer, P., 1999. Lake-level fluctuations at le locle, Swiss Jura, from the Younger Dryas to the Mid-Holocene: A high-resolution record of climate oscillations during the final deglaciation. Géographie physique et Quaternaire 53 (2), 183-197.

Malavieille, J., Lallemand, S.E., Dominguez, S., Deschamps, A., Lu, C.-Y., Liu, C.-S., Schnuerle, P., Angelier, J., Collot, J.Y., Deffontaines, B., Fournier, M., Hsu, S.K., Le Formal, J.P., Liu, S.Y., Sibuet, J.C., Thareau, N., Wang, F., the A. C. T. Scientific Crew, 2002. Arc-continent collision in Taiwan: New marine observations and tectonic evolution. In: Byrne, T.B. and Liu, C.-S. (Eds.), Geology and Geophysics of an Arc-Continent Collision, Taiwan. Geological Society of America Special Papers, 358. The Geological Society of America, Boulder, Colorado, pp. 187-211.

Mark, B.G., Harrison, S.P., Spessa, A., New, M., Evans, D.J.A., Helmens, K.F., 2005. Tropical snowline changes at the last glacial maximum: A global assessment. Quaternary International 138-139, 168-201.

Meierding, T.C., 1982. Late Pleistocene glacial equilibrium-line altitudes in the Colorado Front Range: a comparison of methods. Quaternary Research 18 (3), 289-310.

Milankovic, M., 1941. Kanon der Erdbestrahlung und seine Anwendung auf das Eiszeitenproblem. Königl. Serb. Akad., Spez. Publ., 133, Belgrad, 633 pp.

Milliman, J.D., Lin, S.W., Kao, S.J., Liu, J.P., Liu, C.S., Chiu, J.K., Lin, Y.C., 2007. Short-term changes in seafloor character due to flood-derived hyperpycnal discharge: Typhoon Mindulle, Taiwan, July 2004. Geology 35 (9), 779-782.

Murakami, T., 1987. Effects of the Tibetan Plateau. In: Chang, C.-P. and Krishnamurti, T.N. (Eds.), Monsoon Meteorology. Oxford Monographs on Geology and Geophysics. Oxford University Press, Oxford, New York, pp. 235-270.

Murray, A.S., Marten, R., Johnston, A., Marten, P., 1987. Analysis for naturally occurring radionuclides at environmental concentrations by gamma spectrometry. Journal of Radioanalytical Nuclear Chemistry 115, 263-288.

Murray, A.S., Wintle, A.G., 2000. Luminescence dating of quartz using an improved single-aliquot regenerative-dose protocol. Radiation Measurements 32 (1), 57-73.

Murray, A.S., Olley, J.M., 2002. Precision and accuracy in the optically stimulated luminescence dating of sedimentary quartz: A status review. Geochronometria 21, 1-16.

Murray, A.S., Wintle, A.G., 2003. The single aliquot regenerative dose protocol: potential for improvements in reliability. Radiation Measurements 37 (4-5), 377-381.

Nishiizumi, K., Imamura, M., Caffee, M.W., Southon, J.R., Finkel, R.C., McAninch, J., 2007. Absolute calibration of ^{10}Be AMS standards. Nuclear Instruments and Methods in Physics Research Section B: Beam Interactions with Materials and Atoms 258 (2), 403-413.

Normenausschuß Bauwesen (NABau), 1983. Baugrund; Untersuchung von Bodenproben. Bestimmung der Korngrößenverteilung. DIN 18123. DIN Deutsches Institut für Normung e.V., Beuth. 230-241.

O'Brien, S.R., Mayewski, P.A., Meeker, L.D., Meese, D.A., Twickler, M.S., Whitlow, S.I., 1995. Complexity of Holocene Climate as Reconstructed from a Greenland Ice Core. Science 270 (5244), 1962-1964.

Oba, T., Ikehara, K., Turney, C., 2009. Palaeoceanography of the western Pacific and marginal seas. Journal of Quaternary Science 24 (8), 833-835.

Ochs, M., Ivy-Ochs, S., 1997. The chemical behavior of Be, Al, Fe, Ca and Mg during AMS target preparation from terrestrial silicates modeled with chemical speciation calculations. Nuclear Instruments and Methods in Physics Research Section B: Beam Interactions with Materials and Atoms 123 (1-4), 235-240.

Oerlemans, J., 2005. Extracting a Climate Signal from 169 Glacier Records. Science 308 (5722), 675-677.

Ohmura, A., Kasser, P., Funk, M., 1992. Climate at the equilibrium line of glaciers. Journal of Glaciology 38 (130), 397-411.

Olley, J.M., Murray, A., Roberts, R.G., 1996. The effects of disequilibria in the uranium and thorium decay chains on burial dose rates in fluvial sediments. Quaternary Science Reviews 15 (7), 751-760.

Ono, Y., 1980. Glacial and periglacial geomorphology in Japan. Progress in Physical Geography 4 (2), 149-160.

Ono, Y., 1988. Last Glacial Snowline Altitude and Paleoclimate of the Eastern Asia. The Quaternary Research 26 (3), 271-280. (Japanese with English abstract)

Ono, Y., 1991. Glacial and Periglacial Paleoenvironments in the Japanese Islands. The Quaternary Research 30 (2), 203-211.

Ono, Y., Naruse, T., 1997. Snowline elevation and eolian dust flux in the Japanese Islands during Isotope Stages 2 and 4. Quaternary International 37, 45-54.

Ono, Y., Shiraiwa, T., Dali, L., 2003. Present and last-glacial Equilibrium Line Altitudes (ELAs) in the Japanese high mountains. Zeitschrift für Geomorphologie, N.F. Suppl.-Vol. 130, 217-236.

Ono, Y., Irino, T., 2004. Southern migration of westerlies in the Northern Hemisphere PEP II transect during the Last Glacial Maximum. Quaternary International 118-119, 13-22.

Ono, Y., Shulmeister, J., Lehmkuhl, F., Asahi, K., Aoki, T., 2004. Timings and causes of glacial advances across the PEP-II transect (East-Asia to Antarctica) during the last glaciation cycle. Quaternary International 118-119, 55-68.

Ono, Y., Aoki, T., Hasegawa, H., Dali, L., 2005. Mountain glaciation in Japan and Taiwan at the global Last Glacial Maximum. Quaternary International 138-139, 79-92.

Osmaston, H., 2005. Estimates of glacier equilibrium line altitudes by the Area×Altitude, the Area×Altitude Balance Ratio and the Area×Altitude Balance Index methods and their validation. Quaternary International 138-139, 22-31.

Osmaston, H.A., 2006. Should Quaternary sea-level changes be used to correct glacier ELAs, vegetation belt altitudes and sea level temperatures for inferring climate changes? Quaternary Research 65 (2), 244-251.

Owen, L.A., 1991. Mass movement deposits in the Karakoram Mountains: their sedimentary characteristics, recognition and role in Karakoram landform evolution. Zeitschrift für Geomorphologie, N.F. 35 (4), 401-424.

Owen, L.A., Derbyshire, E., Fort, M., 1998. The Quaternary Glacial History of the Himalaya. In: Owen, L.A. (Ed.), Mountain Glaciation. Quaternary Proceedings, 6. John Wiley & Sons, Chichester, pp. 91-120.

Owen, L.A., Derbyshire, E., Scott, C.H., 2003a. Contemporary sediment production and transfer in high-altitude glaciers. Sedimentary Geology 155 (1-2), 13-36.

Owen, L.A., Finkel, R.C., Haizhou, M., Spencer, J.Q., Derbyshire, E., Barnard, P.L., Caffee, M.W., 2003b. Timing and style of Late Quaternary glaciation in northeastern Tibet. Geological Society of America Bulletin 115 (11), 1356-1364.

Owen, L.A., Haizhou, M., Derbyshire, E., Spencer, J.Q., Bernard, P.L., Nian, Z.Y., Finkel, R.C., Caffee, M.W., 2003c. The timing and style of Quaternary glaciation in the La Ji Mountains, NE Tibet: evidence for restricted glaciation during the latter part of the Last Glacial. Zeitschrift für Geomorphologie, N.F. Suppl.-Vol. 130, 263-276.

Owen, L.A., Spencer, J.Q., Haizhou, M.A., Barnard, P.L., Derbyshire, E., Finkel, R.C., Caffee, M.W., Nian, Z.Y., 2003d. Timing of Late Quaternary glaciation along the southwestern slopes of the Qilian Shan, Tibet. Boreas 32 (2), 281-291.

Owen, L.A., Benn, D.I., 2005. Equilibrium-line altitudes of the Last Glacial Maximum for the Himalaya and Tibet: an assessment and evaluation of results. Quaternary International 138-139, 55-78.

Owen, L.A., Finkel, R.C., Barnard, P.L., Haizhou, M., Asahi, K., Caffee, M.W., Derbyshire, E., 2005. Climatic and topographic controls on the style and timing of Late Quaternary glaciation throughout Tibet and the Himalaya defined by ^{10}Be cosmogenic radionuclide surface exposure dating. Quaternary Science Reviews 24 (12-13), 1391-1411.

Owen, L.A., Caffee, M.W., Finkel, R.C., Seong, Y.B., 2008. Quaternary glaciation of the Himalayan–Tibetan orogen. Journal of Quaternary Science 23 (6-7), 513-531.

Owen, L.A., 2009. Latest Pleistocene and Holocene glacier fluctuations in the Himalaya and Tibet. Quaternary Science Reviews 28 (21-22), 2150-2164.

Panzer, W., 1935. Eiszeitspuren auf Formosa. Zeitschrift für Gletscherkunde 23 (1-3), 81-91.

Peng, T.H., Li, Y.H., Wu, F.T., 1977. Tectonic uplift rates of the Taiwan island since the early Holocene. Memoir of the Geological Society of China 2, 57-69.

Penk, A., Brückner, E., 1901-1909. Die Alpen im Eiszeitalter, 3 Vol., Leipzig, 1199 pp.

Peterse, F., Prins, M.A., Beets, C.J., Troelstra, S.R., Zheng, H., Gu, Z., Schouten, S., Damsté, J.S.S., 2011. Decoupled warming and monsoon precipitation in East Asia over the last deglaciation. Earth and Planetary Science Letters 301 (1-2), 256-264.

Peterson, J., Hope, G., Prentice, M., Hantoro, W., 2002. Mountain environments in New Guinea and the Last Glacial Maximum 'Warm Seas/ Cold Mountains' Enigma in the West Pacific Warm Pool Region. In: Kershaw, P., David, B., Tapper, N., Penny, D. and Brown, J. (Eds.), Bridging Wallace's Line: The Environmental and Cultural History and Dynamics of the SE-Asian-Australian Region. Advances in Geoecology, 34. Catena, Reiskirchen, pp. 173-188.

Peterson, J.A., Chandra, S., Lundberg, C., 2004. Landforms from the Quaternary glaciation of Papua New Guinea: an overview of ice extent during the Last Glacial Maximum. In: Ehlers, J. and Gibbard, P.L. (Eds.), Quaternary Glaciations - Extent and Chronology - Part III: South America, Asia, Africa, Australasia, Antarctica. Developments in Quaternary Science, Volume 2, Part 3. Elsevier, Amsterdam, pp. 313-319.

Porter, S.C., An, Z., 1995. Correlation between climate events in the North Atlantic and China during the last glaciation. Nature 135 (5), 305-308.

Porter, S.C., 2001a. Chinese loess record of monsoon climate during the last glacial-interglacial cycle. Earth-Science Reviews 54 (1-3), 115-128.

Porter, S.C., 2001b. Snowline depression in the tropics during the Last Glaciation. Quaternary Science Reviews 20 (10), 1067-1091.

Porter, S.C., 2005. Pleistocene snowlines and glaciation of the Hawaiian Islands. Quaternary International 138-139, 118-128.

Prentice, M.L., Hope, G.S., Maryunani, K., Peterson, J.A., 2005. An evaluation of snowline data across New Guinea during the last major glaciation, and area-based glacier snowlines in the Mt. Jaya region of Papua, Indonesia, during the Last Glacial Maximum Quaternary International 138-139, 93-117.

Prescott, J.R., Hutton, J.T., 1994. Cosmic ray contributions to dose rates for luminescence and ESR dating: Large depths and long-term time variations. Radiation Measurements 23 (2-3), 497-500.

Preusser, F., Degering, D., Fuchs, M., Hilgers, A., Kadereit, A., Klasen, N., Krbetschek, M., Richter, D., Spencer, J.Q.G., 2008. Luminescence dating: basics, methods and applications. Eiszeitalter und Gegenwart 57 (1-2), 95-149.

Rasmussen, S.O., Andersen, K.K., Svensson, A.M., Steffensen, J.P., Vinther, B.M., Clausen, H.B., Siggaard-Andersen, M.-L., Johnsen, S.J., Larsen, L.B., Dahl-Jensen, D., Bigler, M., Röthlisberger, R., Fischer, H.,

Goto-Azuma, K., Hansson, M.E., Ruth, U., 2006. A new Greenland ice core chronology for the last glacial termination. Journal of Geophysical Research 111 (D06102), 1-16.

Rasmussen, S.O., Vinther, B.M., Clausen, H.B., Andersen, K.K., 2007. Early Holocene climate oscillations recorded in three Greenland ice cores. Quaternary Science Reviews 26 (15-16), 1907-1914.

Reuther, A.U., Ivy-Ochs, S., Heine, K., 2006. Application of surface exposure dating in glacial geomorphology and the interpretation of moraine ages. Zeitschrift für Geomorphologie, N.F. Suppl.-Vol. 142, 335-359.

Richards, B.W.M., 2000. Luminescence dating of Quaternary sediments in the Himalaya and High Asia: a practical guide to its use and limitations for constraining the timing of glaciation. Quaternary International 65-66, 49-61.

Rohling, E.J., Liu, Q.S., Roberts, A.P., Stanford, J.D., Rasmussen, S.O., Langen, P.L., Siddall, M., 2009. Controls on the East Asian monsoon during the last glacial cycle, based on comparison between Hulu Cave and polar ice-core records. Quaternary Science Reviews 28 (27-28), 3291-3302.

Rost, K.T., 1994. Paleoclimatic field studies in and along the Qinling Shan (Central China). GeoJournal 34 (1), 107-120.

Rost, K.T., 2000. Pleistocene paleoenvironmental changes in the high mountain ranges in central China and adjacent regions. Quaternary International 65/66, 147-160.

Ru, J.-C., 2000. The production of Photo Base map in Taiwan, 21st Asian Conference on Remote Sensing. Asian Association of Remote Sensing, Taipei.

Ryu, E., Yi, S., Lee, S.-J., 2005. Late Pleistocene-Holocene paleoenvironmental changes inferred from the diatom record of the Ulleung Basin, East Sea (Sea of Japan). Marine Micropaleontology 55 (3-4), 157-182.

Sawagaki, T., Iwasaki, S., Nakamura, T., Hirakawa, K., 2003. Late Quaternary glaciation in the Hidaka Mountain range, Hokkaido, northernmost Japan: its chronology and deformation till. Zeitschrift für Geomorphologie, N.F. Suppl.-Vol. 130, 237-262.

Sawagaki, T., Aoki, T., Hasegawa, H., Iwasaki, S., Iwata, S., Hirakawa, K., 2004. Late Quaternary glaciations in Japan. In: Ehlers, J. and Gibbard, P.L. (Eds.), Quaternary Glaciations - Extent and Chronology - Part III: South America, Asia, Africa, Australasia, Antarctica. Developments in Quaternary Science, Volume 2, Part 3. Elsevier, Amsterdam, pp. 217-225.

Schäfer, J.M., Tschudi, S., Zhao, Z., Wu, X., Ivy-Ochs, S., Wieler, R., Baur, H., Kubik, P.W., Schluchter, C., 2002. The limited influence of glaciations in Tibet on global climate over the past 170 000 yr. Earth and Planetary Science Letters 194 (3-4), 287-297.

Schaller, M., Hovius, N., Willett, S.D., Ivy-Ochs, S., Synal, H.A., Chen, M.C., 2005. Fluvial bedrock incision in the active mountain belt of Taiwan from in situ-produced cosmogenic nuclides. Earth Surface Processes and Landforms 30 (8), 955-971.

Schulz, G., 2002. Remote Sensing Data and Their Use in Updating Thematic Maps of Pleistocene Climate Elements and Glaciation Boundaries. In: Yang, X. (Ed.), Desert and Alpine Environments: Advances in Geomorphology and Palaeoclimatology. China Ocean Press, Beijing, pp. 100-111.

Seno, T., 1977. The instantaneous rotation vector of the Philippine sea plate relative to the Eurasian plate. Tectonophysics 42 (2-4), 209-226.

Shackleton, N.J., Opdyke, N.D., 1973. Oxygen isotope and palaeomagnetic stratigraphy of Equatorial Pacific core V28-238: Oxygen isotope temperatures and ice volumes on a 105 year and 106 year scale. Quaternary Research 3 (1), 39-55.

Shi, Y., 1989. Discussion on the reconstruction of paleosnowline during glacial period. In: Shi, Y. (Ed.), Problems on Quaternary Glaciation and Environments in Eastern China. Science Press, Beijing, pp. 363–374.

Shi, Y., 1992. Glaciers and glacial geomorphology in China. Zeitschrift für Geomorphologie, N.F. Suppl.-Bd. 86, 51-63.

Shi, Y., Zheng, B., Li, S., 1992. Last glaciation and maximum glaciation in the Qinghai-Xizang (Tibet) Plateau: A controversy to M. Kuhles ice sheet hypothesis. Zeitschrift für Geomorphologie, N.F. Suppl.-Bd. 84, 19-35.

Shi, Y., 2002. Characteristics of late Quaternary monsoonal glaciation on the Tibetan Plateau and in East Asia. Quaternary International 97-98, 79-91.

Siame, L., Chu, H.T., Carcaillet, J., Bourles, D., Braucher, R., Lu, W.C., Angelier, J., Dussouliez, P., 2007. Glacial retreat history of Nanhuta Shan (north-east Taiwan) from preserved glacial features: the cosmic ray exposure perspective. Quaternary Science Reviews 26 (17-18), 2185-2200.

Siame, L.L., Angelier, J., Chen, R.F., Godard, V., Derrieux, F., Bourlès, D.L., Braucher, R., Chang, K.J., Chu, H.T., Lee, J.C., 2011. Erosion rates in an active orogen (NE-Taiwan): A confrontation of cosmogenic measurements with river suspended loads. Quaternary Geochronology 6 (2), 246-260.

Sibuet, J.-C., Hsu, S.-K., 2004. How was Taiwan created? Tectonophysics 379 (1-4), 159-181.

Stauffer, P.H., 1968. Glaciation of Mt. Kinabulu. Geological Society of Malaysia Bulletin 1 (63).

Stone, J.O., 2000. Air pressure and cosmogenic isotope production. Journal of Geophysical Research 105 (B10), 23,753–23,760.

Stott, L., Poulsen, C., Lund, S., Thunell, R., 2002. Super ENSO and Global Climate Oscillations at Millennial Time Scales. Science 297 (5579), 222-226.

Sudgen, D.E., John, B.S., 1976. Glaciers and landscape. A Geomorphological Approach. Arnold, London, 376 pp.

Sun, X., Li, X., Luo, Y., Chen, X., 2000. The vegetation and climate at the last glaciation on the emerged continental shelf of the South China Sea. Palaeogeography, Palaeoclimatology, Palaeoecology 160 (3-4), 301-316.

Suppe, J., 1981. Mechanics of mountain building and metamorphism in Taiwan. Memoir of the Geological Society of China 4, 67-89.

Suppe, J., 1984. Kinematics of arc-continent collision. flipping of subduction, and back-arc spreading near Taiwan. Memoir of the Geological Society of China 6, 21-33.

Takahara, H., Igarashi, Y., Hayashi, R., Kumon, F., Liew, P.-M., Yamamoto, M., Kawai, S., Oba, T., Irino, T., 2010. Millennial-scale variability in vegetation records from the East Asian Islands: Taiwan, Japan and Sakhalin. Quaternary Science Reviews 29 (21-22), 2900-2917.

Tanaka, K., Kano, T., 1934. Glacial topographies in the Nankotaizan Mountain group in Taiwan. The Geographical Review of Japan 10 (3), 169-190. (Japanese)

Tao, S., Chen, L., 1987. A review of recent research on the East Asian summer monsoon in China. In: Chang, C.-P. and Krishnamurti, T.N. (Eds.), Monsoon Meteorology. Oxford Monographs on Geology and Geophysics. Oxford University Press, Oxford, New York, pp. 60-92.

Teng, L.S., 1990. Geotectonic evolution of late Cenozoic arc-continent collision in Taiwan. Tectonophysics 183 (1-4), 57-76.

Teng, L.S., 1996. Extensional collapse of the northern Taiwan mountain belt. Geology 24 (10), 949-952.

Thunell, R., Anderson, D., Gellar, D., Miao, Q., 1994. Sea-Surface Temperature Estimates for the Tropical Western Pacific during the Last Glaciation and Their Implications for the Pacific Warm Pool. Quaternary Research 41, 255-264.

Thunell, R.C., Miao, Q., 1996. Sea Surface Temperature of the Western Equatorial Pacific Ocean during the Younger Dryas. Quaternary Research 46 (1), 72-77.

Tietze, W., Domrös, M., 1987. The Climate of China. GeoJournal 14 (2), 265-266.

Topographic Department Combined Logistics Command, 1995. Topographic Map of Taiwan 1:50,000 Taipei City. (Chinese)

Troll, C., 1973. High mountain belts between the polar caps and the equator: Their definition and lower limit. Arctic and Alpine Research 5 (3, Pt. 2), A19-A27.

Tucker, M., 1996. Methoden der Sedimentologie. Enke, Stuttgart, 366 pp.

Ujiie, H., Ujiie, Y., 1999. Late Quaternary course changes of the Kuroshio Current in the Ryukyu Arc region, northwestern Pacific Ocean. Marine Micropaleontology 37 (1), 23-40.

Vinther, B.M., Clausen, H.B., Johnsen, S.J., Rasmussen, S.O., Andersen, K.K., Buchardt, S.L., Dahl-Jensen, D., Seierstad, I.K., Siggaard-Andersen, M.-L., Steffensen, J.P., Svensson, A., Olsen, J., Heinemeier, J., 2006. A synchronized dating of three Greenland ice cores throughout the Holocene. Journal of Geophysical Research 111 (D13102).

Vita-Finzi, C., Lin, J.-C., 1998. Serial reverse and strike slip on imbricate faults: The Coastal Range of east Taiwan. Geology 26 (3), 279-281.

Wagner, F., Aaby, B., Visscher, H., 2002. Rapid atmospheric CO_2 changes associated with the 8,200-years-B.P. cooling event. Proceedings of the National Academy of Sciences of the United States of America 99 (19), 12011-12014.

Wagner, G.A., 1995. Altersbestimmung von jungen Gesteinen und Artefakten. Physikalische und chemische Uhren in Quartärgeologie und Archäologie. Enke, Stuttgart, 277 pp.

Wang, B., Li, T., 2004. East Asian monsoon - ENSO interactions. In: Chang, C.-P. (Ed.), East Asian Monsoon. World Scientific Series on Meteorology of East Asia. World Scientific, New Jersey, pp. 177-212.

Wang, C.-H., Burnett, W.C., 1990. Holocene Mean Uplift Rates Across an Active Plate-Collision Boundary in Taiwan. Science 248 (4952), 204-206.

Wang, C.-Y., Shin, T.-C., 1998. Illustrating 100 Years of Taiwan Seismicity. Terrestrial, Atmospheric and Oceanic Sciences 9 (4), 589-614.

Wang, J.-H., Lee, M.-F., 2000. Geologic Map of Taiwan 1:500,000. Chen, C.-H. et al. (Eds.). Central Geological Survey, Ministry of Economic Affairs, Taipei

Wang, P., 1999. Response of Western Pacific marginal seas to glacial cycles: paleoceanographic and sedimentological features. Marine Geology 156 (1-4), 5-39.

Wang, Y., Cheng, H., Edwards, R.L., Kong, X., Shao, X., Chen, S., Wu, J., Jiang, X., Wang, X., An, Z., 2008. Millennial- and orbital-scale changes in the East Asian monsoon over the past 224,000 years. Nature 451 (7182), 1090-1093.

Wang, Y.J., Cheng, H., Edwards, R.L., An, Z.S., Wu, J.Y., Shen, C.C., Dorale, J.A., 2001. A High-Resolution Absolute-Dated Late Pleistocene Monsoon Record from Hulu Cave, China. Science 294 (5550), 2345-2348.

Watanabe, T., 1988. Studies of snow accumulation and ablation on perennial snow patches in the mountains of Japan. Progress in Physical Geography 12 (4), 560-581.

Wei, K.-Y., 2002. Environmental changes during the late Quaternary in Taiwan and adjacent seas: an overview of recent results of the past decade (1990-2000). Western Pacific Earth Sciences 2 (2), 149-160.

Wenske, D., Böse, M., Frechen, M., Lüthgens, C., 2011. Late Holocene mobilisation of loess-like sediments in Hohuan Shan, high mountains of Taiwan. Quaternary International 234 (1-2), 174-181.

Wenske, D., Jen, C.-H., Böse, M., Lin, J.-C., in press. Assessment of sediment delivery from successive erosion on stream-coupled hillslopes via a time series of topographic surveys in the central high mountain range of Taiwan. Quaternary International In Press, Corrected Proof.

Whipple, K.X., Kirby, E., Brocklehurst, S.H., 1999. Geomorphic limits to climate-induced increases in topographic relief. Nature 401 (6748), 39-43.

Wintle, A.G., Murray, A.S., 2006. A review of quartz optically stimulated luminescence characteristics and their relevance in single-aliquot regeneration dating protocols. Radiation Measurements 41 (4), 369-391.

Wu, C.-H., Chen, S.-C., 2009. Determining landslide susceptibility in Central Taiwan from rainfall and six site factors using the analytical hierarchy process method. Geomorphology 112 (3-4), 190-204.

Wu, C.C., Kuo, Y.H., 1999. Typhoons affecting Taiwan: Current understanding and future challenges. Bulletin of the American Meteorological Society 80 (1), 67-80.

Xiang, R., Sun, Y., Li, T., Oppo, D.W., Chen, M., Zheng, F., 2007. Paleoenvironmental change in the middle Okinawa Trough since the last deglaciation: Evidence from the sedimentation rate and planktonic foraminiferal record. Palaeogeography, Palaeoclimatology, Palaeoecology 243 (3-4), 378-393.

Xiao, J.L., An, Z.S., Liu, T.S., Inouchi, Y., Kumai, H., Yoshikawa, S., Kondo, Y., 1999. East Asian monsoon variation during the last 130,000 Years: evidence from the Loess Plateau of central China and Lake Biwa of Japan. Quaternary Science Reviews 18 (1), 147-157.

Xiao, S., Li, A., Liu, J.P., Chen, M., Xie, Q., Jiang, F., Li, T., Xiang, R., Chen, Z., 2006. Coherence between solar activity and the East Asian winter monsoon variability in the past 8000 years from Yangtze River-derived mud in the East China Sea. Palaeogeography, Palaeoclimatology, Palaeoecology 237 (2-4), 293-304.

Xu, D., Lu, H., Wu, N., Liu, Z., 2010. 30 000-Year vegetation and climate change around the East China Sea shelf inferred from a high-resolution pollen record. Quaternary International 227 (1), 53-60.

Yang, C., Cui, Z., Wang, S., Sung, Q., 1998. Relicts of the Last Glacial Maximum in Shesan Area. The Symposium on Taiwan Quaternary 7. Proceedings, pp. 8-12.

Yang, C.F., 2000. The Study of Glacial Relicts in Shesan Peak During the Last Glaciation. PhD Thesis, National Taiwan University, Taipei, 256 pp. (Chinese with English abstract)

Yao, Y., Harff, J., Meyer, M., Zhan, W., 2009. Reconstruction of paleocoastlines for the northwestern South China Sea since the Last Glacial Maximum. Science in China Series D: Earth Sciences 52 (8), 1127-1136.

Yi, C., Chen, H., Yang, J., Liu, B., Fu, P., Liu, K., Li, S., 2008. Review of Holocene glacial chronologies based on radiocarbon dating in Tibet and its surrounding mountains. Journal of Quaternary Science 23 (6-7), 533-543.

Yu, S.-B., Liu, C.-C., 1989. Fault creep on the central segment of the Longitudinal Valley fault, eastern Taiwan. Proceedings of the Geological Society of China 32, 209-231.

Yu, S.-B., Chen, H.-Y., Kuo, L.-C., 1997. Velocity field of GPS stations in the Taiwan area. Tectonophysics 274 (1-3), 41-59.

Yu, S.-B., Kuo, L.-C., 2001. Present-day crustal motion along the Longitudinal Valley Fault, eastern Taiwan. Tectonophysics 333 (1-2), 199-217.

Yuan, D., Cheng, H., Edwards, R.L., Dykoski, C.A., Kelly, M.J., Zhang, M., Qing, J., Lin, Y., Wang, Y., Wu, J., Dorale, J.A., An, Z., Cai, Y., 2004. Timing, Duration, and Transitions of the Last Interglacial Asian Monsoon. Science 304 (5670), 575-578.

Zhang, W., Cui, Z., Li, Y., 2006. Review of the timing and extent of glaciers during the last glacial cycle in the bordering mountains of Tibet and in East Asia. Quaternary International 154-155, 32-43.

Zheng, B., Rutter, N., 1998. On the problem of Quaternary Glaciations, and the extent and patterns of Pleistocene Ice Cover in the Qinghai-Xizang (Tibet) Plateau. Quaternary International 45-46, 109-122.

Zhou, H., Zhao, J., Feng, Y., Gagan, M.K., Zhou, G., Yan, J., 2008. Distinct climate change synchronous with Heinrich event one, recorded by stable oxygen and carbon isotopic compositions in stalagmites from China. Quaternary Research 69 (2), 306-315.

Zhou, W., Donahue, D.J., Porter, S.C., Jull, T.A., Li, X., Stuiver, M., An, Z., 1996. Variability of Monsoon Climate in East Asia at the End of the Last Glaciation. Quaternary Research 46 (3), 219-229.

Zhou, W., Head, M.J., Deng, L., 2001. Climate changes in northern China since the late Pleistocene and its response to global change. Quaternary International 83-85, 285-292.

Appendix

Table A1: Transcription of selected Taiwanese geographical units mentioned in the text

Romanised name	Taiwanese Characters	Pinying transciption	other commonly used transcriptions or translations	region/ range	description
3-6-9 hut	三六九山莊	Sān liù jiǔ shān zhuāng		Hsueh Shan	mountain hut
Alishan	阿里山	A lǐ shān		Ali Shan	summit/ mountain range
Ba Tong Guan	八通關	Bā tōng guān	Pa Tung Kuan	Yushan	pass
Central Mountain Range	中央山脈	Zhōng yāng shān mài	Backbone Range	Taiwan	mountain range
Chi Chi earthquake	集集大地震	Jíjí dà dì zhèn		Taiwan	earthquake
Chichiawan Xi	七家灣溪	Qī jiā wān xī	NE-Valley	Hsueh Shan	valley/ river
Chika hut	七卡山莊	Qī kǎ shān zhuāng		Hsueh Shan	mountain hut
Chitsai lake	七彩湖	Qī cǎi hù		Taiwan	lake
Choshui Xi	濁水溪	Chúo shuǐ xī		Taiwan	valley/ river
He Ping Bei Xi	和平北溪	Hé píng běi xī	North Valley	Nanhuta Shan	valley/ river
He Ping Nan Xi	和平南溪	Hé píng nán xī	SE-Valley	Nanhuta Shan	valley/ river
He Ping Xi	和平溪	Hé píng xī	Hoping River	Taiwan	valley/ river
Hengchun	恆春	Héng chūn		Taiwan	peninsula
Hohuan Shan	合歡山	Hé huān shān		Hohuan Shan	mountain range
Hsueh Shan	雪山	Xuě shān	Shesan, Snow Mountains	Hsueh Shan	valley/ river
Ilan	宜蘭	Yí lán	Yilan	Taiwan	city
Lanyang Xi	蘭陽溪	Lán yáng xī		Taiwan	valley/ river
Laonong Xi	荖濃溪	Lǎo nóng xī	NE-Valley	Yushan	valley/ river
Nan Zi Xian Xi	楠梓仙溪	Nán zǐ xiān xī	West valley	Yushan	valley/ river
Nanhu Bei Shan	南湖北山	Nán hú běi shān	Nanhu North summit (1)	Nanhuta Shan	summit
Nanhu Dong Shan	南湖東山	Nán hú dōng shān	Nanhu East Peak	Nanhuta Shan	summit
Nanhu Hut	南湖山莊	Nán hú shān zhuāng		Nanhuta Shan	mountain hut
Nanhu Nan Shan	南湖南山	Nán hú nán shān	Nanhu South Peak	Nanhuta Shan	summit
Nanhu Xi	南湖溪	Nán hú xī	Nanhu/ main /west Valley	Nanhuta Shan	valley/ river
Nanhuta North Peak	南湖大北峰	Nán hú dà shān běi fēng	Nanhu North Peak (1)	Nanhuta Shan	summit
Nanhuta Shan	南湖大山	Nán hú dà shān	Nanhu Main Peak	Nanhuta Shan	summit/ mountain range
Payun hut	排雲山莊	Pái yún shān zhuāng		Yushan	mountain hut
Peishan	北山	Běi shān	Yu Shan North Peak	Yushan	summit
Pingtung	屏東	Píng dōng		Taiwan	county
Qi Shan Xi	旗山溪	Qí shān xī	West valley	Yushan	valley/ river
Sancha Shan	三岔山	Sān chā shān		Sancha Shan	mountain range
Shangyang Shan	向陽山	Xiàng yáng shān		Shangyang Shan	mountain range
Shaofenko	小風口	Xiǎo fēng kǒu		Hohuan Shan	mountain station
Tachia Xi	大甲溪	Dà jiǎ xī	Tachia River, Ta Chia Chi	Taiwan	valley/ river
Tainan	臺南	Tái nán		Taiwan	city
Taipei	台北	Tái běi	Taipeh	Taiwan	city
Taiwan	台灣	Tái wān		Taiwan	country
Tao Sai Xi	陶塞溪	Táo sāi xī	South Valley	Nanhuta Shan	valley/ river
Taroko	太魯閣	Tài lǔ gé			National Park
Toshe basin	頭社盆地	Tóu shè pén dì		Taiwan	mountain basin
Yushan	玉山	Yù shān	Jade mountains	Yushan	summit/ mountain range
	南湖東北峰	Nán hú dōng běi fēng	Nanhu Northeast Peak	Nanhuta Shan	summit
	南湖東南峰	Nán hú dōng nán fēng	Nanhu Southeast Peak	Nanhuta Shan	summit

Notes: The terminology of geographical units and other names is rather inconsistent in non-Chinese maps and publications in Taiwan due to different romanisation. This table provides therefore the traditional Chinese characters, which are used commonly in Taiwan. (1) Caution, different summits, cf. fig. 2.2 for location

Table A2: Temperature and precipitation at meteorological stations in Taiwan

						Temperature (°C)											Precipitation (mm)	
station no.	**station name**	**latitude (N)**	**longitude (E)**	**altitude (m)**	**duration**	**jan**	**feb**	**mar**	**apr**	**may**	**jun**	**jul**	**aug**	**sep**	**oct**	**nov**	**dec**	**year**
Central Weather Bureau of Taiwan stations					*available online from http://www.cwb.gov.tw/eng/index.htm (Apr 11)*													
467530	Alishan	23° 30' 37"	120° 48' 18"	2413	1981-2010	6.2	7.2	9.3	11.4	12.9	14.2	14.6	14.4	13.7	12.3	10.3	7.3	11.2
	Alishan				1981-2010	71.7	137.3	166.5	254.2	493.6	649.6	668.3	809.3	432.9	146.7	46.3	55.9	3932.3
466910	Anbu	25° 11' 11"	121° 31' 13"	826	1981-2010	10.1	10.9	13.0	16.4	19.4	21.8	23.2	22.9	21.0	17.9	14.9	11.4	16.9
	Anbu				1981-2010	294.3	329.2	281.8	247.9	321.2	345.8	266.1	422.5	758.5	703.5	534.7	357.6	4863.1
467610	Chenggong	23° 05' 57"	121° 21' 55"	34	1981-2010	18.9	19.4	21.0	23.2	25.3	27.1	28.1	27.9	26.8	25.2	22.7	20.0	23.8
	Chenggong				1981-2010	67.2	71.8	67.1	89.3	174.3	196.5	246.1	317.6	405.8	265.6	126.6	76.5	2104.4
467480	Chiayi	23° 29' 52"	120° 25' 28"	27	1981-2010	16.5	17.3	19.7	23.0	25.8	27.8	28.6	28.2	27.0	24.5	21.3	17.7	23.1
	Chiayi				1981-2010	23.6	57.4	63.4	103.0	176.2	314.0	369.9	380.2	222.6	27.5	15.2	21.3	1774.3
466900	Danshui	25° 09' 56"	121° 26' 24"	19	1981-2010	15.2	15.6	17.4	21.1	24.5	26.9	28.8	28.6	26.7	23.7	20.6	16.9	22.2
	Danshui				1981-2010	103.9	174.8	194.5	179.3	216.1	243.4	149.2	202.9	299.1	173.9	120.7	97.6	2155.4
467540	Dawu	22° 21' 27"	120° 53' 44"	8	1981-2010	20.3	20.9	22.6	24.7	26.5	28.0	28.6	28.2	27.2	26.0	24.0	21.3	24.9
	Dawu				1981-2010	42.2	44.3	46.4	72.4	192.2	364.4	391.0	429.8	408.7	182.9	82.1	47.3	2303.7
467300	Dongjidao	23° 15' 32"	119° 39' 35"	43	1981-2010	17.8	18.2	20.3	23.3	25.7	27.4	28.4	28.2	27.3	25.3	22.7	19.6	23.7
	Dongjidao				1981-2010	16.9	30.8	44.9	67.7	135.4	183.7	177.3	207.9	120.0	31.5	20.6	17.0	1053.7
467590	Hengchun	22° 00' 20"	120° 44' 17"	22	1981-2010	20.7	21.4	23.2	25.2	27.0	27.9	28.4	28.1	27.4	26.3	24.3	21.7	25.1
	Hengchun				1981-2010	17.9	24.6	20.6	36.5	158.4	374.1	401.8	460.8	330.9	116.5	54.4	25.9	2022.4
467571	Hsinchu	24° 49' 48"	121° 00' 22"	34	1992-2010	15.5	15.9	17.9	21.7	24.9	27.4	29.0	28.7	27.1	24.2	21.2	17.7	22.6
	Hsinchu				1992-2010	64.5	142.1	168.1	164.1	232.8	261.1	141.0	182.4	214.2	62.0	38.1	47.7	1718.1
466990	Hualien	23° 58' 37"	121° 36' 18"	16	1981-2010	18.0	18.4	20.2	22.7	25.1	27.1	28.5	28.2	26.8	24.8	22.2	19.3	23.4
	Hualien				1981-2010	62.2	94.2	85.9	87.0	195.4	221.7	205.2	242.0	399.2	362.7	152.1	69.2	2176.8
467440	Kaohsiung	22° 34' 04"	120° 18' 29"	2	1981-2010	19.3	20.3	22.6	25.4	27.5	28.5	29.2	28.7	28.1	26.7	24.0	20.6	25.1
	Kaohsiung				1981-2010	16.0	20.5	38.8	69.8	197.4	415.3	390.9	416.7	241.9	42.7	18.7	16.2	1884.9
466940	Keelung	25° 08' 25"	121° 43' 56"	27	1981-2010	16.0	16.2	17.9	21.3	24.5	27.3	29.3	28.9	27.0	24.1	21.2	17.7	22.6
	Keelung				1981-2010	331.6	397.0	321.0	242.0	285.1	301.6	148.4	210.1	423.5	400.3	399.6	311.8	3772.0
467620	Lanyu	22° 02' 19"	121° 33' 02"	325	1981-2010	18.5	19.0	20.5	22.4	24.3	25.7	26.3	26.1	25.2	23.8	21.7	19.4	22.7
	Lanyu				1981-2010	248.1	203.9	154.0	149.0	249.3	287.4	231.2	287.9	384.2	305.6	267.0	212.2	2979.8
466950	Pengjiayu	25° 37' 46"	122° 04' 17"	102	1981-2010	15.7	15.9	17.5	20.4	23.4	26.0	28.0	27.9	26.3	23.7	20.7	17.4	21.9
	Pengjiayu				1981-2010	122.6	161.0	169.5	161.6	203.2	194.1	125.8	198.0	236.9	136.8	132.0	112.5	1954.0
467060	Su-ao	24° 36' 06"	121° 51' 52"	25	1982-2010	16.4	16.9	18.8	21.6	24.4	26.9	28.6	28.2	26.6	23.8	20.9	17.7	22.6
	Su-ao				1982-2010	362.8	329.3	200.3	186.9	261.8	246.0	177.2	279.9	535.3	744.8	682.0	433.5	4439.8
467650	Sun Moon Lake	23° 52' 59"	120° 53' 60"	1015	1981-2010	14.2	15.1	16.9	19.2	21.0	22.2	23.0	22.7	22.1	20.7	18.3	15.2	19.2
	Sun Moon Lake				1981-2010	49.1	100.0	124.7	199.5	328.3	436.9	409.9	403.8	232.3	49.7	31.2	36.5	2401.9
467490	Taichung	24° 08' 51"	120° 40' 33"	84	1981-2010	16.6	17.3	19.6	23.1	26.0	27.6	28.6	28.3	27.4	25.2	21.9	18.1	23.3
	Taichung				1981-2010	30.3	89.8	103.0	145.4	231.5	331.2	307.9	302.0	164.5	23.2	18.3	25.9	1773.0
467410	Tainan	22° 59' 43"	120° 11' 49"	14	1981-2010	17.6	18.6	21.2	24.5	27.2	28.5	29.2	28.8	28.1	26.1	22.8	19.1	24.3
	Tainan				1981-2010	17.3	28.1	38.5	79.5	173.6	371.5	357.7	395.1	178.0	27.8	16.7	14.4	1698.2
466920	Taipei	25° 02' 23"	121° 30' 24"	6	1981-2010	16.1	16.5	18.5	21.9	25.2	27.7	29.6	29.2	27.4	24.5	21.5	17.9	23.0
	Taipei				1981-2010	83.2	170.3	180.4	177.8	234.5	325.9	245.1	322.1	360.5	148.9	83.1	73.3	2405.1
467660	Taitung	22° 45' 15"	121° 08' 48"	9	1981-2010	19.5	20.0	21.8	24.1	26.2	27.8	28.9	28.7	27.5	25.7	23.3	20.5	24.5
	Taitung				1981-2010	30.5	40.2	40.5	65.6	155.9	227.8	270.5	302.0	344.6	182.3	79.2	40.5	1779.6
467770	Wuqi	24° 15' 31"	120° 30' 54"	7	1981-2010	16.0	16.3	18.5	22.4	25.5	27.8	29.0	28.8	27.4	24.6	21.4	17.7	23.0
	Wuqi				1981-2010	24.6	81.5	98.5	132.5	213.7	219.1	193.5	211.5	113.2	17.5	16.8	25.3	1347.7
467080	Yilan	24° 45' 56"	121° 44' 53"	7	1981-2010	16.3	16.9	18.9	21.7	24.4	26.8	28.6	28.3	26.5	23.6	20.6	17.5	22.5
	Yilan				1981-2010	147.0	182.3	127.5	138.4	211.7	214.2	155.1	247.8	470.0	442.0	325.1	176.6	2837.7
467550	Yushan (Pei Shan)	23° 29' 21"	120° 57' 06"	3845	1981-2010	-1.1	-0.5	1.1	3.4	5.7	7.1	7.9	7.8	7.1	6.5	4.0	0.8	4.2
	Yushan (Pei Shan)				1981-2010	83.1	120.5	139.1	244.4	414.0	488.2	445.6	519.3	325.2	144.3	77.6	70.0	3071.3
466930	Zhuzihu	25° 09' 54"	121° 32' 11"	607	1981-2010	11.8	12.5	14.7	18.0	21.0	23.3	24.8	24.6	22.7	19.8	16.8	13.3	18.6
	Zhuzihu				1981-2010	232.6	273.5	227.1	207.2	267.4	314.8	247.7	439.5	717.4	683.9	488.8	289.1	4389.0
other stations																		
	Nanhuta Shan	24° 21' 47"	121° 26' 48"	3550	2001-2005	-2.5	-0.6	0.7	4.2	6.4	7.4	8.2	8.2	6.9	5.1	2.8	0.4	3.9
	Nanhuta Shan				2001-2005	45.4	116.5	238.3	194.2	227.0	259.4	619.7	562.8	802.2	316.8	69.7	215.1	3667.0
	Shaofenko	24° 09' 48"	121° 16' 43"	3005	2005-2009	1.6	2.2	3.7	6.0	8.1	9.6	10.6	10.3	9.6	7.9	5.2	1.6	6.4
	Shaofenko				2005-2009	156.0	104.0	311.6	330.0	311.7	514.6	505.8	654.3	550.6	273.4	180.4	97.5	3989.8

Table A3: Comparison of four methods to establish the theoretical ELA over a non-glaciated terrain in four Taiwanese mountain areas

	T (jun)	T (jul)	T (aug)	summer T	annual T	annual P	P (dec)	P (jan)	P (feb)	P (mar)	winter P	alt	laps rate[5] dT/dh	T (ELA)	dT	dh	ELAt
	°C	°C	°C	°C	°C	mm	mm	mm	mm	mm	mm	m	(°C/ m)	°C	°C	m	m
method Ohmura [1]																	
Yushan (61-90)	6.8	7.6	7.4	7.3		3152.1						3845	-0.006	7.0	-0.3	47	3892
Yushan (71-00)	**7.0**	**7.7**	**7.5**	**7.4**		**3054.4**						**3845**	**-0.006**	**6.8**	**-0.6**	**108**	**3953**
Yushan (81-10)	7.1	7.9	7.8	7.6		3071.3						3845	-0.006	6.8	-0.8	134	3979
Nanhuta Shan	7.4	8.2	8.2	7.9		3667.0						3550	-0.006	8.2	0.2	-41	3509
Ali Shan (61-90)	13.8	14.2	13.9	14.0		3962.2						2413	-0.006	8.8	-5.1	855	3268
Ali Shan (81-10)	14.2	14.6	14.4	14.4		3932.3						2413	-0.006	8.8	-5.6	939	3352
Shaofengko	9.6	10.6	10.3	10.2		3989.8						3005	-0.006	8.9	-1.3	212	3217
method Ohmura with winter (dec-mar) precipitation only [2]																	
Yushan (61-90)	6.8	7.6	7.4	7.3			81.5	133.4	161.5	161.4	537.8	3845	-0.006	-0.4	-7.6	1272	5117
Yushan (71-00)	7.0	7.7	7.5	7.4			85.6	116.0	148.9	138.9	489.4	3845	-0.006	-0.5	-7.9	1322	5167
Yushan (81-10)	7.1	7.9	7.8	7.6			70.0	83.1	120.5	139.1	412.7	3845	-0.006	-0.8	-8.4	1401	5246
Nanhuta Shan	7.4	8.2	8.2	7.9			215.1	45.4	116.5	238.3	615.3	3550	-0.006	-0.1	-8.0	1339	4889
Ali Shan (61-90)	13.8	14.2	13.9	14.0			53.7	88.6	113.7	158.8	414.8	2413	-0.006	-0.8	-14.8	2461	4874
Ali Shan (81-10)	14.2	14.6	14.4	14.4			55.9	71.7	137.3	166.5	431.4	2413	-0.006	-0.7	-15.1	2523	4936
Shaofengko	9.6	10.6	10.3	10.2			97.5	156.0	104.0	311.6	669.1	3005	-0.006	0.1	-10.1	1681	4686
0 °C annual isotherm (mean freezing level) [3]																	
Yushan (61-90)					3.8							3845	-0.006	0.0	-3.8	633	4478
Yushan (71-00)					3.9							3845	-0.006	0.0	-3.9	650	4495
Yushan (81-10)					4.2							3845	-0.006	0.0	-4.2	700	4545
Nanhuta Shan					3.9							3550	-0.006	0.0	-3.9	650	4200
Ali Shan (61-90)					10.6							2413	-0.006	0.0	-10.6	1767	4180
Ali Shan (81-10)					11.2							2413	-0.006	0.0	-11.2	1867	4280
Shaofengko					6.4							3005	-0.006	0.0	-6.4	1067	4072
0 °C July isotherm [4]																	
Yushan (61-90)		7.6										3845	-0.006	0.0	-7.6	1267	5112
Yushan (71-00)		7.7										3845	-0.006	0.0	-7.7	1283	5128
Yushan (81-10)		7.9										3845	-0.006	0.0	-7.9	1317	5162
Nanhuta Shan		8.2										3550	-0.006	0.0	-8.2	1367	4917
Ali Shan (61-90)		14.2										2413	-0.006	0.0	-14.2	2367	4780
Ali Shan (81-10)		14.6										2413	-0.006	0.0	-14.6	2433	4846
Shaofengko		10.6										3005	-0.006	0.0	-10.6	1767	4772

[1)] Ohmura et al. (1992) with $P = a + bT + cT^2$, a = 645, b = 296, c = 9, P = annual precipitation, T = summer (JJA) temperature

[2)] Ono (2003)

[3)] Kaser and Osmaston (2002), Hastenrath (2009)

[4)] Porter (2005)

[5)] laps rate after Porter (2001)

bold = applied in Hebenstreit (2006)

Table A4: Locations of sediment analyses and sampling

Location ID	Area	Location	latitude (N)	longitude (E)	altitude, aneroid (m)	sediment interpretation	samples[1]			sediment characteristics [2]			publication [3]
							OSL	EXPO (no.)	grain size	fabric	petro-logy	round-ness	
Hsueh Shan													
Hsu-II	NE-valley	behind lat. moraine	24° 23' 28.3"	121° 15' 41.4"	3040	slope sediment			**xx**				unpubl.
Hsu-III	NE-valley	lateral moraine	24° 23' 28.3"	121° 15' 41.4"	3045	moraine	**xx**		**xx**		**q**	**q**	ZFG, QI
Nanhuta Shan													
Nan-Ia	Upper valley	middle rock ridge	24° 22' 02.3"	121° 26' 43.8"	3510	erratic boulder		**1**					QSR
Nan-Ib	Upper valley	middle rock ridge	24° 22' 04.4"	121° 26' 43.1"	3485	erratic boulder		**2**					QSR
Nan-II	Upper valley	north cliff	24° 22' 31.3"	121° 26' 44.9"	3520	schist moraine	**x**		**xx**	**x**	**xx**	**xx**	QI
Nan-III	Upper valley	northern part	24° 22' 21.9"	121° 26' 43.3"	3480	schist moraine	**x**		**x**	**x**	**xx**	**xx**	QI
Nan-IIIa	Upper valley	northern part	24° 22' 22.1"	121° 26' 41.3"	3485	erratic boulder		**5**					QSR
Nan-IV	Upper valley	"kame"	24° 22' 15.4"	121° 26' 43.3"	3425	glaciofluvial sed.	**x**		**x**	**q**	**x**	**xxx**	QI, ZFG
Nan-V	SE-valley	terrace behind moraine	24° 21' 04.7"	121° 27' 51.4''	3180	glaciofluvial sed.	**xx**		**xx**				QI, ZFG
Nan-Vb	SE-valley	moraine top	24° 21' 04.7"	121° 27' 51.5"	3190	bbm		**6**			**x**	**q**	QSR, QI
Nan-VI	SE-valley	slope	24° 21' 14.9"	121° 27' 38.8"	3200	slope sediment	**x**		**xx**				ZFG, Kl, QI
Nan-VII	Lower valley	lateral (N-) moraine	24° 22' 11.9"	121° 26' 35.2"	3375	schist moraine	**xx**		**xx**	**x**	**x**	**x**	QI, ZFG
Nan-VIII	Lower valley	slope	24° 22' 19.8"	121° 26' 02.2"	3420	slope sediment	**x**		**(xx)**				Kl, QI, QSR
Nan-IXb	Lower valley	2nd moraine top	24° 22' 04.8"	121° 26' 32.3"	3385	bbm		**4**			**q**	**q**	QSR
Nan-IXb	Lower valley	2nd moraine, prox. base	24° 22' 06.6"	121° 26' 32.3"	3380	bbm		**3**					QSR
Nan-NX	Nanhu valley		24° 22' 13.8"	121° 23' 43.1"	2250	moraine			**x**	**x**	**x**	**xxx**	QI
Yushan													
Yu-I	NE-valley	"Panzer"-moraine	23° 28' 57.5"	120° 57' 52.7"	3140[4]	moraine			**xx**	**q**	**q**	**x**	photo QI
total:							11	6	17	4	8	12	

(1) x represents one sample or analysis, (x) = Klose (2007)
(2) q = qualitativ description
(3) ZFG = Hebenstreit and Böse (2003), QI = Hebenstreit et al. (2006), QSR = Hebenstreit et al. (2011), Kl = Klose (2006)
(4) GPS altitude

Table A5: Results of 17 grain size analyses in %

Date (ddmmyy):		201000/	201000/	220301/	200300/	210300/	210300/	210300/	210300/	220300/	170301/	240301/	040300/	040300/	050300/	050300/	280302/	280302/
depth:		60 cm	90 cm	110 cm	80 cm	40 cm	80 cm	45 cm	55 cm	x	x	x	35 cm	50 cm	40 cm	80 cm	x	x
sample no.:		**Nan-II/1**	**Nan-II/2**	**Nan-III**	**Nan-IV**	**Nan-V/1**	**Nan-V/2**	**Nan-VI/1**	**Nan-VI/2**	**Nan-VII/1**	**Nan-VII/2**	**Nan-NX**	**Hsu-II/1**	**Hsu-II/2**	**Hsu-III/1**	**Hsu-III/2**	**Yu-I/1**	**Yu-I/2**
total sample:		100.00	100.00	100.00	100.00	100.00	100.00	100.00	100.00	100.00	100.00	100.00	100.00	100.00	100.00	100.00	100.00	100.00
gravel sieving	20-63 mm	19.06	13.48	2.30	2.92	0.00	0.00	0.00	0.00	0.00	6.15	10.94	0.00	0.00	0.00	0.00	11.98	10.40
	6.3-20 mm	28.35	11.71	20.13	15.60	0.00	0.00	0.00	0.00	11.64	24.69	36.44	5.98	1.62	10.95	20.67	20.92	16.10
	2-6.3 mm	27.53	15.39	33.83	30.91	0.76	3.22	0.05	0.37	28.42	33.65	25.34	3.25	4.10	6.91	17.43	21.05	24.33
sieve and pipette analysis	1000-2000 µm	11.68	6.68	10.52	22.15	0.99	6.62	0.28	0.77	15.00	12.61	7.29	1.35	2.59	0.96	2.13	9.36	6.65
	630-1000 µm	4.45	4.00	4.15	11.10	0.95	7.11	0.72	1.10	7.12	5.37	4.23	0.60	1.46	0.33	0.75	4.64	3.19
	315-630 µm	3.53	5.38	4.56	7.94	1.50	16.56	7.36	5.05	8.57	5.08	5.22	1.45	3.39	0.52	0.99	6.22	4.37
	200-315 µm	0.59	1.32	0.12	1.90	1.58	10.68	14.82	8.14	4.50	0.29	0.80	2.24	5.10	0.66	1.49	3.87	3.42
	125-200 µm	0.45	1.66	0.79	1.09	3.39	7.75	16.72	9.97	3.84	0.37	0.82	5.42	9.78	1.11	5.97	3.67	3.92
	63-125 µm	0.76	3.98	1.33	0.91	11.13	9.88	16.88	17.01	4.86	1.23	0.56	9.77	15.53	3.62	9.22	4.21	4.97
	20-63 µm	1.39	11.10	8.12	1.09	16.23	12.61	17.90	17.46	4.79	3.23	1.71	16.26	9.42	30.12	10.69	5.90	6.23
	6.3-20 µm	0.78	9.48	5.16	1.15	25.64	13.15	11.91	19.81	4.11	2.44	1.86	9.61	13.49	18.04	8.68	0.66	4.05
	2-6.3 µm	0.78	10.52	4.81	2.06	25.64	9.44	9.77	14.93	3.37	2.80	1.45	12.61	13.23	10.80	7.58	2.42	3.46
	< 2 µm	0.65	5.29	4.17	1.18	12.19	2.98	3.61	5.41	3.78	2.10	3.33	31.46	20.30	15.98	14.39	5.09	8.92
Percentage of matrix fractions																		
Σ sand		**85.64**	**38.76**	**49.09**	**89.16**	**19.69**	**60.55**	**56.80**	**42.18**	**73.22**	**70.26**	**69.39**	**22.94**	**40.13**	**8.77**	**33.22**	**69.43**	**53.93**
Σ silt		**11.77**	**52.33**	**41.37**	**8.50**	**68.03**	**36.37**	**39.59**	**52.39**	**20.47**	**23.84**	**18.41**	**42.40**	**38.33**	**71.78**	**43.53**	**19.50**	**27.93**
Σ clay		**2.59**	**8.91**	**9.54**	**2.34**	**12.29**	**3.08**	**3.61**	**5.43**	**6.31**	**5.90**	**12.20**	**34.65**	**21.53**	**19.46**	**23.25**	**11.07**	**18.14**
Percentage of total sample																		
Σ gravel		**74.94**	**40.58**	**56.26**	**49.44**	**0.76**	**3.22**	**0.05**	**0.37**	**40.06**	**64.49**	**72.72**	**9.23**	**5.72**	**17.85**	**38.10**	**53.96**	**50.84**
Σ sand		**21.46**	**23.04**	**21.47**	**45.08**	**19.54**	**58.60**	**56.77**	**42.03**	**43.89**	**24.95**	**18.93**	**20.83**	**37.84**	**7.20**	**20.56**	**31.97**	**26.51**
Σ silt		**2.95**	**31.09**	**18.10**	**4.30**	**67.51**	**35.20**	**39.57**	**52.19**	**12.27**	**8.46**	**5.02**	**38.49**	**36.14**	**58.96**	**26.95**	**8.98**	**13.73**
Σ clay		**0.65**	**5.29**	**4.17**	**1.18**	**12.19**	**2.98**	**3.61**	**5.41**	**3.78**	**2.10**	**3.33**	**31.46**	**20.30**	**15.98**	**14.39**	**5.09**	**8.92**

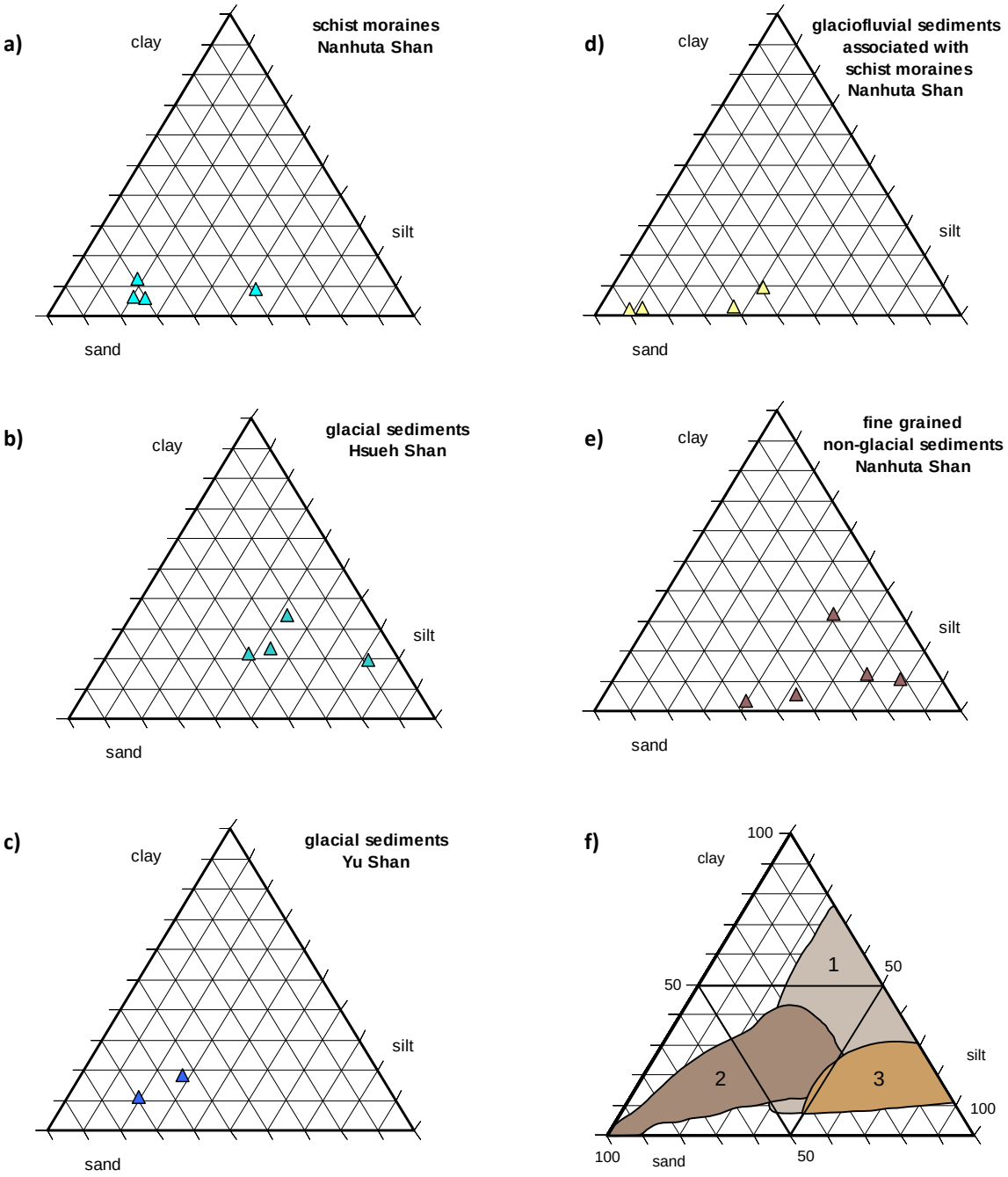

Figure A1: Ternary diagrams of grain size distributions and respective facies interpretations of sediments in three study areas, including the following samples (cf. appendix table A5):

a) Nan-II/2, Nan-VII/1, Nan-VII/2, Nan-NX
b) Hsu-II/1, Hsu-II/2, Hsu-III/1, Hsu-III/2
c) Yu-I/1, Yu-I/2
d) Nan-II/1, Nan-III, Nan-IV, Nan-V/2
e) Nan-V/1, Nan-VI/1, Nan-VI/1, Nan-VIII/1*, Nan-VIII/2*
(*Klose, 2007, there Va, Vb)
f) Envelopes of common natural grain size distributions in soils: 1 – weathered rock, 2 – glacial material, 3 – Loess (Hartge and Horn, 1992)

Table A6: Results of clast counting

Loc-ID	depth [cm]		roundness class 1	2	3	4	petrography slate	quartzite	Σ(n)	l [cm]
Nan-II	40	n	21	24	5	0	39	11	50	5-20
		%	***42.0***	***48.0***	***10.0***	***0.0***	***78.0***	***22.0***		
Nan-II	80	n	5	21	12	2	35	5	40	3-10
		%	***12.5***	***52.5***	***30.0***	***5.0***	***87.5***	***12.5***		
Nan-III	0	n	17	19	9	0	36	9	45	4-50
		%	***37.8***	***42.2***	***20.0***	***0.0***	***80.0***	***20.0***		
Nan-III	80	n	4	27	9	0	38	2	40	4-15
		%	***10.0***	***67.5***	***22.5***	***0.0***	***95.0***	***5.0***		
Nan-IV	20	n	23	14	3	0	n.a.	n.a.	40	5-10
		%	***57.5***	***35.0***	***7.5***	***0.0***				
Nan-IV	50	n	10	21	8	1	33	7	40	4-15
		%	***25.0***	***52.5***	***20.0***	***2.5***	***82.5***	***17.5***		
Nan-IV	100	n	2	14	24	10	n.a.	n.a.	50	3-5
		%	***4.0***	***28.0***	***48.0***	***20.0***				
Nan-VII	x	n	21	50	28	1	94	6	100	10-20
		%	***21.0***	***50.0***	***28.0***	***1.0***	***94.0***	***6.0***		
Nan-NX	x	n	3	19	8	0	27	3	30	5-10
		%	***10.0***	***63.3***	***26.7***	***0.0***	***90.0***	***10.0***		
Nan-NXb	x	n	17	10	3	0	n.a.	n.a.	30	5-15
		%	***56.7***	***33.3***	***10.0***	***0.0***				
Nan-NXc	x	n	0	3	22	25	n.a.	n.a.	50	5-10
		%	***0.0***	***6.0***	***44.0***	***50.0***				
Nan-Vb (moraine top)	0	n	n.a.	n.a.	n.a.	n.a.	3	27	30	10-50
		%	***n.a.***	***n.a.***	***n.a.***	***n.a.***	***10.0***	***90.0***		
Yu-I	x	n	6	25	19	0	n.a.	n.a.	50	5-15
		%	***12.0***	***50.0***	***38.0***	***0.0***				

n = number of counted clastes
l = lengh of counted clastes
n.a. = not applied

Table A7: Comparison of ^{10}Be exposure ages calculated under alternative scaling models

Sample	Lal (1991)/ Stone (2000)	Desilets et al. (2003, 2006)	Dunai (2001)	Lifton et al. (2005)	Lal/ Stone, time-dependent
	exposure age ± external uncertainty (ka)				
Nanhuta Shan (Hebenstreit et al. 2011)					
Expo1	9.181 ± 1.091	8.893 ± 1.273	9.263 ± 1.322	8.795 ± 1.123	9.049 ± 1.058
Expo2	10.192 ± 1.033	9.921 ± 1.280	10.266 ± 1.320	9.773 ± 1.090	10.069 ± 0.998
Expo3	9.538 ± 1.085	9.343 ± 1.299	9.687 ± 1.342	9.222 ± 1.134	9.429 ± 1.054
Expo4	10.443 ± 1.167	10.223 ± 1.404	10.561 ± 1.446	10.060 ± 1.218	10.318 ± 1.132
Expo5	2.954 ± 0.640	3.252 ± 0.750	3.308 ± 0.763	3.299 ± 0.731	3.263 ± 0.703
Expo6	14.142 ± 1.349	13.960 ± 1.738	14.282 ± 1.771	13.608 ± 1.446	13.953 ± 1.298
Nanhuta Shan (Siame et al., 2007, recalculated)					
NHTS-2, §	12.169 ± 2.915	11.807 ± 2.982	12.180 ± 3.073	11.535 ± 2.815	12.027 ± 2.870
NHTS-5	6.005 ± 0.949	5.978 ± 1.059	6.197 ± 1.096	5.993 ± 0.988	6.042 ± 0.947
NHTS-6, §	17.762 ± 4.928	16.835 ± 4.860	17.213 ± 4.966	16.338 ± 4.595	17.177 ± 4.751
NHTS-7	9.594 ± 1.450	9.293 ± 1.589	9.655 ± 1.647	9.170 ± 1.450	9.481 ± 1.419
NHTS-9	5.780 ± 2.274	5.788 ± 2.324	5.985 ± 2.402	5.805 ± 2.300	5.848 ± 2.298
NHTS-10	6.260 ± 0.927	6.179 ± 1.040	6.420 ± 1.078	6.190 ± 0.961	6.261 ± 0.918
NHTS-12e, §	6.162 ± 2.152	6.229 ± 2.232	6.451 ± 2.310	6.243 ± 2.200	6.181 ± 2.155
NHTS-13a	12.343 ± 2.135	12.260 ± 2.337	12.579 ± 2.394	11.992 ± 2.149	12.212 ± 2.097
NHTS-14	6.440 ± 1.830	6.329 ± 1.868	6.583 ± 1.941	6.339 ± 1.825	6.415 ± 1.818
NHTS-15	8.531 ± 2.423	8.208 ± 2.422	8.568 ± 2.527	8.151 ± 2.346	8.370 ± 2.371
NHTS-16	9.597 ± 2.043	9.297 ± 2.114	9.659 ± 2.194	9.174 ± 1.999	9.485 ± 2.009
NHTS-17	7.512 ± 1.368	7.283 ± 1.448	7.599 ± 1.509	7.275 ± 1.368	7.362 ± 1.332
NHTS-19, §	10.757 ± 1.938	10.486 ± 2.067	10.833 ± 2.132	10.305 ± 1.918	10.624 ± 1.901
NHTS-20b	9.721 ± 1.389	9.451 ± 1.547	9.800 ± 1.601	9.320 ± 1.401	9.609 ± 1.358

Notes:

The surface exposure ages were calculated with the CRONUS-Earth online exposure age calculator, version 2.2. See Balco et al. (2008) for full documentaion of all five scaling schemes. For sample details and ^{10}Be concentrations of the Siame samples, see Siame et al., 2007. We assumed 5 cm sample thickness and 2.65 g/cm^3 rock density for their samples. We used the 07KNSTD standard for our samples and the NIST_30600 standard for Siame's samples.

§ … these samples are not included in further discussion due to different geomorphological interpretation (see Hebenstreit et al., 2011, chapter 6)

Table A8: Calculations of error weighted mean ages of ^{10}Be and OSL samples

sample			x_i	σ
			(ka)	
Hsueh Shan				
Hsu-III	lateral moraine		51.0 ±	10.0
Hsu-III	lateral moraine		56.0 ±	4.0
		$\mu \pm \sigma_\mu$	55.3 ±	3.7
Nanhuta Shan				
plateau				
NHTS-9			5.8 ±	2.3
NHTS-10			6.2 ±	1.0
NHTS-14			6.3 ±	1.8
NHTS-15			8.2 ±	2.3
NHTS-16			9.2 ±	2.0
		$\mu \pm \sigma_\mu$	6.7 ±	0.7
rock ridge and Lower Valley				
Expo1	ridge		8.8 ±	1.1
Expo2	ridge		9.8 ±	1.1
Expo3	bbm		9.2 ±	1.1
Expo4	bbm		10.1 ±	1.2
NHTS-7	ridge		9.2 ±	1.5
NHTS-20b	ridge		9.3 ±	1.4
Expo 1-4		$\mu \pm \sigma_\mu$	9.4 ±	0.6
all ridge		$\mu \pm \sigma_\mu$	9.3 ±	0.6
Expo3 & 4 (bbm)		$\mu \pm \sigma_\mu$	9.6 ±	0.8
schist moraine (OSL)				
Nan-II	Upper Valley		8.7 ±	1.0
Nan-III	Upper Valley		9.0 ±	2.0
Nan-VII	Lower Valley		9.7 ±	0.7
II+III+VII		$\mu \pm \sigma_\mu$	9.3 ±	0.6
Lower Valley (Nan-VII, Expo 3 & 4)		$\mu \pm \sigma_\mu$	**9.7 ±**	**0.5**
Upper Valley, Lower Valley & rock ridge		$\mu \pm \sigma_\mu$	**9.4 ±**	**0.4**
SE-Valley				
Expo6	bbm		13.6 ±	1.4
NHTS-13a	whaleback rock		12.0 ±	2.1
		$\mu \pm \sigma_\mu$	**13.1 ±**	**1.2**
post-glacial				
Expo5	exhumed glacial boulder		3.3 ±	0.7
Nan-VI	slope		3.1 ±	0.3
Nan-VIII	slope		3.3 ±	0.9
		$\mu \pm \sigma_\mu$	**3.1 ±**	**0.3**

Nan-xy = OSL samples, Hebenstreit et al., 2006

EXPOx = ^{10}Be samples, Hebenstreit et al., 2011

NHTS-xy = ^{10}Be samples, Siame et al., 2007

Scaling of ^{10}Be ages after Lifton et al., 2005

mean calculation after Bevington and Robinson (1992) $\mu = \frac{\sum (x_i / \sigma_i^2)}{\sum (1/\sigma_i^2)}$ $\sigma_\mu = \sqrt{1/\sum (1/\sigma_i^2)}$

samples not included in mean calculation:

NHTS-2, -6, -12a, -19	(different geomorph. Interpretation, cf. table A7)
NHTS-5, -17	(possibly eroded boulders)
Nan-IV	(less reliable OSL age)
Nan-V, -VIIb	(representing backwasting stage)

List of publications

Peer reviewed journals

Hebenstreit, R., Ivy-Ochs, S., Kubik, P.W., Schlüchter, C., Böse, M., 2011. Lateglacial and early Holocene surface exposure ages of glacial boulders in the Taiwanese high mountain range. Quaternary Science Reviews 30 (3-4), 298-311.

Hebenstreit, R., Böse, M., Murray, A., 2006. Late Pleistocene and early Holocene glaciations in Taiwanese mountains. Quaternary International 147 (1), 76-88.

Hebenstreit, R., 2006. Present and former equilibrium line altitudes in the Taiwanese high mountain range. Quaternary International 147 (1), 70-75.

Hebenstreit, R., Böse, M., 2003. Geomorphological evidence for a Late Pleistocene glaciation in the high mountains of Taiwan dated with age estimates by optically stimulated luminescence (OSL). Zeitschrift für Geomorphologie, N.F. Suppl.-Vol. 130, 31-49.

Book chapter

Böse, M., Hebenstreit, R., 2011. Late Pleistocene and Early Holocene Glaciations in the Taiwanese High Mountain Ranges. In: Ehlers, J., Gibbard, P.L. and Hughes, P.D. (Eds.), Quaternary Glaciations - Extent and Chronology - A Closer Look. Developments in Quaternary Science, 15. Elsevier, Amsterdam, pp. 1003 -1012.

Conference contributions

Hebenstreit, R., Ivy-Ochs, S., Kubik, P., Böse, M., 2010. Latest Pleistocene and Early Holocene Surface Exposure Ages of Glacial Boulders in the Taiwanese High Mountain Range. EGU General Assembly 2010. Geophysical Research Abstracts, Vienna, p. EGU2010-12229.

Böse, M., Hebenstreit, R., Ivy-Ochs, S., 2007. Surface exposure dating of glacial boulders in the high mountain range of Taiwan and its implication for the Late Glacial equilibrium line altitude. XVII INQUA Congress. Quaternary International 167-168, Cairns, p. 37.

Böse, M., Klose, C., Hebenstreit, R., 2006. Differentiated denudation in the High Mountains of Taiwan, EGU General Assembly, Vienna, pp. A-02175.

Hebenstreit, R., 2004. Geomorphological studies on the Late Pleistocene Glaciation in the High Mountains of Taiwan. In: National Taiwan University and Free University Berlin (Eds.), Morphodynamics in the Mountains of Taiwan since the Late Pleistocene. Abstracts of the Taiwan-German Quaternary Symposium, Taipei, p. 5.

Böse, M., Hebenstreit, R., 2003. Geomorphological Studies on the Late Pleistocene Glaciation in the high Mountains of Taiwan. XVI INQUA Congress, Reno Hilton Hotel and Conference Center, Nevada, p. 72.

Böse, M., Hebenstreit, R., 2001. Geomorphologische Befunde zur spätpleistozänen Vergletscherung im Hochgebirge von Taiwan. 27. Jahrestagung des Deutschen Arbeitskreises für Geomorphologie, Berlin, pp. 10-11.

Böse, M., Hebenstreit, R., 2001. Geomorphologic Evidence of Late Pleistocene Glaciation in the High Mountains of Taiwan. Fifth International Conference on Geomorphology. Transactions of the Japanese Geomorphological Union, Tokyo, p. C-28.

Hebenstreit, R., Reißmann, C., Böse, M., 2001. Geomorphic Evidence of a Late Pleistocene Glaciation in the High Mountains of Taiwan. In: International Geosphere-Biosphere Programme - IGBP (Editor), Challenges of a Changing Earth. Global Change Open Science Conference. Challenges of a Changing Earth, Amsterdam, p. 180.

Hebenstreit, R., Böse, M., 2001. Late Pleistocene Glaciation in the High Mountain Range of Taiwan, Dated by Optically Stimulated Luminescence (OSL). Fifth International Conference on Geomorphology. Transactions of the Japanese Geomorphological Union, Tokyo, p. C-88.

Böse, M., Hebenstreit, R., Martens, H., 2000. Zur Gebirgsvergletscherung von Taiwan. In: Ivy-Ochs, S., Oberholzer, P. and Schlüchter, C. (Eds.), DEUQUA 2000, Hauptversammlung, Bern, p. 10.

Hebenstreit, R., Martens, H., 2000. Vorzeitliche Vergletscherung des Nanhuta Shan, Taiwan. In: Ivy-Ochs, S., Oberholzer, P. and Schlüchter, C. (Eds.), DEUQUA 2000, Hauptversammlung, Bern, p. 22.

Hebenstreit, R., Martens, H., 2000. Ancient Glaciation of Nanhuta Shan, Sino-German Geomorphological Workshop - Glacial Landforms, Taipei.

Curriculum Vitae

For data privacy protection the curriculum vitae is not part of the online version of this dissertation.

Eidesstattliche Erklärung

Hiermit erkläre ich, dass ich die vorliegende Arbeit selbständig angefertigt und keine als die angegebenen Quellen und Hilfsmittel verwendet habe. Die Beiträge der Co-Autoren der wissenschaftlichen Veröffentlichungen und technische Hilfe anderer Personen sind im Rahmen der Danksagung (Acknowledgements) dargelegt.

Ich erkläre, dass ich diese Dissertation in dieser oder anderer Form in keinem früheren Promotionsverfahren, sondern erstmalig am Fachbereich Geowissenschaften der Freien Universität Berlin eingereicht habe. Der Inhalt der dem Verfahren zugrunde liegenden Promotionsordnung ist mir bekannt.

Berlin, den 29.08.2011

Robert Hebenstreit